MICROCOPY RESOLUTION TEST CHART

NATIONAL BUREAU OF STANDARDS-1963-A

DOT/FAA/CT-85/32

AD-A171 215

# Development of an Operating Profile for Bias Aircraft Tires

Paul C. Durup
Max A. Gamon
Lockheed-California Company

June 1986
Final Report

DTIC
ELECTE
AUG 2 5 1986
E

US Department of Transportation
**Federal Aviation Administration**

DTIC FILE COPY

86

## NOTICE

ADA 171 215

Technical Report Documentation Page

| 1. Report No. | 2. Government Accession No. | 3. Recipient's Catalog No. |
|---|---|---|
| DOT/FAA/CT-85/32 | | |

| 4. Title and Subtitle | 5. Report Date |
|---|---|
| DEVELOPMENT OF AN OPERATING PROFILE FOR AIRCRAFT TIRES | June 1986 |
| | 6. Performing Organization Code |
| | DTS-48 |

| 7. Author's) | 8. Performing Organization Report No. |
|---|---|
| Paul Durup, Max Gamon, Stephen Bobo,* S.K. Clark** | |

| 9. Performing Organization Name and Address | 10. Work Unit No. (TRAIS) |
|---|---|
| +Lockheed California Company<br>Burbank, California 91520 | FA6A7/A6254 |
| | 11. Contract or Grant No. |
| | DTRS57-80-C-00190 |
| | 13. Type of Report and Period Covered |

| 12. Sponsoring Agency Name and Address | |
|---|---|
| Federal Aviation Administration<br>800 Independence Ave., S.W.<br>Washington, DC 20590 | Final Report<br>June 1980 – December 1985 |
| | 14. Sponsoring Agency Code |
| | AWS-340 |

16. Abstract

This report describes the procedures of analysis and dynamometer testing that were used to develop data and supporting technology for improving the maintenance and continued airworthiness of civil aircraft tires. As related to the inspection, retread and repair of aircraft tires under Advisory Circular AC 145-41, improved criteria which characterize typical tire operating environments and operating scenarios (associated with long range, medium range, and short haul transport airplanes) are defined. Based upon these criteria and scenarios which include tire loading, temperature, and roll distances, means to assess tire fatigue life were developed. Results of this effort may be used for the identification of in-service acceptance criteria and prescribed retread limits.

| 17. Key Words | 18. Distribution Statement |
|---|---|
| Aircraft Tires, Temperature, Stress, Brake Heating, Burst Tests, Dynamometer Tests, Retreading | DOCUMENT IS AVAILABLE TO THE PUBLIC THROUGH THE NATIONAL TECHNICAL INFORMATION SERVICE, SPRINGFIELD, VIRGINIA 22161 |

| 19. Security Classif. (of this report) | 20. Security Classif. (of this page) | 21. No. of Pages | 22. Price |
|---|---|---|---|
| Unclassified | Unclassified | | |

Form DOT F 1700.7 (8-72)     Reproduction of completed page authorized

A

## PREFACE

This report presents results of a study aimed at improving procedures for maintenance, inspection, repair, and retreading of aircraft tires. The study was performed by the Lockheed California Company (Paul C. Durup, Principal Investigator) under Contract DTRS-80-C-00190. Technical Monitors of the contract were Richard M. Johnson (FAA Technical Center) and Stephen N. Bobo (DOT/Transportation Systems Center). Under a subcontract, the Goodyear Tire and Rubber Company, under the direction of Harold Saviers and Edward Demors, provided valuable assistance in obtaining, inspecting, and retreading tires, instrumenting test tires, analyzing tire failures, consulting on test methods, and analyzing test results. Dynamometer testing was performed at the Flight Dynamics Laboratory, Wright Patterson Air Force Base, under the supervision of Igors Skriblis.

The report contains contributions by Stephen N. Bobo, and by Samuel K. Clark of the University of Michigan, who provided experimental data obtained under Contract 84-P-00607.

## TABLE OF CONTENTS

# LIST OF ILLUSTRATIONS

LIST OF ILLUSTRATIONS (CONTINUED)

## LIST OF ILLUSTRATIONS (CONTINUED)

LIST OF TABLES

# EXECUTIVE SUMMARY

The FAA is responsible for insuring the continued airworthiness of aircraft tires. Recent accidents prompted a review of rules and advisories related to testing and maintenance of tires. Accordingly, a study was performed to examine the validity of tire tests now called for under TSO C62-c and AC 145-4. Since radials are being introduced into the fleet, the report will serve as a baseline for examination of the standards relative to radial tires.

The study consisted initially of development of a tire heating model, since a relationship was believed to exist between heating and tire failure. Then, a series of dynamometer and flight tests were performed to validate the model. Subsequently, attempts were made to relate tire failure to distance and load, since both result in heating. These attempts were inconclusive, but there was some evidence that time at temperature might be the dominant factor. Consequently, an experimental study was undertaken, based on operational profiles of tires in three classes of service on aircraft (short, intermediate, and long haul), which demonstrated a dependence of ply adhesion on time at temperature. The data obtained suggest a finite safe upper limit of service life of tires depending on the class of service.

# INTRODUCTION

## PURPOSE.

The FAA has the responsibility to insure the continued airworthiness of aircraft tires. It does so by certifying that new tires meet certain performance standards under TSO C62-c; by performing surveillance of repair stations under FAR Part 139; and by reviewing process specifications and maintenance, repair, and retreading procedures of repair stations licensed to carry out repairs of aircraft tires. The document which addresses maintenance, repair and retreading of aircraft tires is AC 145-4.

Recently, TSO C62-c and AC 145-4 were both upgraded to reflect the increased demands imposed by widebody aircraft in the commercial fleet. In addition to TSO C62-c and AC 145-4 test requirements, airframe manufacturers, airline operators, and aircraft tire manufacturers are devising different tests to increase the assurance that tires will perform their function with a reduced probability of failure. Some airlines rely on inspections to determine when a tire should be removed from service and others have set up policy regarding the arbitrary number of retreads permitted before the tire is removed from service (some examples are none, five, and seven). The tests, inspections, and retread policies, while in the direction of increasing tire safety, do not directly provide a measure of the actual service life of a tire. The objective of this work is to develop an appropriate procedure for assuring the continued airworthiness of aircraft tires. To do so, it is necessary to determine the type of service tires encounter over their life and the damage this service imposes.

## BACKGROUND.

The service life of tires is influenced by a number of environmental factors such as loading, carcass temperature, roll distance, contained gas pressure, foreign object damage, runway crown, and ground maneuvers. While foreign object damage cannot be accounted for in an analysis of the fatigue life of a tire, but rather is an inspectable item, the other listed factors can be represented in estimating the service life of tires. One way to accomplish the representation is to define the ground taxi history for airplanes having certain missions.

For instance, long range airplanes would be characterized by high loads during takeoff taxi. The long flight will cool the tire very close to ambient; thus the tire will be at an extremely low temperature at touchdown and carcass temperature most likely will not be of concern during rollout, braking, and subsequent taxi. On the other hand, airplanes that are used on short haul flights (less than an hour) are usually on the ground for very short periods of time (about one half hour). The temperature of the tire carcass does not have sufficient time to cool to ambient and will sequentially increase in temperature as each flight is made, as illustrated in figure 1.
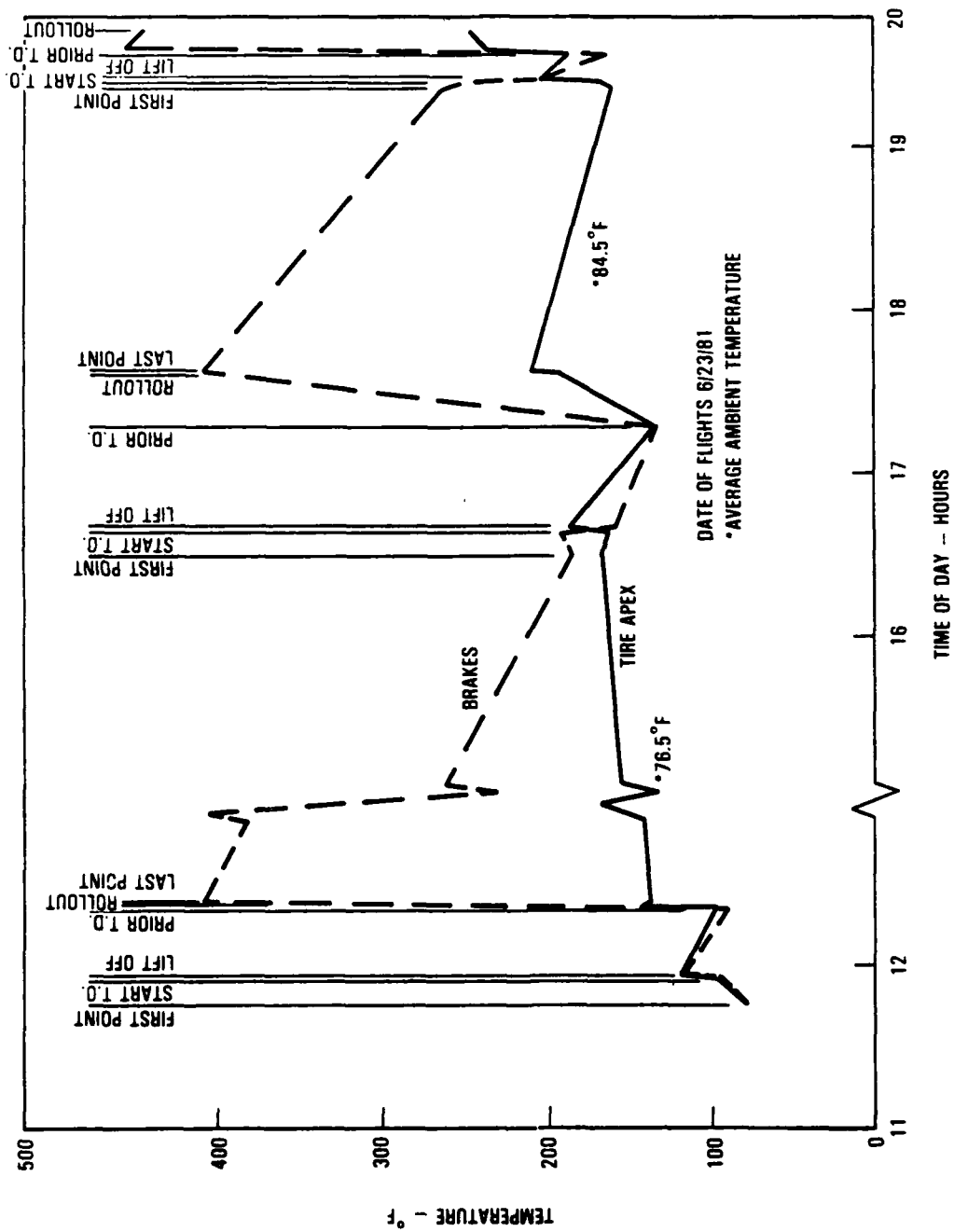
FIGURE 1. TEMPERATURE HISTORY, TIRE APEX AND BRAKES

2

In actuality, transport airplanes fall into three categories: short haul, medium range, and long range. By defining a set of missions for each category in much the same manner as used for developing an airframe structural fatigue spectrum, a representative tire usage can be developed. These tire spectra, for each of the categories, will provide a series of loadings and roll distances which represent tire experience on a flight-by-flight basis. However, if the spectra are applied as tests, the test calendar time will be prohibitive, the predominant pacing function being the time to cool the tires in between simulated flights. Accordingly, some method is needed to reduce the number of test runs similar to that of the S-N curves used in some fatigue tests of metal structures. To obtain such a curve, the relationship of the loading to the number of cycles to failure is needed for tires.

However, since there is evidence that tire heat will alter the number of flexural cycles that a tire can withstand, the problem of defining tire fatigue for use in developing a practical tire test regime will have to account for temperature as well as flexural cyclic loading. This project has developed a method for obtaining tire fatigue curves using practical testing times and loads, and taking into account the effects of temperature. The curves can then be used for simulating actual operations.

Lateral loads, while occurring in only about 5 percent of a typical taxi operation, impose increased forces on the tire which add to its rate of fatigue degradation. The larger lateral loads are normally encountered in airplanes equipped with multi-wheeled tandem-type landing gears because the wheels cannot caster in a turn. The stresses imposed by lateral loads in tires have been accounted for in this project in a manner similar to the process which has been developed in metal fatigue studies; i.e., resulting stresses from combined loads are resolved into equivalent stresses. During the testing, a system of equivalent axial loads was developed which gives fatigue effects similar to a given series of lateral loads.

In addition to the self-generated heat produced by tires, other potential heat factors that can influence tire carcass temperatures are the heat developed by rolling friction, brakes, ambient temperature and cooling developed by the motion of air over the tire. Because rubber is a very poor conductor of heat, the temperature of the tire will not immediately react thermally to external sources of heating or cooling. Therefore, in developing an analytical model of the tire heat experience, exposure time is important. The analytical model was developed to support the production of the scenarios. The importance of brake heat on carcass heat depends on the efficiency of the heat shield as well as the amount and severity of the braking.

Inasmuch as it is difficult to obtain carcass temperatures during actual service operations, it has been necessary to obtain data through instrumented flight testing simulating a typical service flight, through instrumented dynamometer tests, and through contributions of measured data from previous flights and dynamometer tests.

3

PROGRAM SCOPE.

Figure 2 is a flowchart depicting the interrelationships of tasks aimed first at finding the rate of degradation of a tire with service, and then determining the point at which airworthiness falls below an acceptable limit.

Initially, a typical operating profile was determined for each of three classes of service: short, intermediate, and long haul. Next, a model was developed, which accounts for the various means by which fatigue is introduced into a tire. The two major degrading influences on tires are heating and the cyclic stress of rolling through the contact patch. The model, therefore, accounts for the number of cycles (revolutions) the tire experiences and the resultant heat buildup from load, speed, lateral force, and other factors. Dynamic testing was then used to confirm the ability of the model to predict the temperature rise at various points in the tire, and in particular, the hottest point. Although the testing program provided a direction for further work, it did not demonstrate an ability, unaided, to determine the upper service life of a tire from assumptions about known operating conditions. The data spread, as discussed in the upcoming section on Service Tire Remaining Life, was too great to permit rigorous prediction of tire life.

It was thus necessary to develop engineering data which could be used to predict tire safe upper service limits based on some factor, such as temperature, which is related to the severity of service the tire encounters.

Accordingly, an effort was directed at determining the long-term effects of elevated temperature on tires. If a laboratory test could be devised to quantify the degradation of some measurable parameter in a tire as a function of time at temperature, then the data could be used to determine the upper service limit on a tire based on measurement of that parameter. An excellent candidate parameter which could provide the key to the amount of exposure to fatigue is interply adhesion. This parameter is measured on all classes of aircraft tires as a part of the quality assurance provisions of FAA advisories relating to tire maintenance. AC 145-4 recommends adhesion tests of the buff line interface and the outer ply layer of the tire carcass. Adhesion tests of tire samples exposed to different temperature environments were conducted in order to determine the relationship between adhesion and time-at-temperature.

In order to determine the impact of temperature on the service life of a tire, it was necessary to establish the relationship between time-at-temperature (from the adhesion experiment) and the time-in-service, during which a tire is above a given temperature threshold from the operating profiles and test data. This relationship was established and led to a rationale for predicting an upper service limit.

## TIRE OPERATING ENVIRONMENT

### TIRE HEATING.

ANALYTICAL METHODS. Analytical predictions of tire heating are required for this study in order to supply temperature data to the tire operation scenarios developed later in this report. Tire heating is a highly complex phenomenon

4
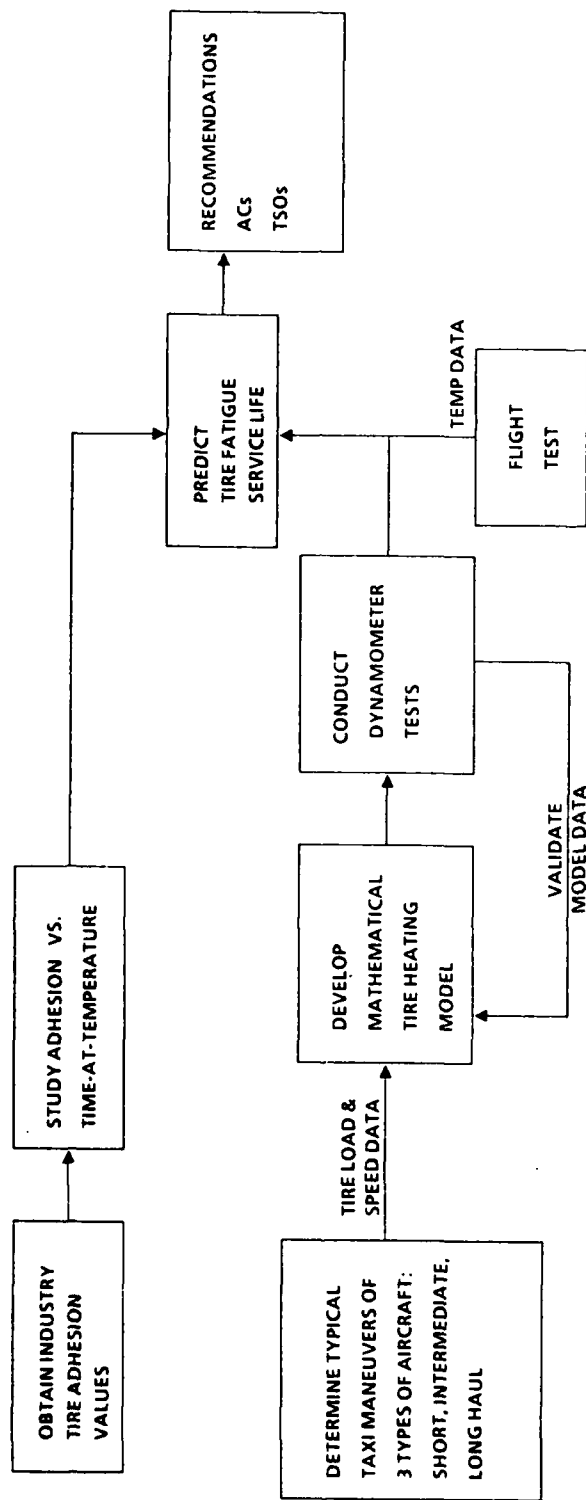
FIGURE 2. TIRE DEGRADATION AND AIRWORTHINESS FLOWCHART

5

involving hysteretic losses in the cyclic stressing of the tire materials, energy input from the tread/pavement contact region, conduction within the tire structure, and convection and radiation to the surrounding air. In addition, tire heating from braking involves a complex combination of radiation, convection and conduction heat transfer mechanisms. While these problems have been treated analytically, the more successful solutions have involved fairly complex finite element models of the tire (references 1, 2) or the wheel/tire/brake assembly (reference 3). For the current study a simpler approach is desirable, in order to keep the scope of the tire-heating analysis development in proper perspective to the total program effort.

Accordingly, lumped parameter thermal models are employed, in which the spatial variation of temperature within the tire is ignored. This technique is justified because, for the aircraft tires being considered, the critical region of the tire is known by previous test and experience to be the apex region. Unpublished comprehensive dynamometer test data for 50 x 20-20 tires clearly indicate that the apex region attains the highest temperatures, averaging about 40°F higher than the shoulder region. Therefore, a complete temperature profile of the tire is not necessary; only a reasonably accurate prediction of the apex temperature rise is required. Furthermore, the low thermal conductivity of tire materials results in very little heat transfer in the direction of tread-shoulder-sidewall-apex, at any given circumferential position. These considerations lead to the tire apex heating model presented in the following section.

Tire Apex Heating Model. Figure 3 illustrates the tire apex heating model. The tire is shown broken into three sections i, j and k; any number of sections can be used. Each section behaves independently of the others, since the heat conduction between sections is essentially zero. For each section, there is an integral heat generation term $\mu$ iFV, a convective heat transfer from the tire to the surrounding air, and the time variation of the lumped thermal energy of the tire section. (The periodic heat conduction to the pavement surface for sections in contact with the pavement is not shown, since the focus of the subsequent analysis is on the apex region where such conduction does not exist.) These terms lead to the governing differential equation shown in figure 3. The closed-form solution to this equation is also shown in figure 3; the nomenclature is identified in table 1.

The input parameters $\mu_{o_i}$, $\alpha_i$, $H_i$ and $m_i$ are all representative of the ith section, and, therefore, their magnitudes depend upon how finely the tire is broken down. However, from the equations in figure 3, the parameters $T_i$ and $\Delta T_{f_i}$ involve ratios of the input data, so that the time history for $\Delta T_i$ is independent of the location of the ith section if $\mu_{o_i}$, $\alpha_i$ and $H_i$ are all proportional to $m_i$ (and $c_i$ is the same for all sections). In reality, however, the $\mu_i = \mu_{o_i} - \alpha_i T_i$ will vary with position along the meridian of the tire, with sections undergoing greater strains having larger $\mu_i$. In other words, areas of higher strain will have higher internal heat generation rates, and these will lead to higher tire temperatures.

6

$\mu_i\,FV$

$H_i\,(T_i \cdot T_a)$

$T_a$

$i$   $T_i$

$K_{ij}\,(T_i - T_j) \approx 0$

$i$   $T_j$

$k$   $T_k$

F

**DIFFERENTIAL EQUATION:**

$$m_i c_i \dot{T}_i = \mu_i FV - H_i\,(T_i - T_a)$$

**SOLUTION:**

$$\Delta T_i(t) = \Delta T_{fi}\left(1 - e^{-1/\tau i}\right)$$

$$\Delta T_{fi} = \frac{\mu_{oi}FV + H_i T_{ai}}{H_i + a_i FV} - T_{oi}$$

$$\tau_i = \frac{m_i c_i}{H_i + a_i\,FV}$$

$$\mu_i = C_V C_\delta\,(\mu_{oi} - \alpha_i T_i)$$
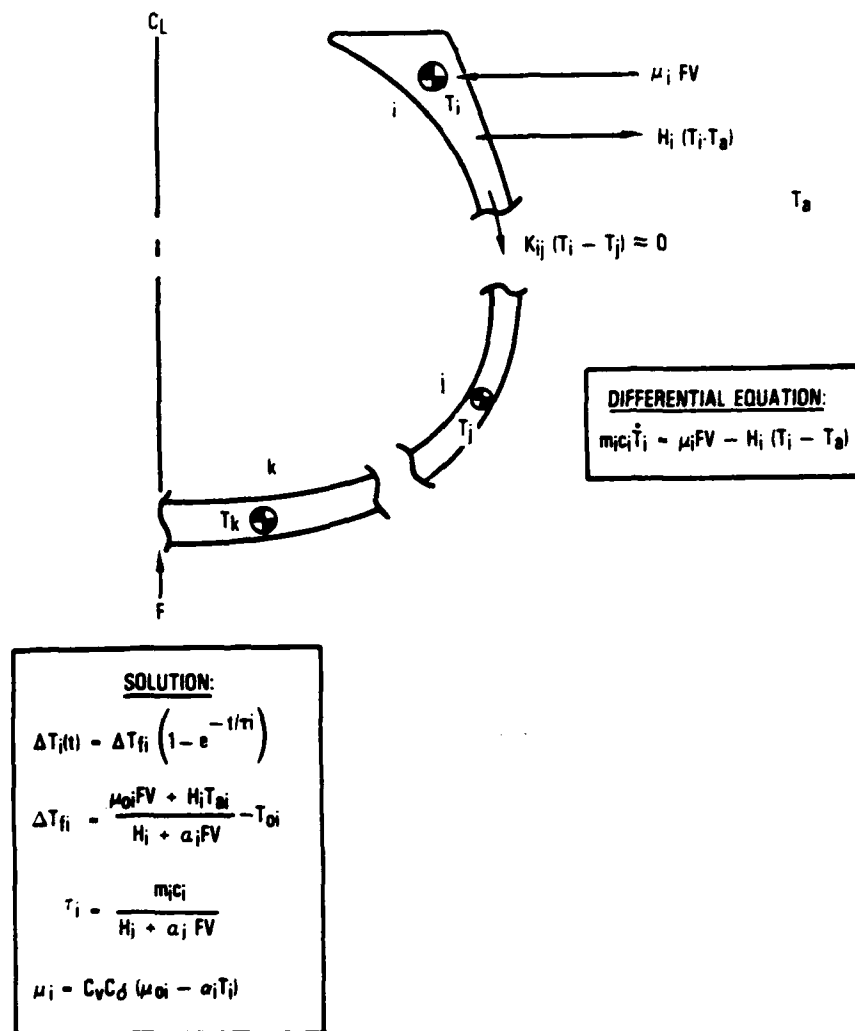
FIGURE 3.   ANALYTICAL MODEL OF TIRE HEATING DUE TO ROLLING

TABLE 1.  TERMINOLOGY FOR TIRE HEATING DUE TO ROLLING

| Quantity | Unit | Description |
|---|---|---|
| $c_i$ | $\frac{\text{Ft-pounds}}{\text{Pound} \cdot ^oF}$ | Specific heat of ith tire section (material property) |
| $C_J$ | -- | Velocity factor for $\mu_i$ |
| $C_\Delta$ | - | Tire deflection factor for $\mu_i$ |
| F | Pounds | Total tire vertical load |
| $H_i$ | $\frac{\text{Ft-pounds}}{^oF \text{ sec}}$ | Convective heat transfer coefficient for ith tire section |
| $m_i$ | Pounds | Weight of the ith tire section |
| t | Sec | Time |
| $T_a$ | $^oF$ | Ambient air temperature |
| $\Delta T_i(t)$ | $^oF$ | Time varying temperature of ith tire section, relative to the initial temperature $T_{0_i}$ |
| $\Delta T_{f_i}$ | $^oF$ | Final steady state temperature of ith tire section, relative to the initial temperature $T_{0_i}$ |
| $T_{0_i}$ | $^oF$ | Initial temperature of ith tire section |
| V | Ft/sec | Tire rolling velocity |
| $\tau_i$ | sec | Time constant of ith section |
| $\mu_i$ | — | Portion of total rolling friction coefficient yielding internal heat generation in section i |
| $\mu_{0_i}$ | — | Value of $\mu_i$ at $T_i = 0^oF$ |
| $a_i$ | $1/^oF$ | Slope of $\mu_i$ vs $T_i$ curve |

All the input parameters in table 1 can be calculated in a straightforward fashion except for $\mu_i$.  This is a complex function of the tire construction, materials, tire deflection (or vertical load and inflation pressure), and rolling velocity.  The following qualitative observations on the nature of $\mu_i$ can be made.

$\mu_i$ depends upon the local strain and strain rate, with higher strains and strain rates yielding higher $\mu_i$.

Higher strains result from larger tire deflections.

Higher cyclic frequency of strain applications results from higher velocities for a given load.

$\mu_i$ decreases with temperature, which reflects the variation with temperature of the loss factor of viscoelastic materials typical of tire construction.

8

$\mu_i$ is dependent on the mass of the ith section relative to the total tire mass. This is true because the summation of all the $\mu_i$ over the tire is equal to the total rolling friction coefficient, $\mu$. Therefore, the more finely the tire is broken down into sections for analysis, the lower the $\mu_i$ for each section.

It is assumed that the above factors can be simulated analytically by employing the empirical factors $C_v$ and $C_\delta$ in the equation for $\mu_i$ (figure 3). The parameters $\mu_o$ and $\alpha$ (dropping the subscript i, since the present study is focusing only on the tire apex region), as well as $C_v$ and $C_\delta$ are determined from experimental tire test data. Figures 4 and 5 show the resulting curves for the dimensionless factors $C_v$ and $C_\delta$. The experimentally determined values for $\mu_o$ and $\alpha$ are:

$$\mu_o = 0.01432 \text{ (dimensionless)}$$

$$\alpha = 22.58 \times 10-6 \ 1/°F$$

The experimental data used to derive the empirical parameters, $\mu_o$, $\alpha$, $C_v$ and $C_\delta$ consist of dynamometer tests of 50 x 20 - 20 tires performed at Wright-Patterson Air Force Base and at Goodyear. The applicability of the parameters to other tire sizes is unknown. The test results and correlation with analytical results, using the model just described, are presented in an upcoming section.

Contained Air Heating Model. Figure 6 shows the lumped thermal model used to calculate the time history of contained air temperature. Table 2 defines the nomenclature used in figure 6. In this model the contained air is heated by convection from the tire and cooled by convection to the wheel. The tire and wheel temperatures are not treated as unknowns in the analysis. The tire apex temperature from the analysis described in the preceeding section is used, and the wheel temperature is assumed constant. The first assumption is acceptable because only a tiny fraction (less than 0.2 percent) of the energy generated in the tire apex is required to heat the contained air. Therefore, the cooling effect on the tire apex of heat transfer to the contained air can be ignored. Similarly, the assumption of constant wheel temperature (in the absence of braking) is reasonable since the thermal inertia of the wheel is on the order of 33 times thermal inertia of the contained air. Also, the wheel can reject heat to the atmosphere to balance the heat input from the contained air (and tire apex via conduction). Although the contained air is heated by the entire inner surface of the tire, the apex temperature is used as a characteristic temperature of the whole tire. The model parameters are then determined empirically to obtain the best fit with test data.

The same dynamometer test data used to determine the apex heating parameters are used to determine one of the parameters in the contained air model. The parameter $\gamma$, which is the ratio of the tire-to-air convective heat transfer coefficient to the sum of the tire-to-air plus air-to-wheel coefficients, is chosen to provide the best fit of the test data. The mass of contained air is

9
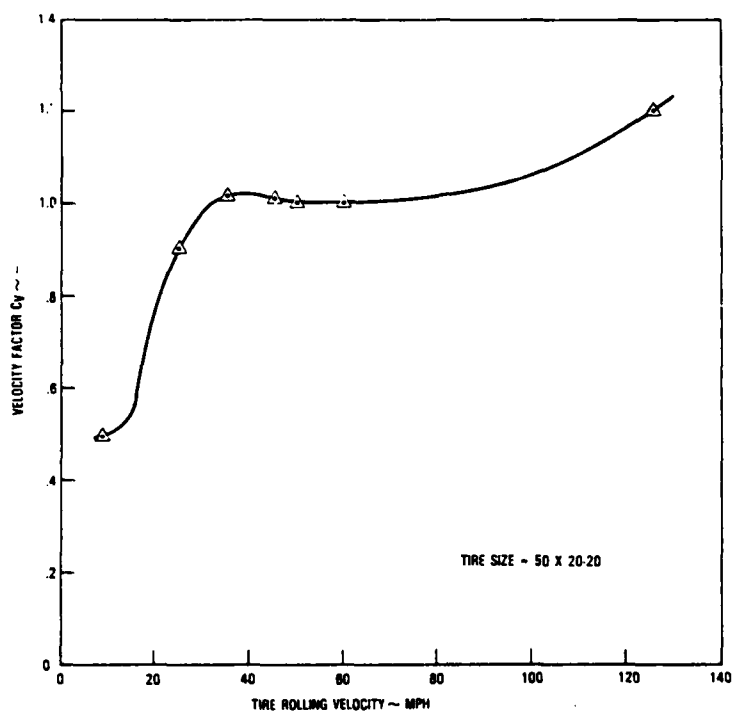
FIGURE 4.   VELOCITY FACTOR, TIRE APEX HEATING MODEL
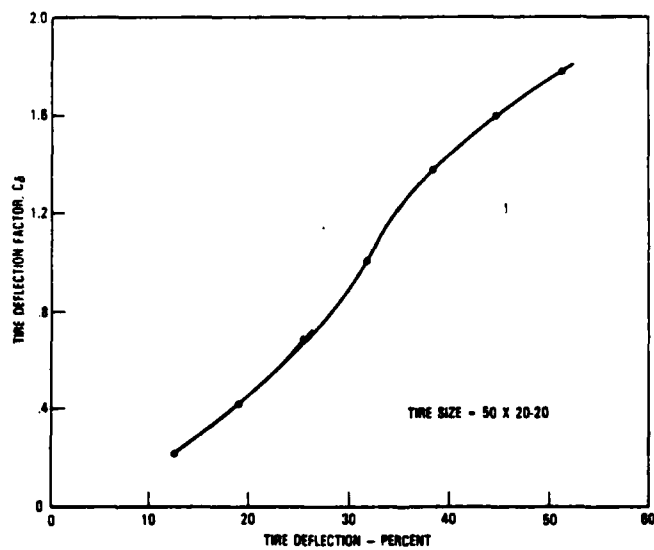


FIGURE 5.   TIRE DEFLECTION FACTOR, TIRE APEX HEATING MODEL
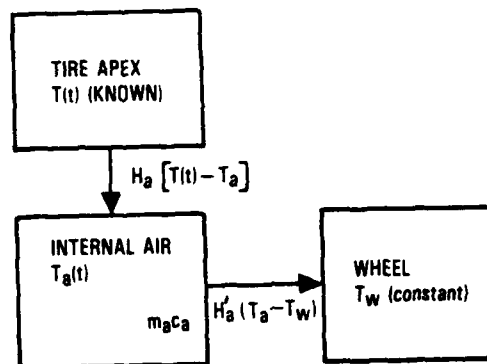
10

FIGURE 6. ANALYTICAL MODEL OF CONTAINED AIR HEATING

TABLE 2.   TERMINOLOGY FOR CONTAINED AIR HEATING

| Quantity | Unit | Description |
|---|---|---|
| $c_a$ | $\dfrac{\text{Ft-pounds}}{\text{Pound-}^\circ\text{F}}$ | Specific heat of contained air, constant volume |
| $H_a$ | $\dfrac{\text{Ft-Pounds}}{^\circ\text{F-Sec}}$ | Convective heat transfer coefficient, tire to contained air |
| $H_a'$ | $\dfrac{\text{Ft-Pounds}}{^\circ\text{F-Sec}}$ | Convective heat transfer coefficient, contained air to wheel |
| $m_a$ | Pounds | Weight of contained air |
| $\Delta T_a$ | $\text{F}^\circ$ | Time varying contained air temperature, relative to initial contained air temperature |
| $T_{ao}$ | $^\circ\text{F}$ | Initial contained air temperature |
| $T_0$ | $^\circ\text{F}$ | Initial apex temperature |
| $\Delta T_f$ | $^\circ\text{F}$ | Final steady state apex temperature, relative to initial apex temperature $T_0$ |
| $T_W$ | $^\circ\text{F}$ | Constant wheel temperature |
| $\tau$ | Sec | Time constant for tire apex section |
| $\tau_a$ | Sec | Time constant for contained air |

taken as 1/3 of the total air mass, to correspond to the assumption that the tire apex region represents 1/3 of the total tire weight. This procedure yields a γ of 0.43. The tire-to-air convective heat transfer coefficient, $H_a$, is estimated using conventional procedures, and the remaining parameters ($m_a$, $c_a$) can be readily calculated. The degree of correlation between test and analytical results is discussed in an upcoming section.

The closed-form solutions for the tire apex and contained air temperatures require that the velocity be constant. For accelerated takeoffs or decelerated landing rollouts, the continuous velocity variation can be represented by a series of constant velocity steps. The calculated final temperature from one step is used as the initial temperature for the following step. Alternatively, numerical integration can be used to directly integrate the governing equations of motion.

> Brake Heating Model. The contribution of brake heating during the landing rollout in negligible until after the airplace comes to a stop, since the tire conduction is so low that the heat generated within the brakes takes a long time to increase the tire temerature. This conveniently allows the calculations of tire temperature rise during and after landing rollout to be separated into two phases.

- Tire heating due to internally generated heat during the landing rollout until the airplace stops, or braking ceases.

- Subsequent fire heating during the brake cool-down phase with the airplace stopped or taxiing at low speed.

The first effect is handled with the equations in figure 3, and the second effect is handled with a separate analysis described in this section.

This phase of the analysis focuses on the transfer of heat from a brake at high temperature to a tire which is either stopped or still rolling at low speed. During this phase there is no energy input to the brakes, since brake application has ceased, but there may be energy input to the tire if it is still rolling. In its simplest form, this problem can be solved with the analytical model shown in figure 7. This model employs only two lumped thermal masses, representing the brake heat sink and the tire. In this case, the tire refers to the tire apex section, since portions of the tire farther removed from the rim will undergo lesser temperature rise due to transfer of brake heat. The brake heat sink is initially at a much higher temperature than the tire, and during brake cool-down heat is transferred to the tire via conduction and radiation to the wheel and then conduction to the tire bead. Simultaneously, heat is transferred from the brake to atmosphere and from the tire to the atmosphere by convection. In addition, if the tire is rolling, internal heat is generated within the tire.

The governing differential equations for this system are:

$$m_1 c_1 \dot{T}_1 + (K + H_1) T_1 - KT_2 = H_1 T_a$$

$$m_2 c_2 \dot{T}_2 - KT_1 + (K + H_2 + \alpha FV) T_2 = H_2 T_a + \mu_o FV$$

The closed-form solution to this system of equations is shown in table 3, while table 4 defines the nomenclature. From Table 3 it can be seen that the form of the equations for $T_1$ and $T_2$ is simple, involving a steady state temperature and two decaying exponential transient terms for each mass. The time constants are proportional to $mc/H_T$, the thermal inertia divided by the total system heat transfer coefficient. The steady state temperatures for both the masses are just the ambient temperature $T_a$ for the zero velocity case, and $T_a$ plus an increment dependent on velocity for the rolling tire case.

TEST RESULTS AND CORRELATION WITH ANALYSIS. Dynamometer tests of 50 x 20-20 tires, conducted both at Wright/Patterson (WPAFB) and Goodyear, were used to determine the empirical constants in the tire apex and contained air heating models. Table 5 summarizes the test conditions for the WPAFB tests; Table 6 presents the same data for the Goodyear tests. The WPAFB tests used 34 ply rating tires with a rate load of 57,000 pounds, while the Goodyear tests were performed with 32 ply rating tires having a rated load of 53,800 pounds. Both sets of data were weighted equally in determining the empirical tire constants; i.e., the 32 and 34 ply rating tires were assumed to be identical thermally.

13

BRAKE

$T_1$
$m_1c_1$

$H_1(T_1 - T_a)$

$K(T_1 - T_2)$

$T_a$

$\mu FV$

TIRE

$T_2$
$m_2c_2$

$H_2(T_2 - T_a)$
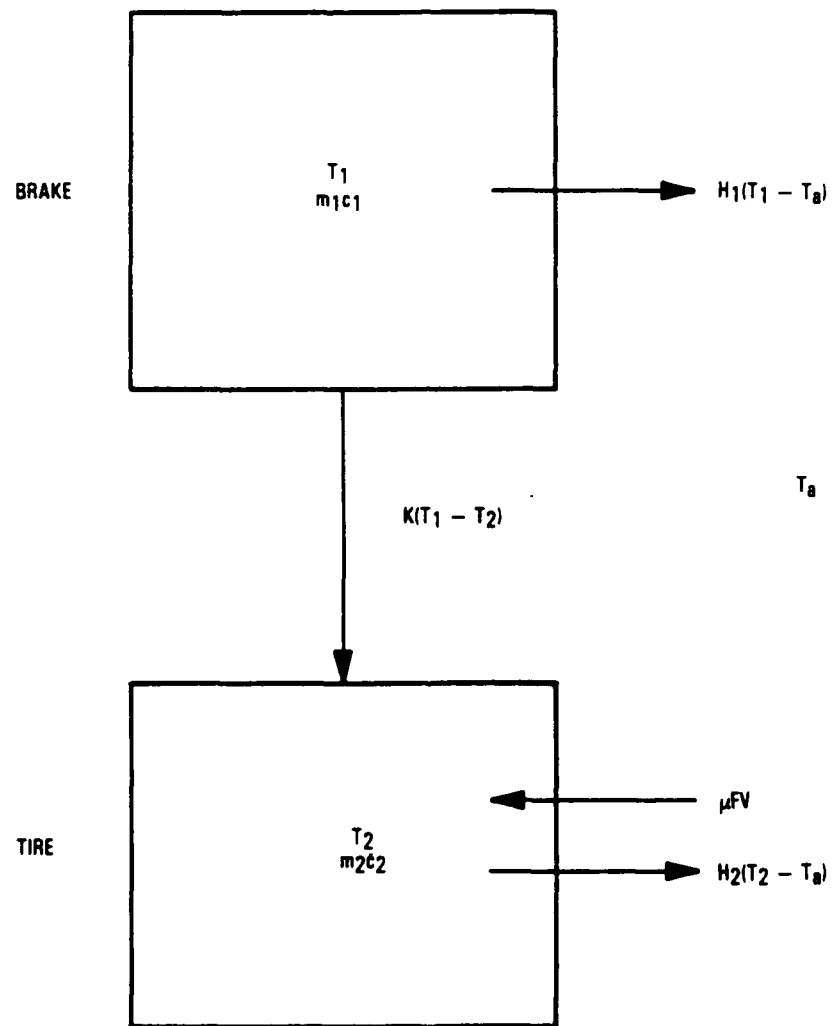
FIGURE 7. ANALYTICAL MODEL FOR TIRE HEATING DUE TO BRAKING

14

TABLE 3. EQUATIONS FOR TIRE HEATING DUE TO BRAKING

$mc \overset{\Delta}{=} m_1 c_1 + m_2 c_2$  $\qquad r' \overset{\Delta}{=} m_1 c_1 / mc$

$H \overset{\Delta}{=} H_1 + H_2'$  $\qquad r \overset{\Delta}{=} H_1 / H$  $\qquad\qquad H_2' \overset{\Delta}{=} H_2 + \alpha' FV$

$H_T \overset{\Delta}{=} K + H$  $\qquad \alpha \overset{\Delta}{=} K / H_T$

$$f = \frac{\left\{ \alpha^2 + 2\alpha(1-\alpha)\left[(r-r')\left(r(1-r')-r'\right) + (1-r)r'^2\right] + (r-r')^2(1-\alpha)^2 \right\}^{1/2}}{r'(1-r')}$$

$$g = \frac{\alpha + r(1-\alpha) + r'(2r-1)(\alpha-1)}{r'(1-r')}$$

$$F = \frac{r'f}{2\alpha} \qquad\qquad G = \frac{\alpha + r(1-\alpha) - r' \cdot g/2}{\alpha} \qquad\qquad \overline{B}_1 = G + F$$

$$\overline{B}_2 = G - F$$

$$\Delta T_{1V} = \frac{a}{(1-\alpha)\left[\alpha + r(1-r)(1-\alpha)\right]} \quad \frac{(\mu_0 - a' T_a) F'V}{H_T}$$

$$\Delta T_{2V} = \frac{\left[a + r(1-a)\right]}{(1-a)\left[a + r(1-r)(1-a)\right]} \quad \frac{(\mu_0 - a' T_a) F'V}{H_T}$$

$$\Delta T_1 = T_a - T_{10} + \Delta T_{1V}$$

$$\Delta T_2 = T_a - T_{20} + \Delta T_{2V}$$

$$C_1 = \frac{-\overline{B}_2 \, \Delta T_1 + \Delta T_2}{\overline{B}_2 - \overline{B}_1} \qquad\qquad C_2 = \frac{\overline{B}_1 \Delta T_1 - \Delta T_2}{\overline{B}_2 - \overline{B}_1}$$

$$\tau_1 = \frac{2mc}{H_T} \frac{1}{(g-f)} \qquad\qquad \tau_2 = \frac{2mc}{H_T} \frac{1}{(g+f)}$$

$$T_1(t) = T_a + \Delta T_{1V} + C_1 e^{-t/\tau_1} + C_2 e^{-t/\tau_2}$$

$$T_2(t) = T_a + \Delta T_{2V} + \overline{B}_1 C_1 e^{-t/\tau_1} + \overline{B}_2 C_2 e^{-t/\tau_2}$$

TABLE 4. NOMENCLATURE FOR TIRE HEATING DUE TO BRAKING

| Quantity | Units | Description |
|---|---|---|
| $\overline{B}_1$ | — | Nondimensional constant |
| $\overline{B}_2$ | — | Nondimensional constant |
| $C_1$ | $^oF$ | Constant for transient portion of $T_1$ |
| $C_2$ | $^oF$ | Constant for transient portion of $T_2$ |
| f | — | Nondimensional constant |
| F | — | Nondimensional constant |
| F' | Pounds | Tire vertical load |
| g | — | Nondimensional constant |
| G | — | Nondimensional constant |
| H | $\dfrac{\text{ft-pounds}}{^oF\text{-sec}}$ | Total system effective convective heat transfer coefficient |
| $H_1$ | | Convective heat transfer coefficient for brakes |
| $H_2$ | | Convective heat transfer coefficient for tires |
| $H_2'$ | | Effective convective heat transfer coefficient for tire |
| $H_T$ | | Total system heat transfer coefficient (conduction + convection) |
| K | | Conductive heat transfer coefficient between brake and tire |
| mc | ft-pound/$^oF$ | Total system thermal inertia (product of mass and specific heat) |
| $m_1c_1$ | ft-pound/$^oF$ | Thermal inertia of brake heat sink |
| $m_2c_2$ | ft-pound/$^oF$ | Thermal inertia of tire |
| r | — | Nondimensional constant |
| r' | — | Nondimensional constant |
| $T_a$ | $^oF$ | Ambient temperature |
| $T_1$ | $^oF$ | Time varying temperature of brake |
| $T_2$ | $^oF$ | Time varying temperature of tire |
| $T_{10}$ | $^oF$ | Initial temperature of brake |
| $T_{20}$ | $^oF$ | Initial temperature of tire |
| V | ft/sec. | Rolling velocity |
| $a$ | — | Nondimensional constant |
| $a'$ | 1/$^oF$ | Slope of $\mu$ vs. $T_2$ curve |
| $\Delta T_1$ | $^oF$ | Temperature change constant |
| $\Delta T_2$ | $^oF$ | Temperature change constant |
| $\Delta T_{1V}$ | $^oF$ | Temperature change increment due to rolling, brake |
| $\Delta T_{2V}$ | $^oF$ | Temperature change increment due to rolling, tire |
| $\mu$ | — | Portion of total rolling friction coefficient causing tire internal heat generation |
| $\mu_0$ | — | Value of $\mu$ at $T_2 = 0^oF$ |
| $\tau_{1,2}$ | seconds | Time constants for transient temperature response |

TABLE 5.  WRIGHT/PATTERSON DYNAMOMETER TEST CONDITIONS,
50 x 20-20 34 PR TIRES

| Radial Load Ratio | Radial Load ~ Pounds | Velocity, M.P.H. |
|---|---|---|
| 0.4 | 22,800 | 50. |
| 0.6 | 34,200 | 50 |
| 0.8 | 45,600 | 50 |
| 1.0 | 57,000 | 50. |
| 1.2 | 68,400 | 50. |
| 1.4 | 79,800 | 50 |
| 1.6 | 91,200 | 50. |
| 1.8 | 102,600 | 50. |
| 2.0 | 114,000 | 50. |
| | | |
| 1.0 | 57,000 | 10. |
| 1.0 | 57,000 | 80. |
| 1.0 | 57,000 | 130. |

Rated Load = 57,000 pounds

TABLE 6.  GOODYEAR DYNAMOMETER TEST CONDITIONS,
50 x 20-20 32 PR TIRES

| Radial Load Ratio | Radial Load ~ Pounds | Velocity, M.P.H. |
|---|---|---|
| 1.0 | 53,800 | 15 |
| 1.0 | 53,800 | 25 |
| 1.0 | 53,800 | 35 |
| 1.0 | 53,800 | 45 |
| 1.0 | 53,800 | 60 |
| | | |
| 0.84 | 45,300 | 35 |
| 0.84 | 45,300 | 35 |
| 1.00 | 53,800 | 35 |
| 1.30 | 69,940 | 35 |
| 1.60 | 86,080 | 35 |

Rated Load = 53,800 pounds

17

The final values of the empirical constants were presented in the previous section on Analytical Methods. Figures 8 through 13 show the degree of correlation obtained between test and analysis for the WPAFB dynamometer tests. These figures cover a radial load range from 34,200 pounds to 114,000 pounds, representing 0.6 to 2.0 times the rated load. All these results are at a constant velocity of 50 mph. Although the test data are used to quantify the empirical constants, there are not enough constants to allow fine-tuning each temperature time-history curve. The degree of correlation exhibited, therefore, represents the ability of the simplified theory to model all the factors that influence the apex and contained air temperatures. The load variations represented by figures 8 through 13 are used to define $C_\delta$, the variation of $\mu_0$ and with tire deflection. Overall, the degree of correlation is quite good, considering the simplicity of the analytical model. In figures 10 and 12, the test apex temperatures increase rapidly at the end. This is due to carcass separation just prior to tire failure, which leads to a rapid build-up of internal heat generation. The theory is not intended to model this rapid heat build-up. The purpose of the theory is to yield temperature data for tire operating scenarios, and normal operations involve neither carcass separation nor tire temperatures above 350°F. Therefore, the divergence of test and analytical data at such high temperatures is of no concern in the present application.

Figures 14 through 19 compare the analytical results with the Goodyear dynamometer data. Since these data cover a range of velocities from 15 to 60 mph, they are used to define $C_V$, the variation of $\mu_0$ and $\alpha$ with velocity. The initial temperature for the apex and contained air is not known for the Goodyear data. Both are assumed to be 100°F. For these cases the apex temperature correlation is good, but the contained air temperatures do not correlate as well. In particular, the rapid rise in contained air temperatures after 600 seconds in figure 15 is not matched by the theory. However, these test data are inconsistent with the other results at different velocities, so the test data may be suspect in that case. WPAFB data are also used to define $C_V$ at the velocity extremes of 10 and 130 mph.

The analytical model, employing the empirical constants developed from dynamometer test data, was used to predict the apex temperature time-histories or the 50 x 20-20 tires mounted on the L-1011 during flight testing at Palmdale. Figures 20 and 21 show the comparisons between test and analytical apex temperatures for a takeoff roll and a landing rollout, respectively. In both cases the theoretical predictions are substantially below the test data. The rate of temperature increase agrees during the middle portion of each run, but the initial test temperature build-up is much more rapid than that for the theory. Despite the poor correlation event in figures 20 and 21, the peak temperatures in each case are predicted within 15°F.

The heating of the tire apex due to brake heating does not appear to be very significant for brake temperatures resulting from normal landing rollouts. Figures 22 and 23 show time histories of the tire apex and brake sensor temperatures for two flight tests of the L-1011. At the conclusion of Flight 1701, temperature readings were taken for 30 minutes after the airplane was parked. From figure 22, it can be seen that the tire apex cools from 230 to 162°F during the "STATIC" phase from 11:16 to 11:50 AM. During this same time the brake is cooling from 570 to 450°F, yet the heat rejected by the brake does not appear to be heating the tire. It could be argued that the tire apex would have cooled at an even faster rate, had the brakes not been hot. However,

18
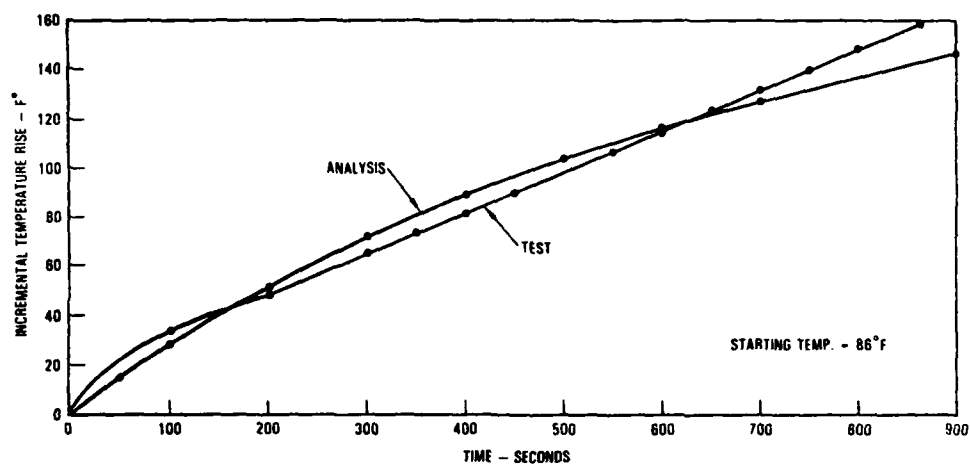
FIGURE 8. TIRE APEX TEMPERATURE RISE; VELOCITY 50 MPH, RADIAL LOAD 34,200 POUNDS
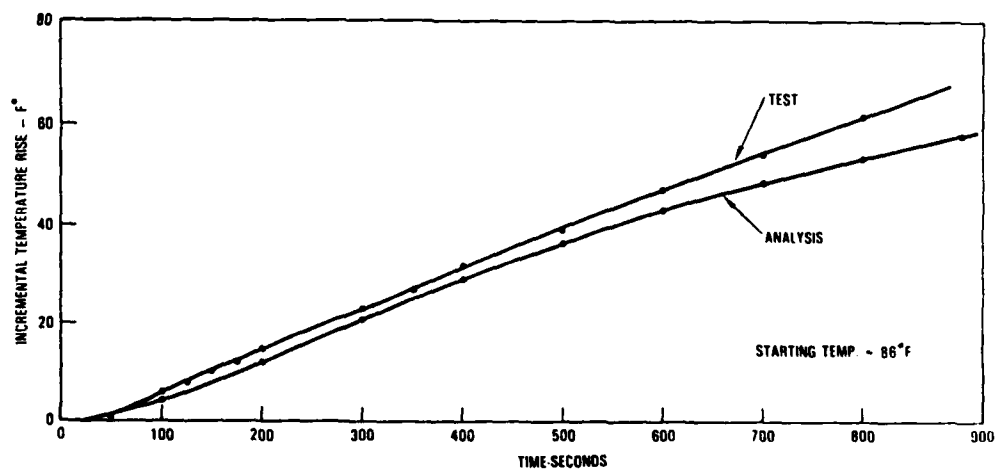


FIGURE 9. CONTAINED AIR TEMPERATURE RISE; VELOCITY 50 MPH, RADIAL LOAD 34,200 POUNDS

19
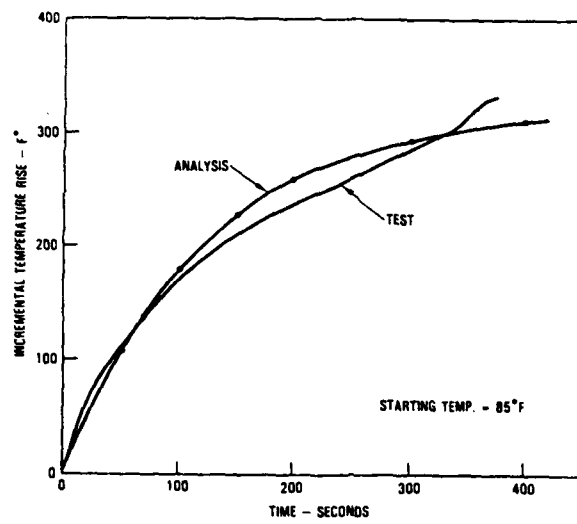
FIGURE 10. TIRE APEX TEMPERATURE RISE; VELOCITY 50 MPH,
RADIAL LOAD 79,800 POUNDS
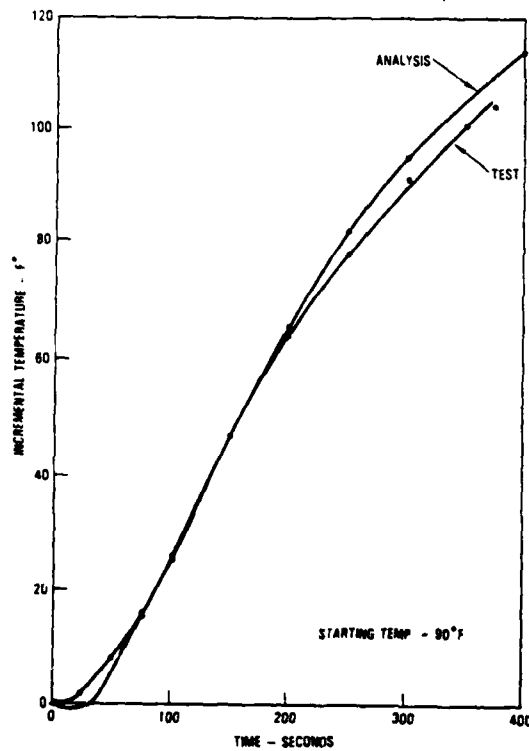


FIGURE 11. CONTAINED AIR TEMPERATURE RISE; VELOCITY 50 MPH,
RADIAL LOAD 79,800 POUNDS

20
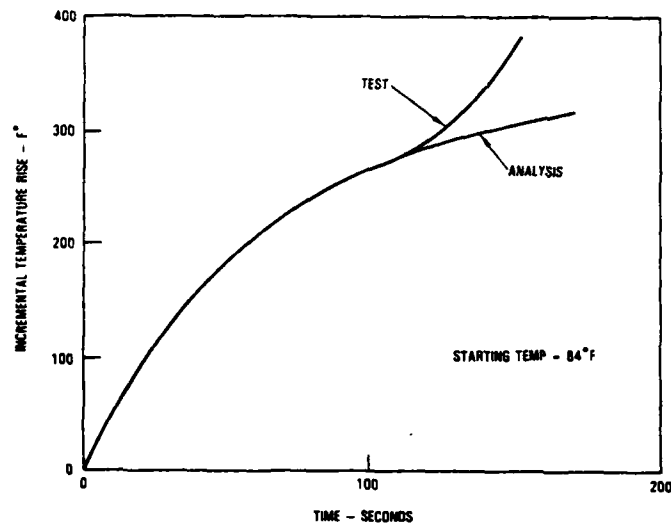
FIGURE 12. TIRE APEX TEMPERATURE RISE; VELOCITY 50 MPH,
RADIAL LOAD 114,000 POUNDS
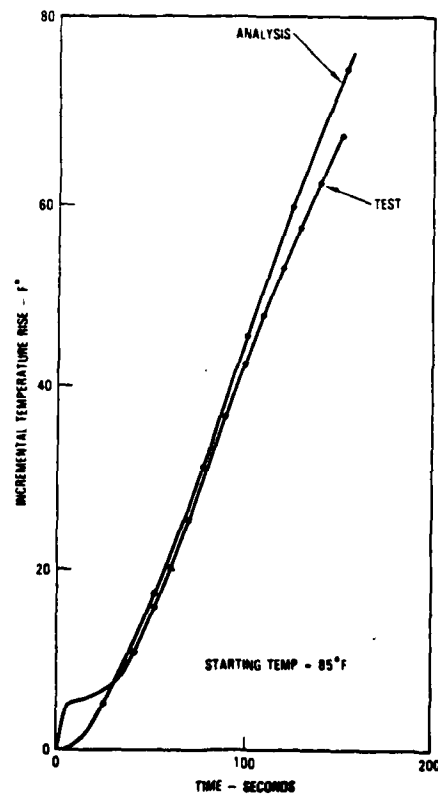


FIGURE 13. CONTAINED AIR TEMPERATURE RISE; VELOCITY 50 MPH,
RADIAL LOAD 114,000 POUNDS

21
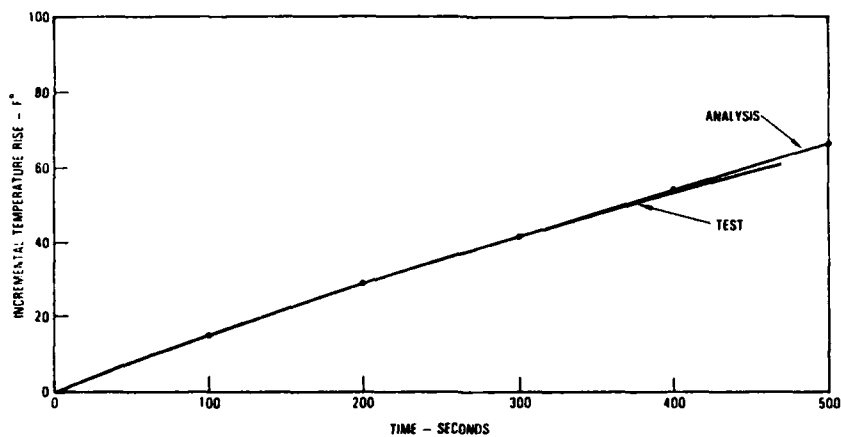
FIGURE 14.   TIRE APEX TEMPERATURE RISE; VELOCITY 15 MPH, RADIAL LOAD 53,800 POUNDS
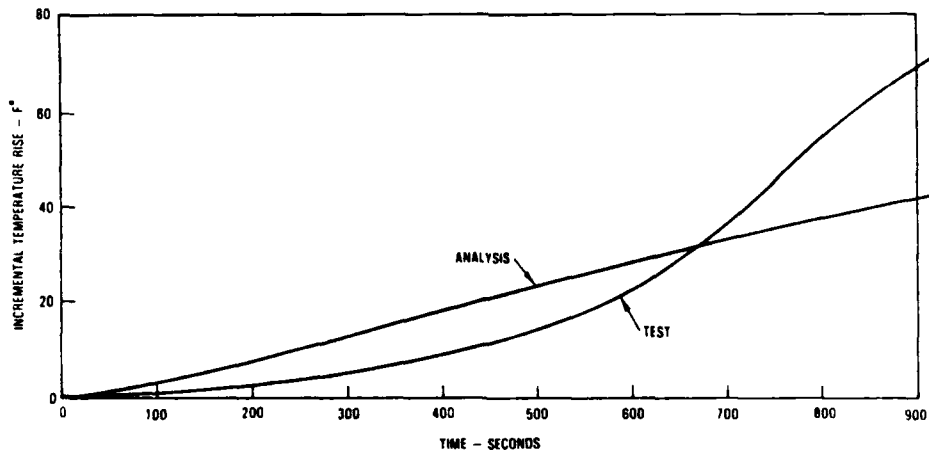


FIGURE 15.   CONTAINED AIR TEMPERATURE RISE; VELOCITY 15 MPH, RADIAL LOAD 53,800 POUNDS
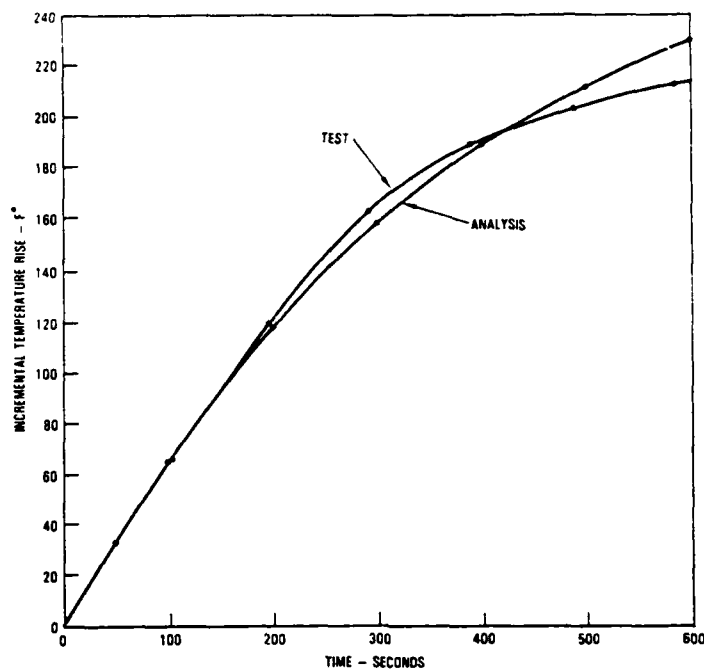
FIGURE 16. TIRE APEX TEMPERATURE RISE; VELOCITY 35 MPH,
RADIAL LOAD 53,800 POUNDS
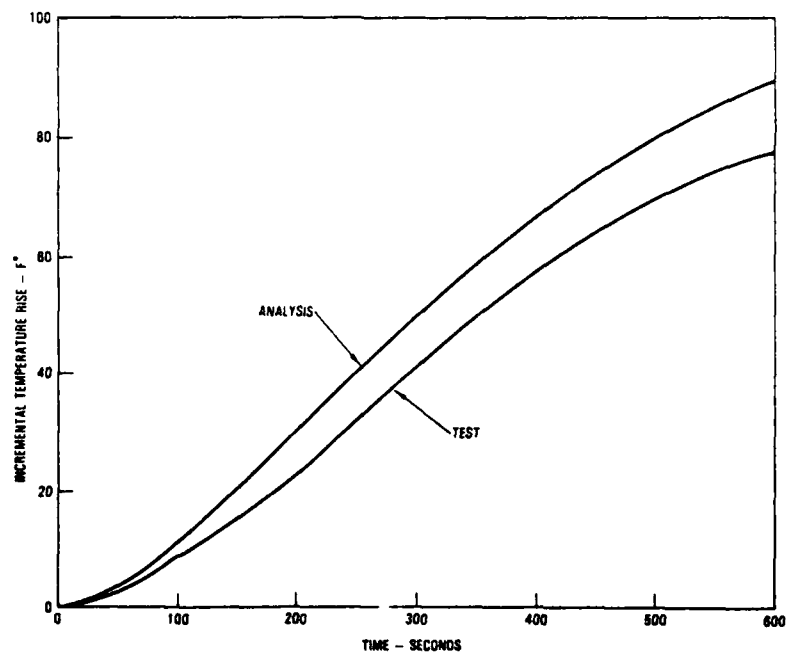


FIGURE 17. CONTAINED AIR TEMPERATURE RISE; VELOCITY 35 MPH,
RADIAL LOAD 53,800 POUNDS
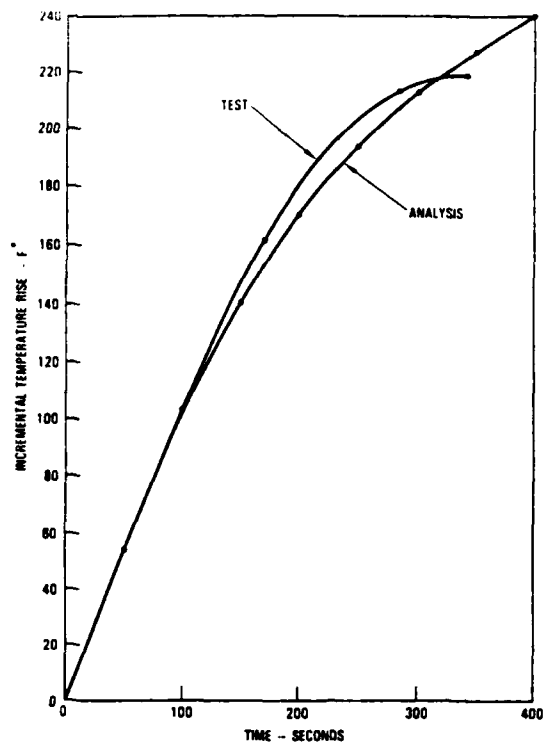
FIGURE 18. TIRE APEX TEMPERATURE RISE; VELOCITY 60 MPH, RADIAL LOAD 53,800 POUNDS
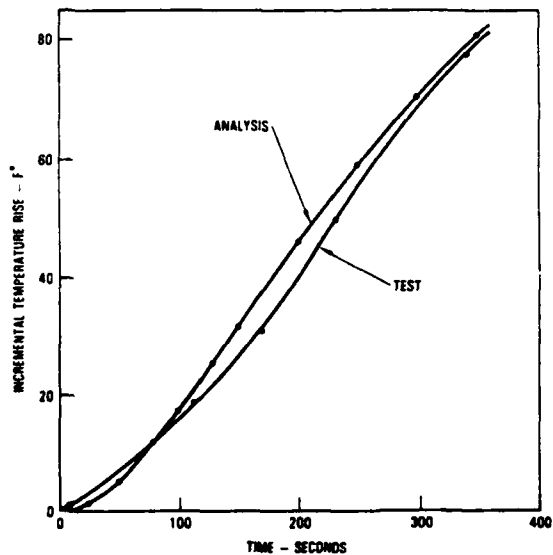


FIGURE 19. CONTAINED AIR TEMPERATURE RISE; VELOCITY 60 MPH, RADIAL LOAD 53,800 POUNDS
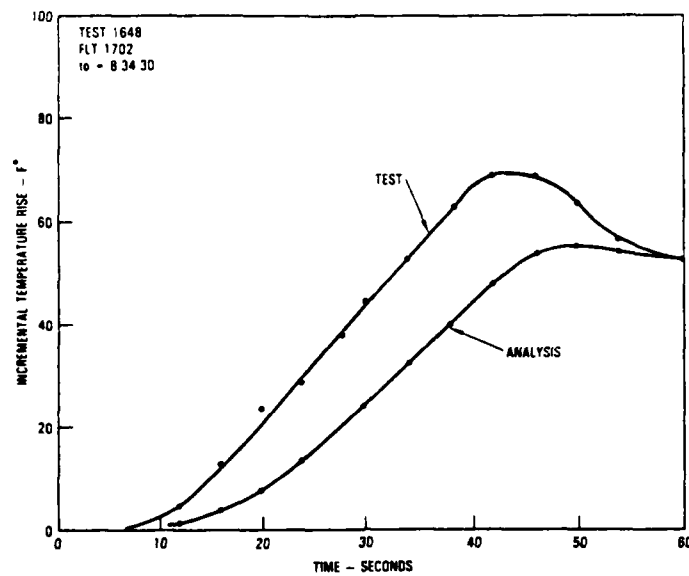
FIGURE 20. TIRE APEX TEMPERATURE RISE, TAKEOFF ROLL
STARTING TEMPERATURE 114.8°F
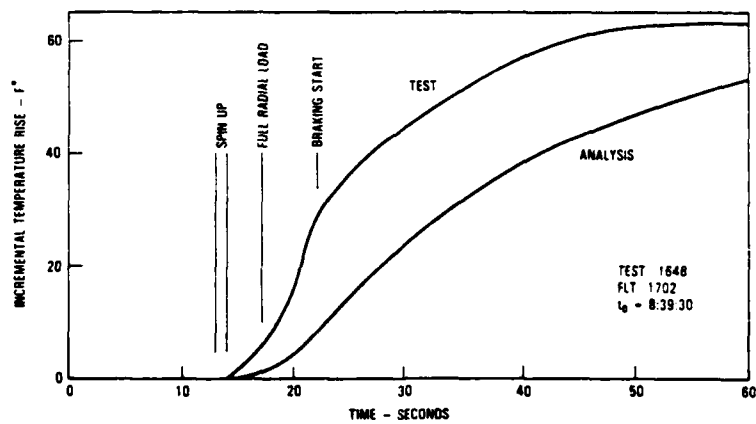


FIGURE 21. TIRE APEX TEMPERATURE RISE, LANDING ROLL OUT;
STARTING TEMPERATURE 140°F

25
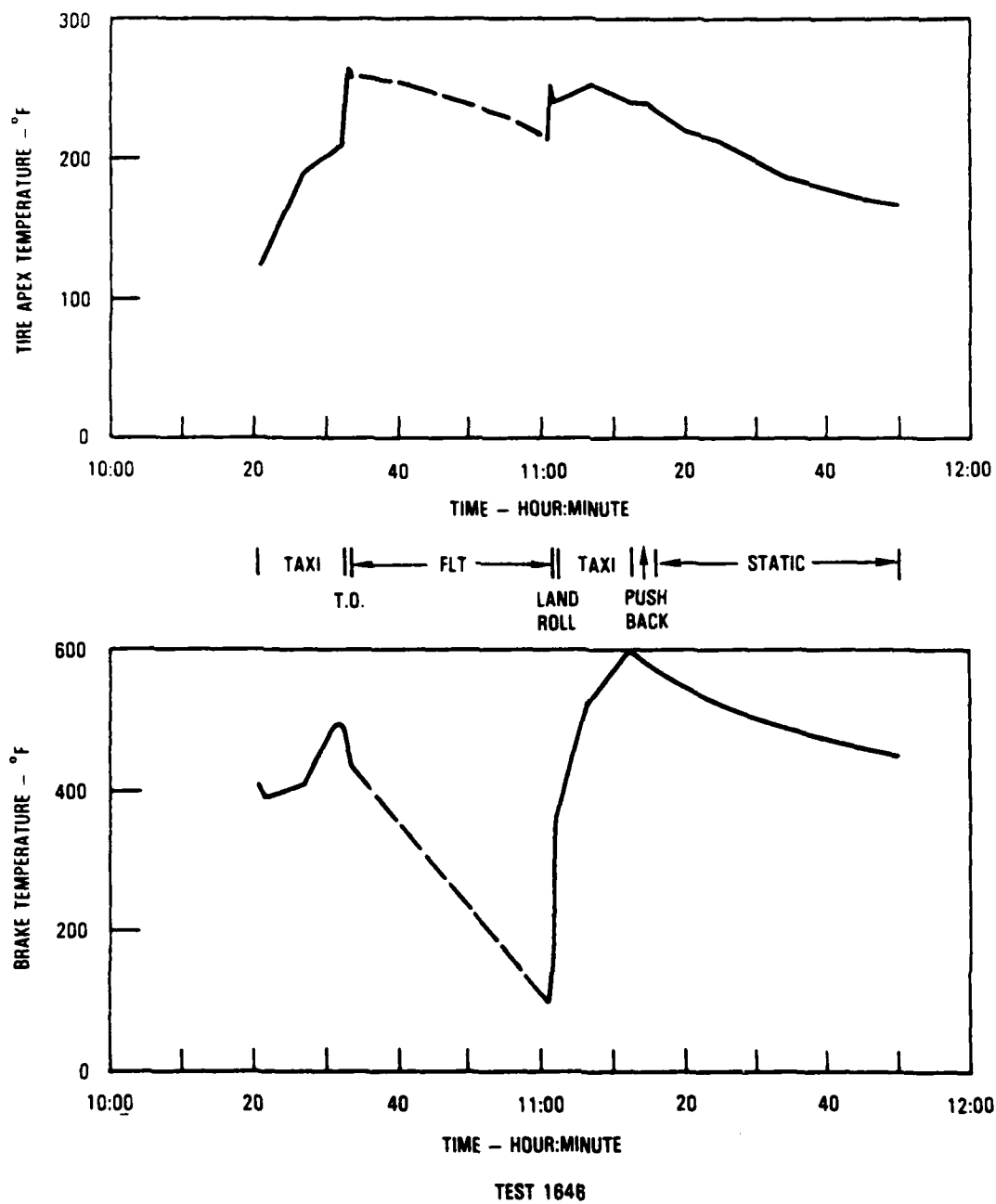
FIGURE 22. TIRE AND BRAKE TEMPERATURES, FLIGHT 1701, 5/29/81

26
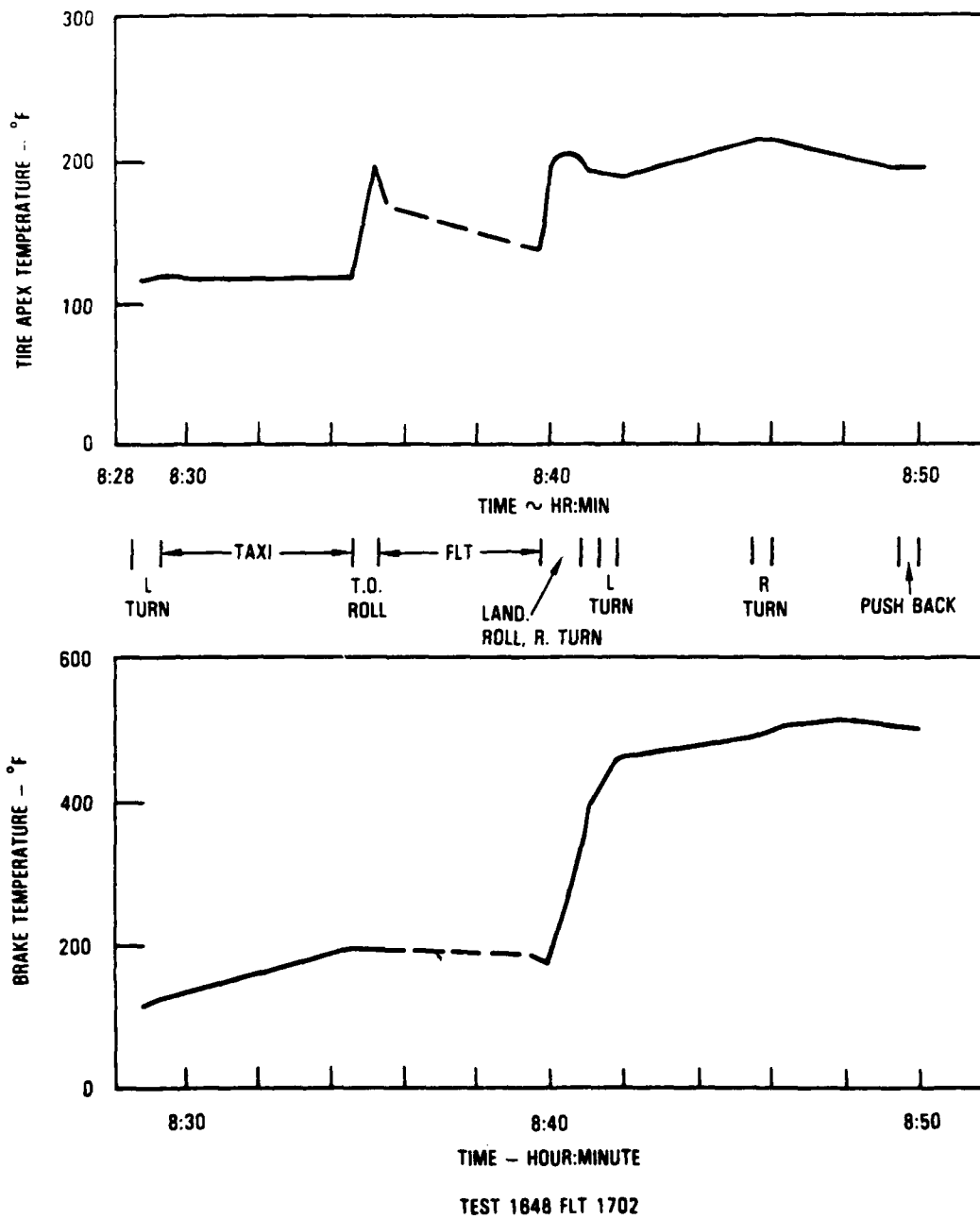
FIGURE 23. TIRE AND BRAKE TEMPERATURES, FLIGHT 1702, 5/29/81

27

analysis of static cooldown, using the tire apex heating model which correlates well with dynamometer test data, indicates that the apex cooling rate shown in figure 22 is greater (not less) than the model would predict for zero airflow over the tire. The convective heat transfer coefficient is strongly dependent on the velocity of airflow over the tire. The apex cooldown rate shown in figure 22 can be duplicated analytically by assuming an airflow of approximately five miles per hour over the tire. Unfortunately, surface wind was not monitored during the flight test, but a five miles per hour wind would not be unusual.

What the test data seem to indicate is that the tire cooling rate is on the order of what would be expected with no heat input from the brake. Furthermore, the apex temperature rise during taxiing and takeoff for Flight 1701 can be duplicated within about $\pm 5$ degrees with the apex heating analytical model. The tire apex temperature variations in figure 23 Flight 1702 are also about what would be predicted due to tire rolling, without any heat input from the brakes.

Figure 24 shows additional detail of temperature variations during the landing rollout, taxi and cooldown phases of Flight 1701. It is interesting to note that there is a significant difference between the temperatures of the inner and outer sides of the wheel. The brake is within the inner side of the wheel, which therefore gets considerably hotter than does the outer side of the wheel due to heat transfer from the brake. The inner side of the tire apex temperature is also higher than the outer side apex temperature; however, the difference that existed prior to touchdown remains virtually constant during rollout, taxi and static cooldown.

It seems clear that a considerably more elaborate analytical model than the two-mass system shown in figure 7 would be required to accurately simulate the type of behavior evident in figure 24. However, since the effect of brake heating on tire apex temperature seems to be minor compared to tire heating due to rolling, no attempt was made to develop a more sophisticated brake heating model.

The L-1011 incorporates a heat shield between the brakes and the wheel, to reduce the amount of heat transfer between the brake stack and the inner side of the wheel. An airplane without such a shield may exhibit significant tire heating due to braking. For the L-1011 however, only a rejected takeoff at high gross weight would heat the brakes enough to provide a significant heat input to the tires.

     SCENARIO APPLICATION FORMAT. Appendix A provides a step-by-step procedure for the application of the tire apex and gas heating equations to tire operation scenarios.

TIRE OPERATION SCENARIOS.

     Scenarios are a prerequisite for developing tire qualification test spectra for the long range, medium range and short haul transport airplanes. The scenarios presented are developed using typical mission mixes for operations from a representative airport which is a composite of several airports.
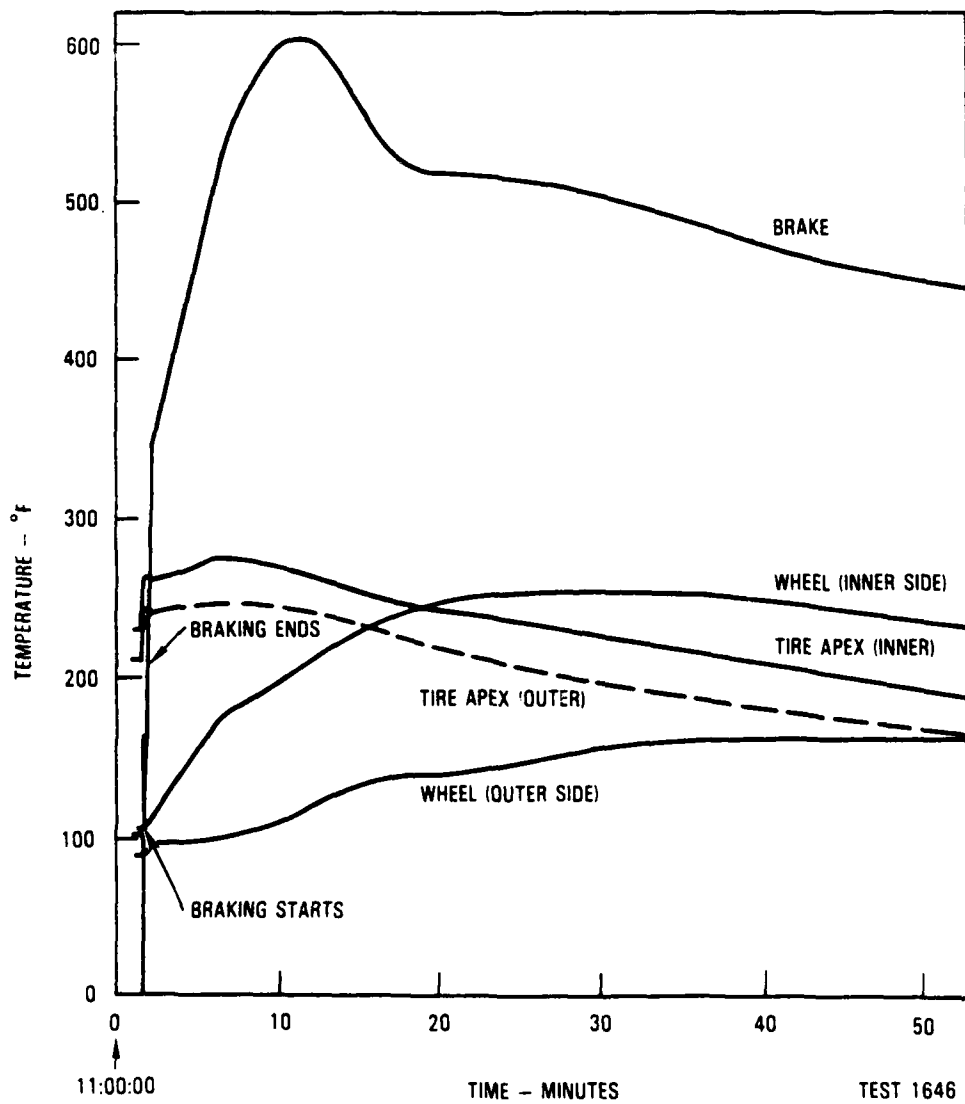
FIGURE 24.  BRAKE, WHEEL AND TIRE TEMPERATURES, FLIGHT 1702, 5/29/81

CHARACTERISTICS OF A REPRESENTATIVE AIRPORT. Table 7 presents most of the salient airport ground operations characteristics (see reference 4) affecting the tires during ground operations and is used in developing the scenarios. Runway crown, which influences the load distribution on multi-wheeled landing gears, is accounted for as a discrete input to tire loads where appropriate.

The average taxi distances for takeoffs and landings and the average turns encountered during these operations are used in the scenarios. A thirty-five foot radius turn is added at the end of the landing sequence to account for tight turns that may occur during close towing maneuvers.

TABLE 7. REPRESENTATIVE AIRPORT GROUND OPERATIONS CHARACTERISTICS

| | Takeoff | | | | Landing | | | |
|---|---|---|---|---|---|---|---|---|
| | | No. of Turns | | | | No. of Turns | | |
| | | Radius — Feet | | | | Radius — Feet | | |
| Airport | Taxi Distance Feet | 65 | 90 | 150 | Taxi Distance Feet | 65 | 90 | 150 |
| San Francisco International | 10,220 | 1 | 2 | 3 | 8,540 | 1 | 1 | 3 |
| John F. Kennedy International | 15,520 | 2 | 1 | 2 | 14,840 | 1 | 1 | 3 |
| Dulles International | 13,850 | 2 | 1 | 0 | 11,720 | 1 | 1 | 1 |
| O'Hare International | 15,920 | 2 | 1 | 2 | 11,060 | 2 | 1 | 2 |
| Honolulu International | 13,080 | 1 | 1 | 2 | 12,600 | 2 | 1 | 2 |
| Los Angeles International | 12,300 | 1 | 2 | 3 | 9,160 | 1 | 1 | 4 |
| Average All Airports | 13,500 | 2 | 2 | 2 | 11,300 | 1 | 1 | 2 |

AIRPLANE MISSION MIXES. The mission mixes are a composite of predicted flights by potential operators condensed to provide a means by which representative loadings can be established for the life of the airplane. Tables 8, 9 and 10 provide the mission mixes for the long range, medium range and short haul transport category of airplanes. Training flights are represented by only a small number of flights and have been combined with missions closest in weight to reduce the number of scenarios.

The short haul flights are sequential with no refueling in between flights and a stopover time for off load and on load of passengers of approximately thirty minutes.

## TABLE 8. MISSION MIX, LONG RANGE

| Non-Dimensional Weight | | Percent of Flights | Flight Time Hours |
|---|---|---|---|
| Takeoff | Landing | | |
| 0.940 | 0.611 | 5.2 | 9.4 |
| 0.846 | 0.616 | 17.4 | 6.8 |
| 0.818 | 0.690 | 12.2 | 3.6 |
| 0.736 | 0.615 | 12.2 | 3.6 |
| 0.729 | 0.690 | 26.5 | 1.0 |
| 0.652 | 0.615 | 26.5 | 1.0 |

## TABLE 9. MISSION MIX, MEDIUM RANGE

| Non-Dimensional Weight | | Percent of Flights | Flight Time Hours |
|---|---|---|---|
| Takeoff | Landing | | |
| 0.958 | 0.711 | 15.2 | 5.6 |
| 0.900 | 0.808 | 10.9 | 1.9 |
| 0.847 | 0.808 | 30.2 | 0.6 |
| 0.787 | 0.704 | 10.4 | 1.9 |
| 0.745 | 0.708 | 33.3 | 0.6 |

## TABLE 10. MISSION MIX, SHORT HAUL

| Non-Dimensional Weight | | Percent of Flights | Flight Time Minutes |
|---|---|---|---|
| Takeoff | Landing | | |
| 0.916 | 0.871 | 20 | 60 |
| 0.865 | 0.834 | 20 | 45 |
| 0.820 | 0.798 | 20 | 45 |
| 0.792 | 0.747 | 20 | 60 |
| 0.741 | 0.711 | 20 | 45 |

31

TAXI SCENARIOS.  The data for the representative airport were used to establish distances traveled, number of tire revolutions, and time for takeoff and landing taxi operations for each of the categories of airplanes.  The taxi speeds used are best estimates and vary depending upon the pilot.  Tire loads are calculated using the weight of the airplane from the mission mixes and an algorithm which provides wheel loads during ground maneuvers including runway crown effects.  Tire apex temperature includes tire generated and brake heat. Tire pressure is a function of the contained gas, temperature which is influenced by the tire apex temperature and time.  Temperatures are adjusted for landing depending upon the flight time.

Figures 25 through 30 present the scenarios for the long-range transport and figures 31 through 35 show the scenarios for the medium-range transport.  It is assumed that the time on the ground between flights is sufficient to allow the tire apex and gas temperature to reach ambient, which is taken conservatively to be 100°F.  Allowance is made for the landing gear being extended during the landing approach for ten minutes, which either makes the tire apex temperature greater or less than the tire gas temperature, depending on the length of the flight.  The apex temperature always leads the gas temperature when exposed to changes in the immediate environmental temperature.

Figures 36 through 40 illustrate the scenarios for the short-haul transport. The ramp times are given along with corresponding changes in the tire apex and gas temperatures.  Again the ambient temperature is assumed to be 100°F.  In the case of the short-haul airplane, the landing gear extended time is assumed to be five minutes.


# TIRE FATIGUE LIFE

## INTRODUCTION.

Several different types of tests were performed to obtain data for development of and correlation with analytical methods.  In addition, data were obtained from industry tests and from flight tests performed in support of other programs.  Part of the data obtained under this program was from three types of dynamometer tests, namely:  rate of temperature build-up, cycling tests to a given tire temperature and constant temperature tests.  Limited flight testing provided the remaining portion of the data obtained in the program.

The rate of temperature build-up on new tires provided data by which temperature rise could be observed for straight roll and for yawed roll under different combinations of radial and lateral loading conditions.  The data thus obtained were used to obtain equivalent radial loads for given combinations of radial and lateral loads.

Cycling tests, performed on service tires, were designed to provide a means of comparing, relatively, the life remaining for the tires as a function of the flights made.  New tire cycling and constant temperature tests were designed to provide data reflecting the heat and load effects on the life of tires.  The data were then used to establish tire fatigue curves for various cycling temperatures.  Since it is desired that a tire be able to withstand a rejected takeoff (RTO) at the end of its service life, each tire subjected to these tests was exposed to a run representing a taxi to takeoff, takeoff, and a rejected takeoff.

FIGURE 25. SCENARIO, LONG RANGE, 5.2 PERCENT OF FLIGHTS, NON-DIMENSIONAL WEIGHT 0.940 TAKEOFF 0.611 LANDING

33
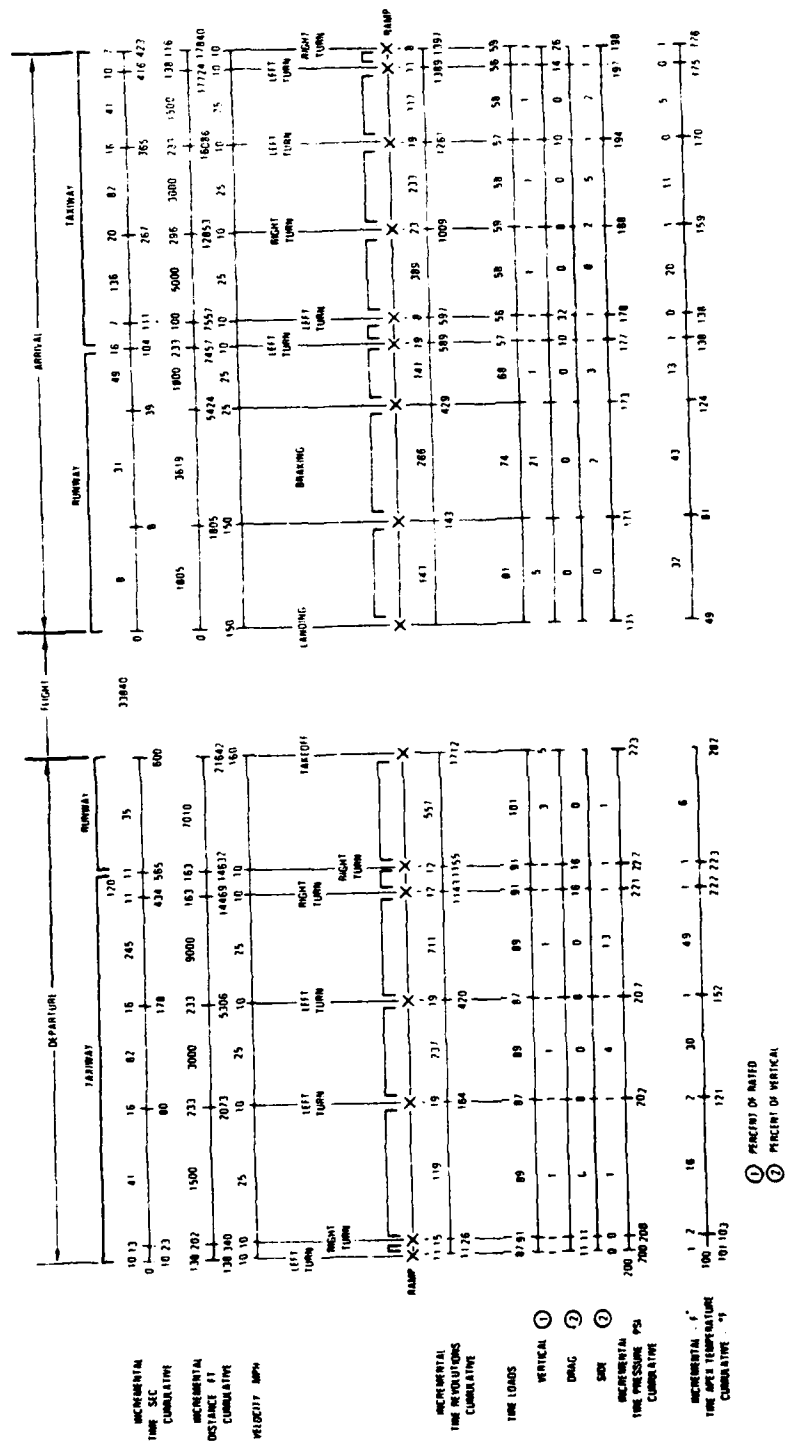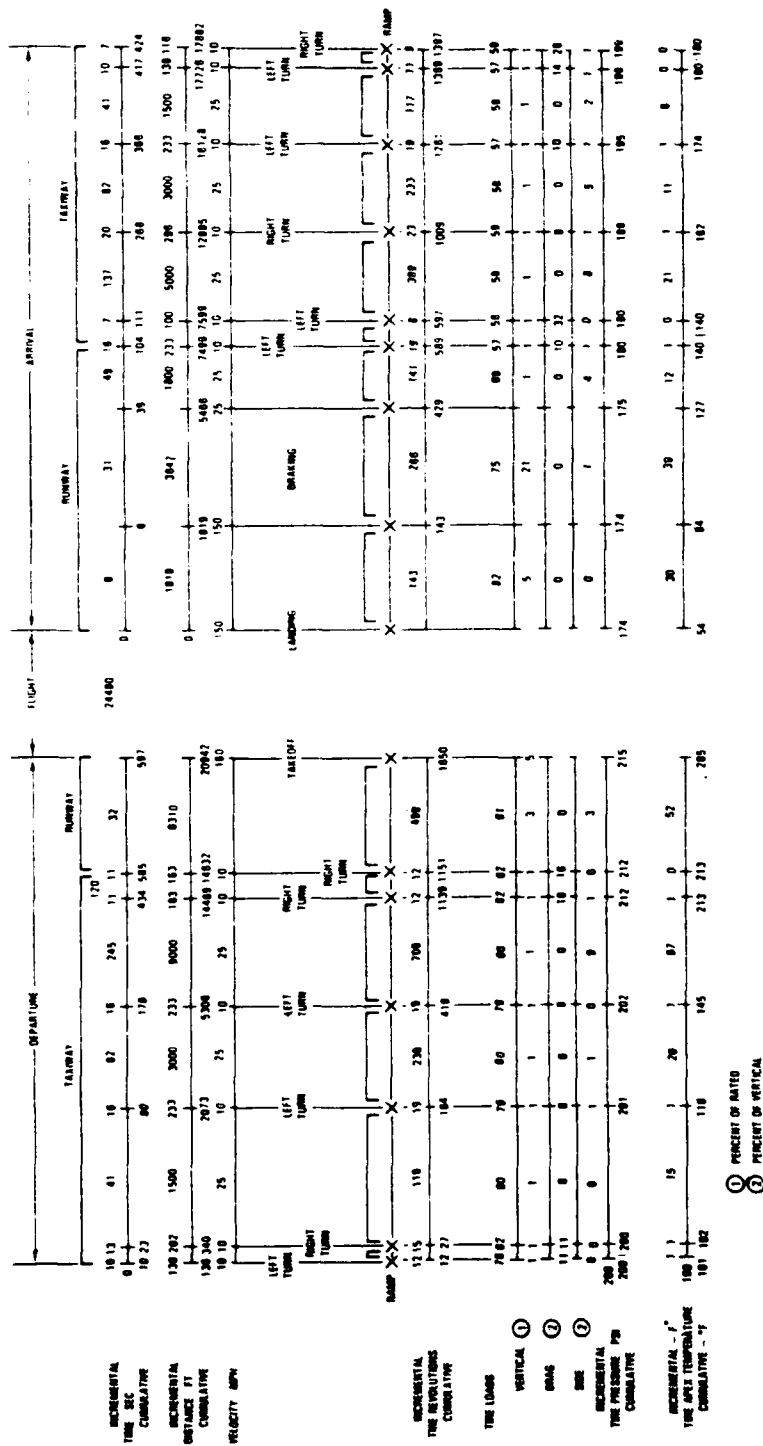
FIGURE 26. SCENARIO, LONG RANGE, 17.4 PERCENT OF FLIGHTS, NON-DIMENSIONAL WEIGHT 0.846 TAKEOFF 0.616 LANDING
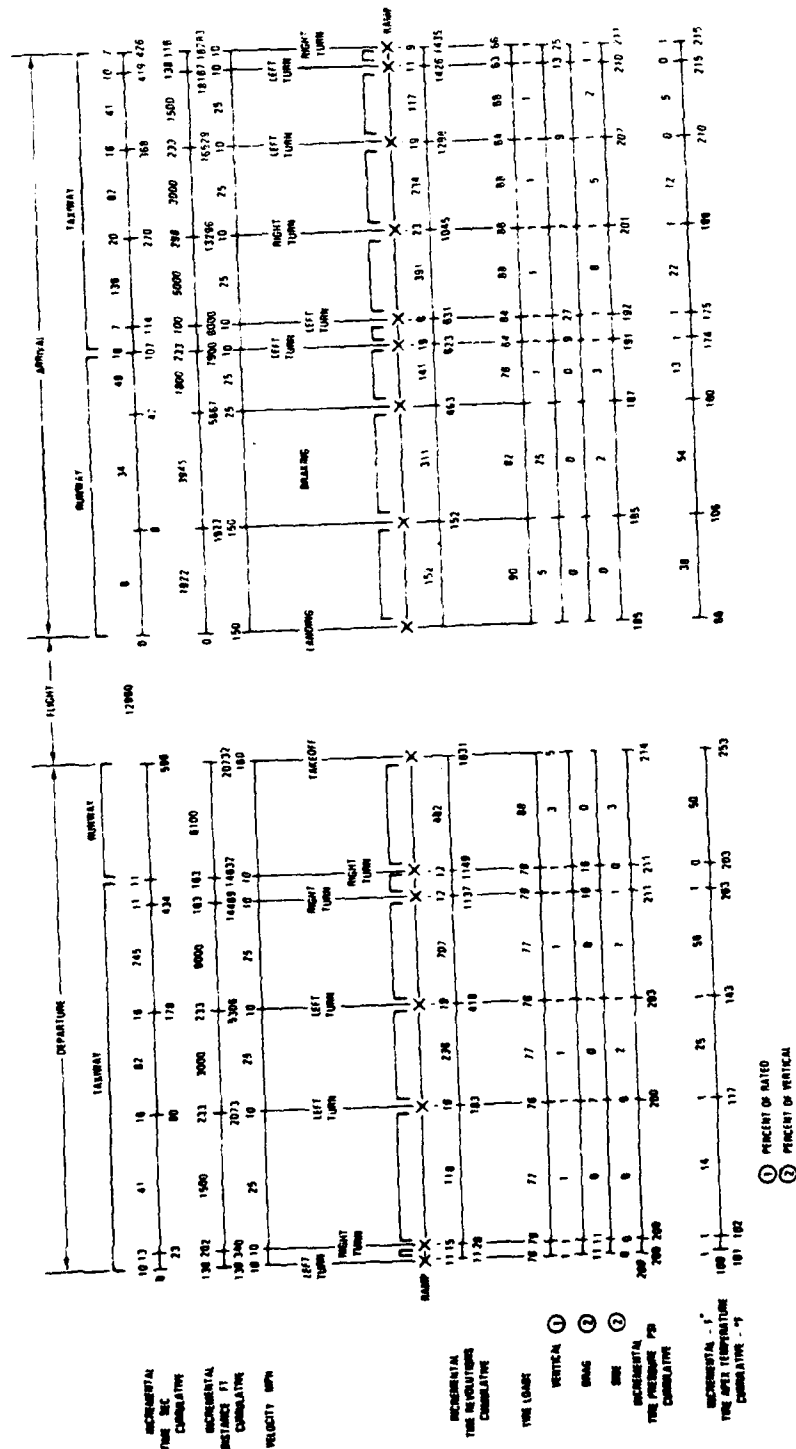
FIGURE 27. SCENARIO, LONG RANGE, 12.2 PERCENT OF FLIGHTS, NON-DIMENSIONAL WEIGHT 0.818 TAKEOFF 0.690 LANDING

FIGURE 28.   SCENARIO, LONG RANGE, 12.2 PERCENT OF FLIGHTS, NON-DIMENSIONAL WEIGHT
0.736 TAKEOFF 0.615 LANDING

FIGURE 29.   SCENARIO, LONG RANGE, 26.5 PERCENT OF FLIGHTS, NON-DIMENSIONAL WEIGHT
0.729 TAKEOFF 0.690 LANDING

37

FIGURE 39. SCENARIO, LONG RANGE, 26.5 PERCENT OF FLIGHTS, NON-DIMENSIONAL WEIGHT 0.652 TAKEOFF 0.615 LANDING.
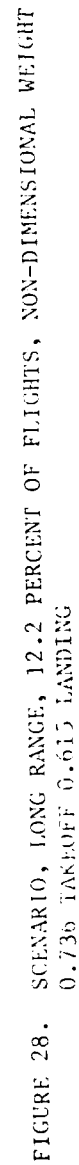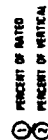
38
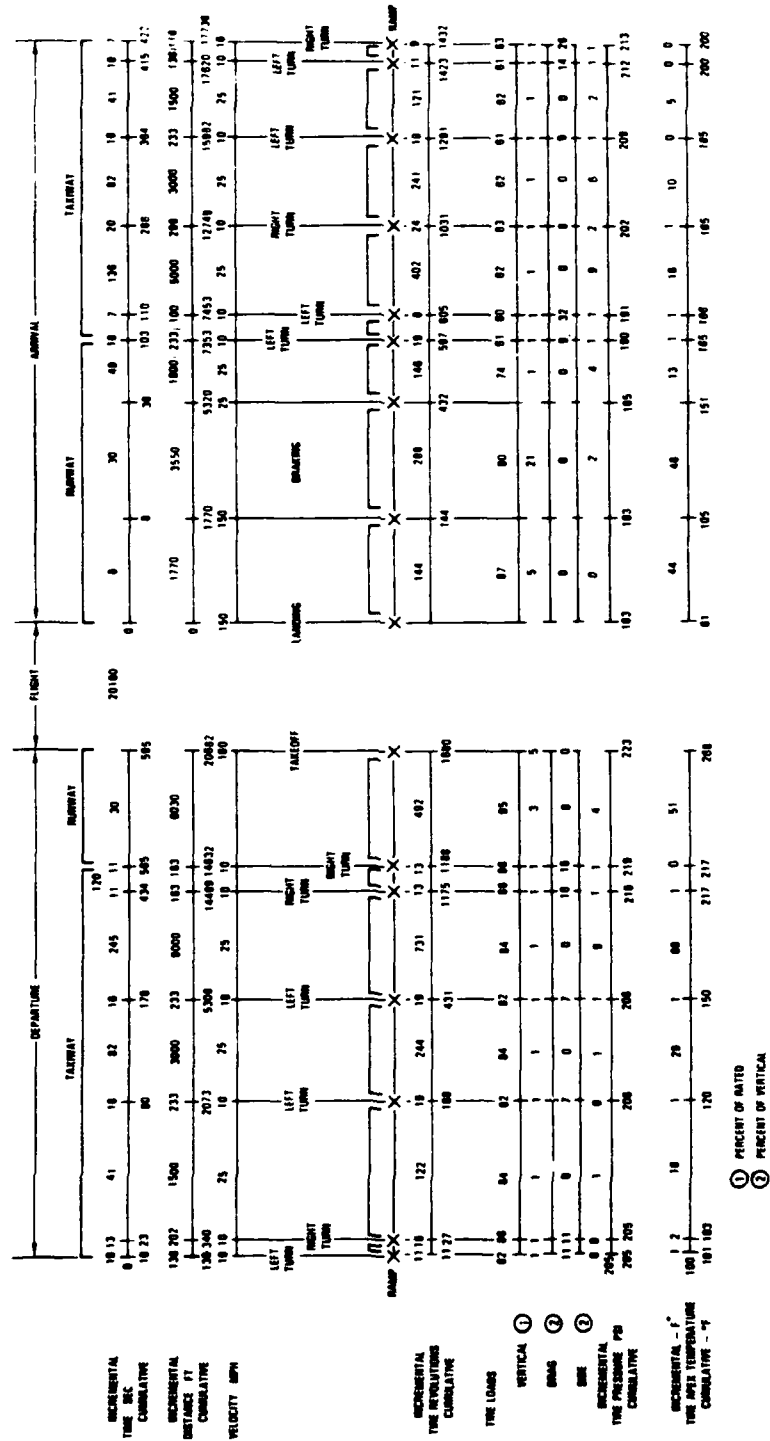
FIGURE 31. SCENARIO, MEDIUM RANGE, 15.2 PERCENT OF FLIGHTS, NON-DIMENSIONAL WEIGHT 0.958 TAKEOFF 0.711 LANDING

39

FIGURE 32. SCENARIO, MEDIUM RANGE, 10.9 PERCENT OF FLIGHTS, NON-DIMENSIONAL WEIGHT 0.900 TAKEOFF 0.800 LANDING

FIGURE 33. SCENARIO, MEDIUM RANGE, 30.2 PERCENT OF FLIGHTS, NON-DIMENSIONAL WEIGHT 0.847 TAKEOFF 0.808 LANDING

41
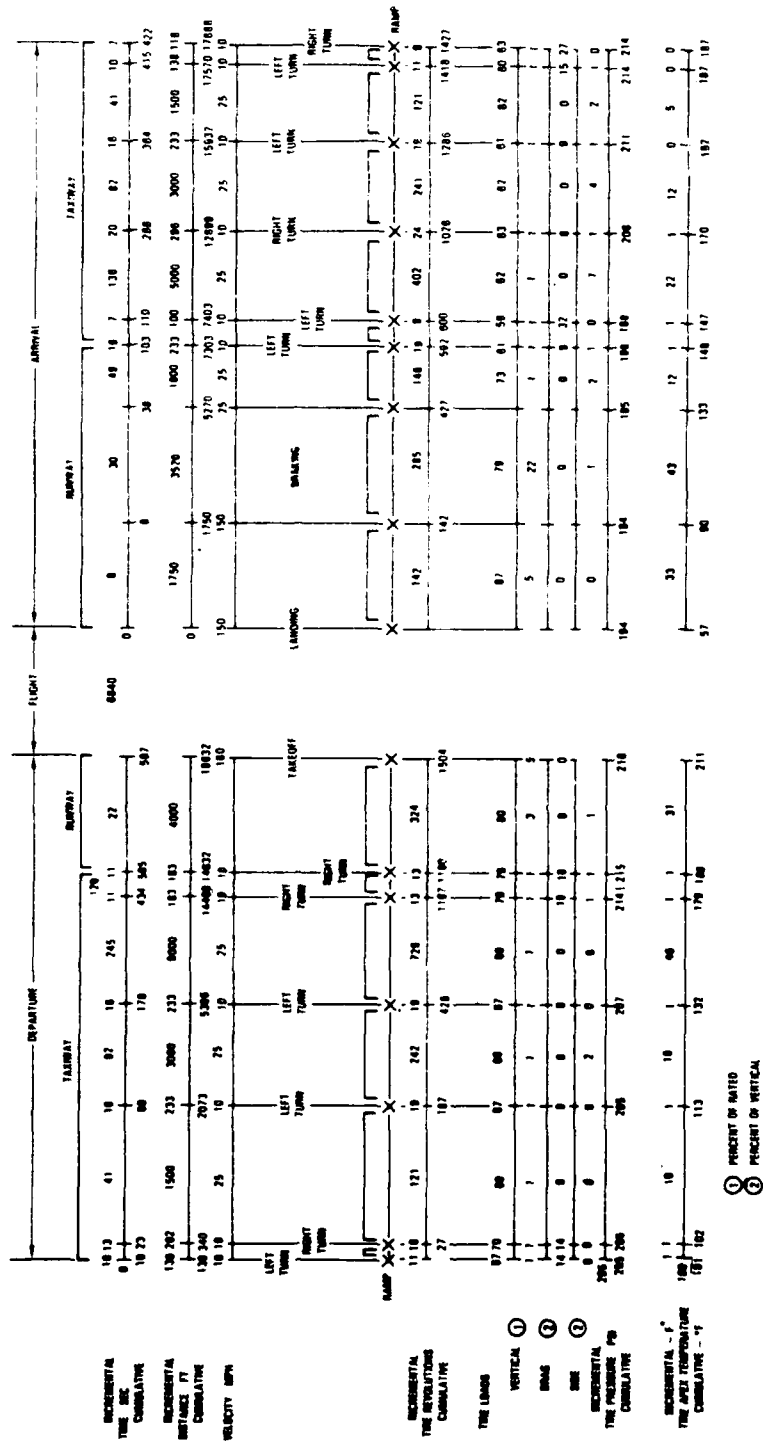
FIGURE 34. SCENARIO, MEDIUM RANGE, 10.4 PERCENT OF FLIGHTS, NON-DIMENSIONAL WEIGHT 0.787 TAKEOFF 0.704 LANDING

42

FIGURE 35.   SCENARIO, MEDIUM RANGE, 33.3 PERCENT OF FLIGHTS, NON-DIMENSIONAL WEIGHT
0.745 TAKEOFF 0.708 LANDING

FIGURE 36. SCENARIO, SHORT HAUL, FIVE LANDINGS, NONREFUELED FLIGHTS, FIRST LEG.

44
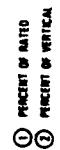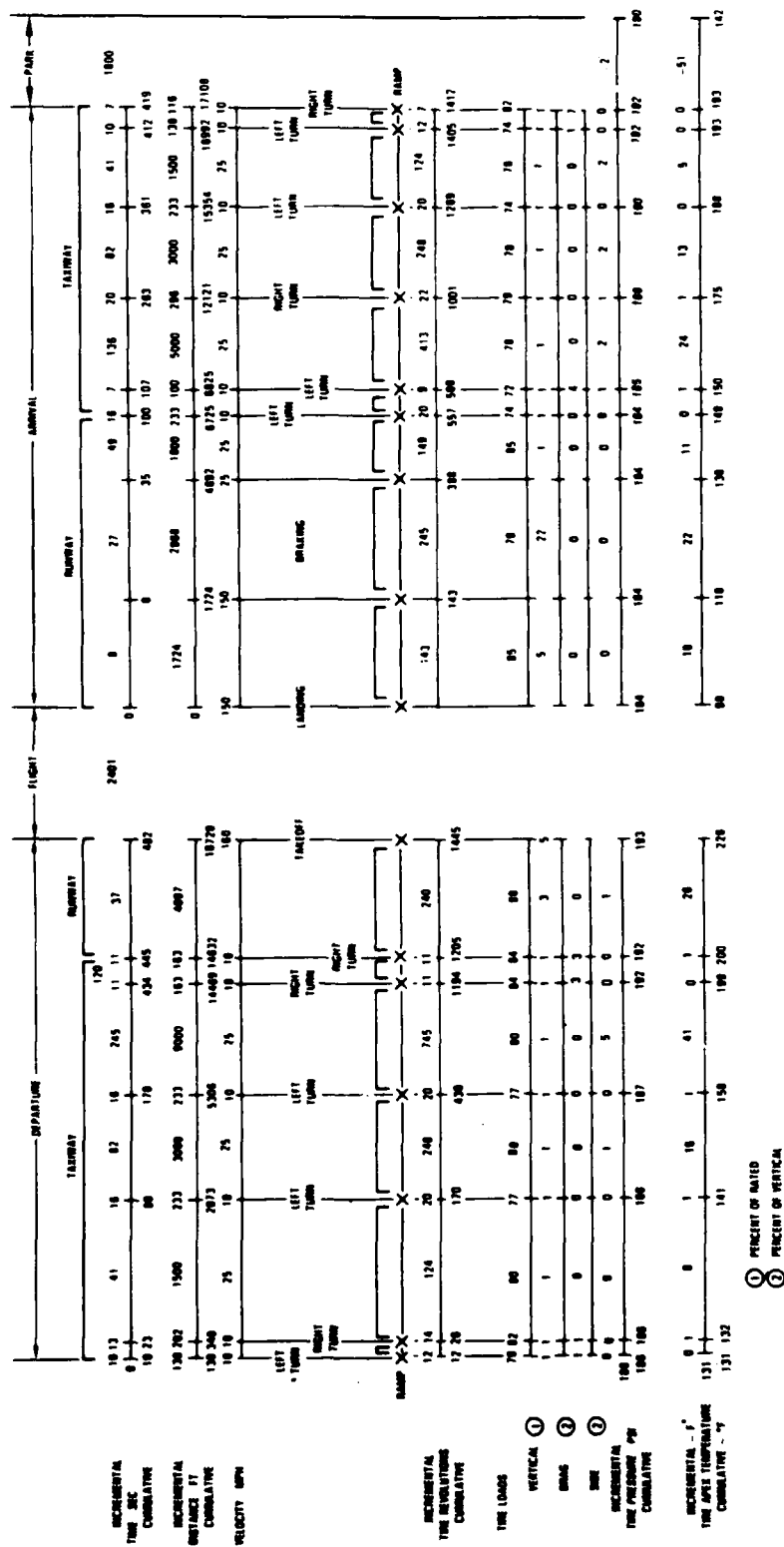
FIGURE 37. SCENARIO, SHORT HAUL, FIVE LANDINGS, NONREFUELED FLIGHTS, SECOND LEG

FIGURE 38. SCENARIO, SHORT HAUL, FIVE LANDINGS, NONREFUELED FLIGHTS, THIRD LEG

FIGURE 39.   SCENARIO, SHORT HAUL, FIVE LANDINGS, NONREFUELED FLIGHTS, FOURTH LEG
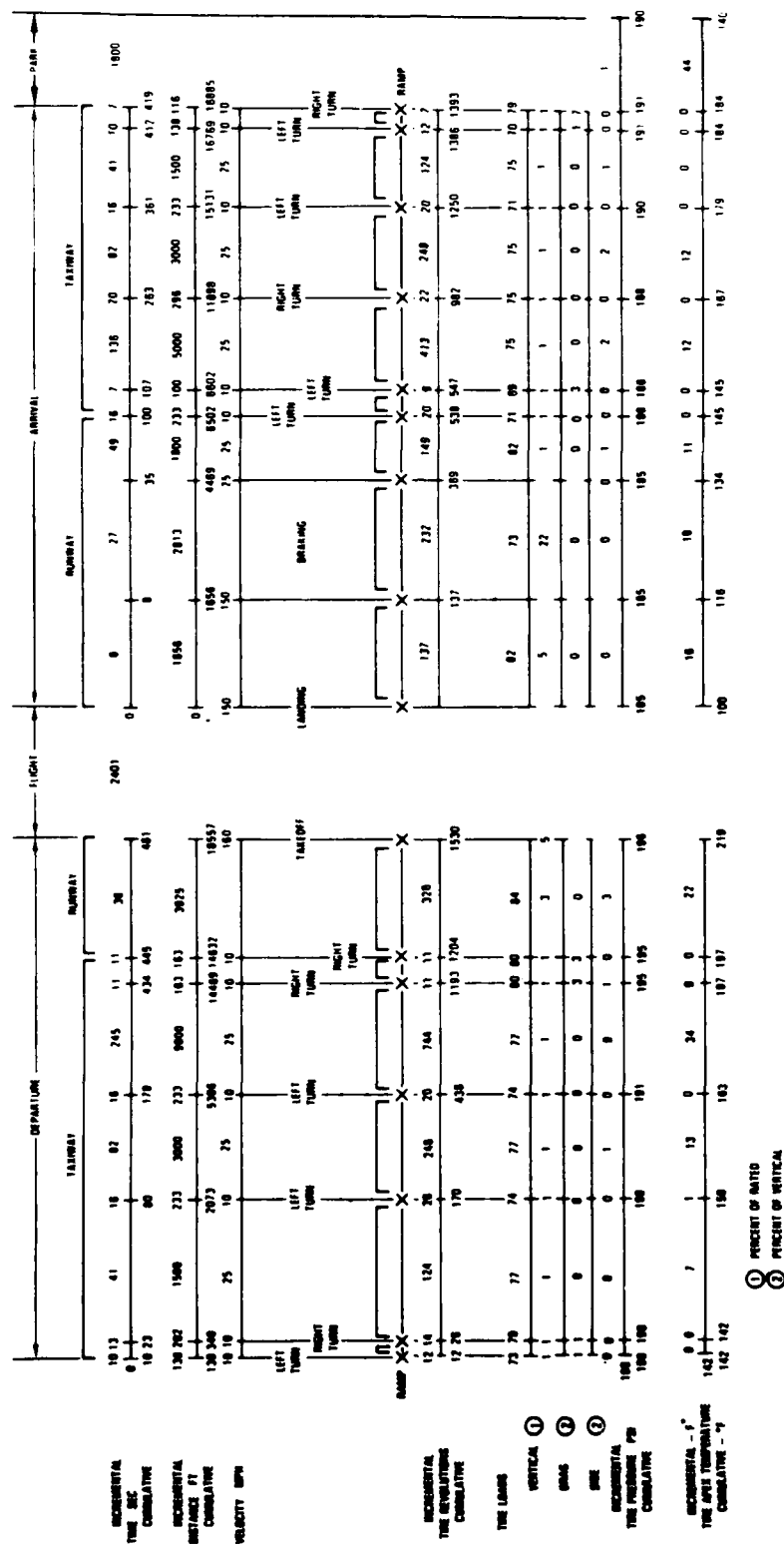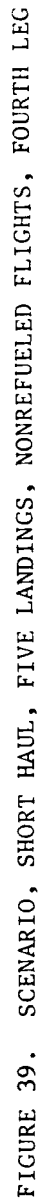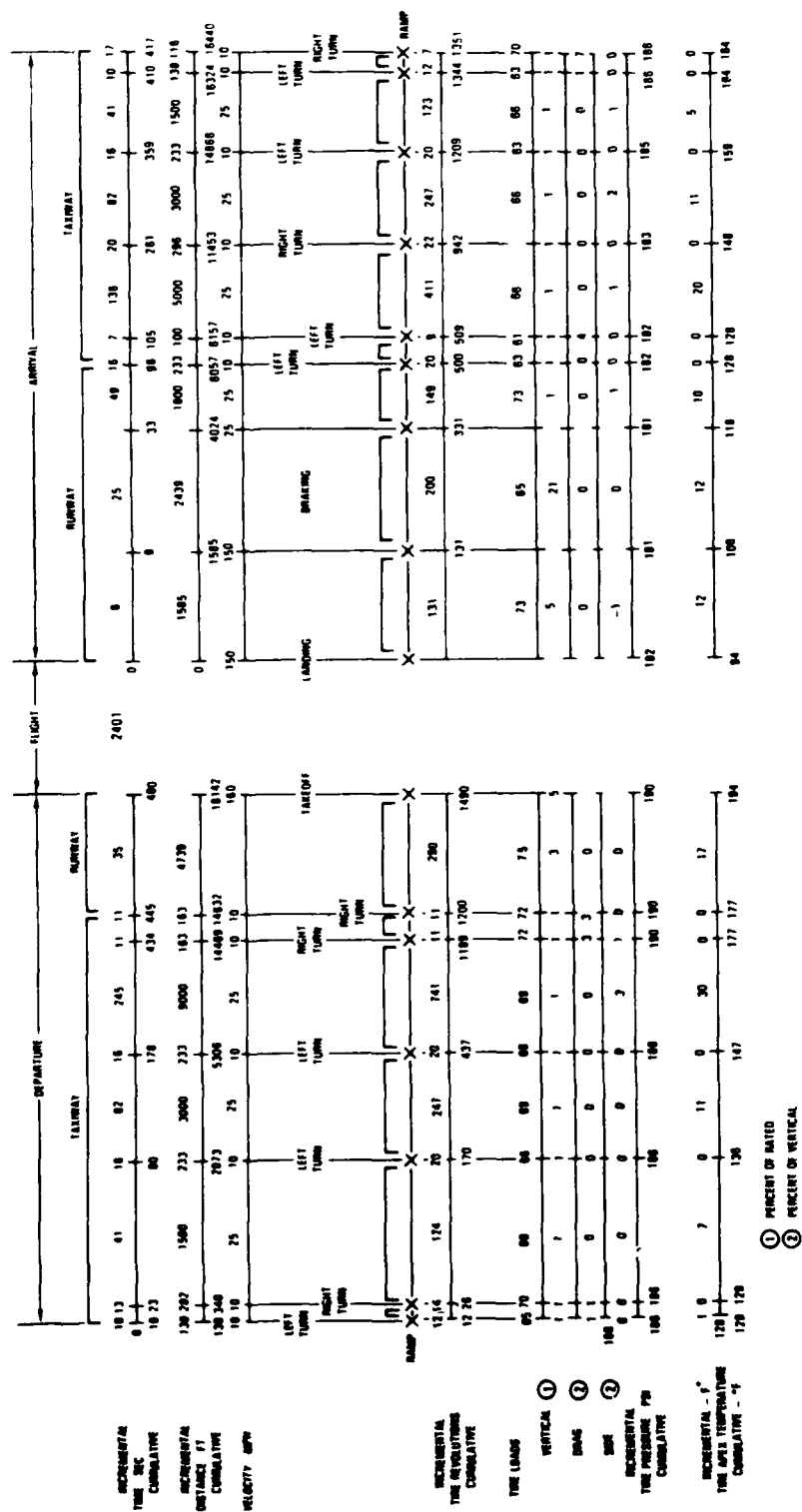
FIGURE 40. SCENARIO, SHORT HAUL, FIVE LANDINGS, NONREFUELED FLIGHTS, LAST LEG

## SERVICE TIRES REMAINING STRENGTH.

There has been past evidence that tire materials, namely the fabric, deteriorate in strength when exposed to load and heat. Review of retreading techniques indicates that the deterioration from the process will cause minimal to no damage. However, under service operations tire apex temperatures can be expected to reach 220 to 280°F, depending on taxi distances. Burst tests performed by a tire manufacturer best illustrate the loss in strength encountered during service.

Hydrostatic burst tests were performed on two different size tires, 50 x 20-20 and 49 x 17, with each tire for a given size, having the same number of retreads. The results of the tests are given in tables 11 and 12.

The data indicate that the burst pressure of a 50 x 20-20 tire with five retreads can range from 57.0 to 79.0 percent of that of a new tire, and for a 49 x 17 tire with seven retreads, it can range from 50.4 to 85.7 percent. The average for the 50 x 20-20 tire is about 68.6 percent, and for the 49 x 17 is about 61.0. The 68.6 percent burst pressure is approximately the burst pressure of a new tire if it were at a temperature of about 250°F. All the burst test failures occurred in the crown or shoulder area of the tire.

The burst pressure test data scatter for a new 50 x 20-20 tire is about +5 percent, and for a new 49 x 17 tire is about +4 percent. The burst pressure test data scatter for the 50 x 20-20 and 49 x 17 service tires are +10 and +35 percent, respectively. If the one 49 x 17 tire that performed far better than the others is eliminated from the group, the average scatter is +14 percent.

Figure 41 shows the variation of number of tire retreads with the ratio of burst pressure to rated pressure. The ratio of the average burst pressure to rated pressure for the 50 x 20-20 service tires is 3.6 at ambient temperature. Again, if the 49 x 17 service tire data point of 790 psi is eliminated, the ratio of the average burst pressure to the rated pressure at ambient temperature is shown as being 3.0. These points are significant in that they show that the strength of tires deteriorates with use. The ratio is further reduced if the pressure increase due to service operations is considered. For instance, at an apex temperature of 260°F, which is common, the tire internal pressure can reach 233 psi. The ratio for the tires with five retreads is reduced from 3.6 to 3.2 and for the tires with seven retreads, from 3.0 to 2.6. Considering that the foregoing operations are average and that longer taxi distances are encountered at some airports, tires with more than seven retreads would have even less strength capability. This situation is not only from the increase in tire pressure due to heat, but also from a reduction in burst strength due to temperature, as shown in figure 42.

The data scatter from the burst tests increases with the number of retreads as shown in figure 43. The scatter in the new tires of 4 to 5 percent can be attributed to manufacturing differences, while the scatter above 4 to 5 percent can be attributed to operational use. Considering the scatter, the ratio of burst to rated pressure for the tires with five retreads is further reduced to 2.9, and for the tires with seven retreads to 2.2. This potential loss in strength indicates that retreading tires more than five times increases the risk of service failure considerably. In addition, a margin is needed to provide strength for an overload due to a failure of a tire on the same axle.

TABLE 11.   BURST TESTS 50 x 20-20, 34 PR TIRES
NUMBER OF RETREADS:   5

| Tire Serial Number | Number of Landings | Burst Press. – PSI | Percent of New Tire Burst Press.** |
|---|---|---|---|
| 01150140 | 904* | 741 | 65.6 – 72.6 |
| 01340261 | 853* | 644 | 57.0 – 63.1 |
| 83050294 | 901* | 753 | 66.6 – 73.8 |
| 91200348 | 899 | 806 | 71.3 – 79.0 |
| Average | 889 | 736 | 65.1 – 72.1 |

*Incomplete records.  Estimated by finding the average number of landings per retread for the known history between retreads and using this value for unknown cases.

**The new tire burst pressure from tests is 1075 ±55 psi.  1130 psi is used for the lower percentage value and 1020 psi is used for the higher value.

TABLE 12.   BURST TESTS 49 x 17, 28 PR TIRES
NUMBER OF RETREADS:   7

| | Burst Pressure, PSI | Percent of New Tire Burst Pressure* |
|---|---|---|
| | 620 | 62.1 – 67.2 |
| | 513 | 51.4 – 55.6 |
| | 790 | 79.2 – 85.7 |
| | 503 | 50.4 – 54.6 |
| | 563 | 56.4 – 61.1 |
| | 520 | 52.1 – 56.4 |
| Average | 585 | 58.6 – 63.4 |

*The new tire burst pressure from tests is 960 ±38 psi.  998 psi is used for the lower percentage value and 922 psi is used for the higher value.
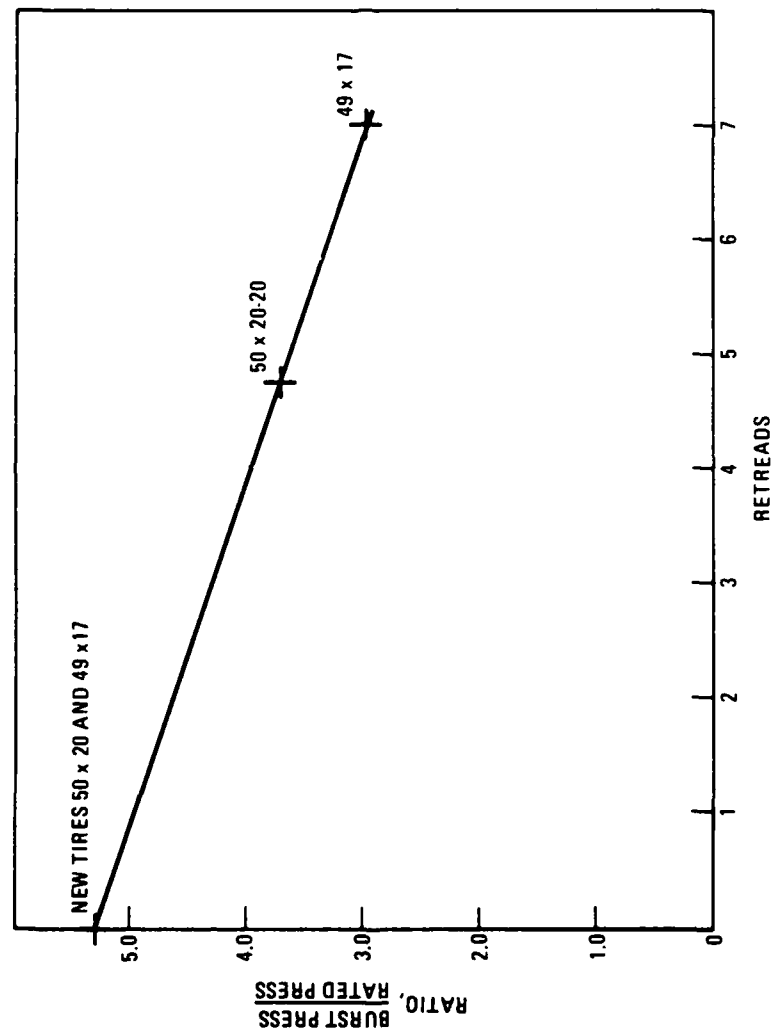
FIGURE 41. TIRE BURST STRENGTH AS A FUNCTION OF THE NUMBER OF RETREADS
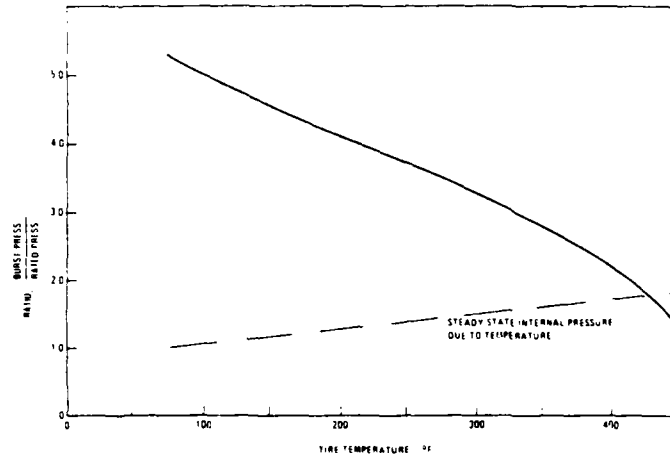
FIGURE 42.  TIRE BURST STRENGTH AS A FUNCTION OF TIRE TEMPERATURE
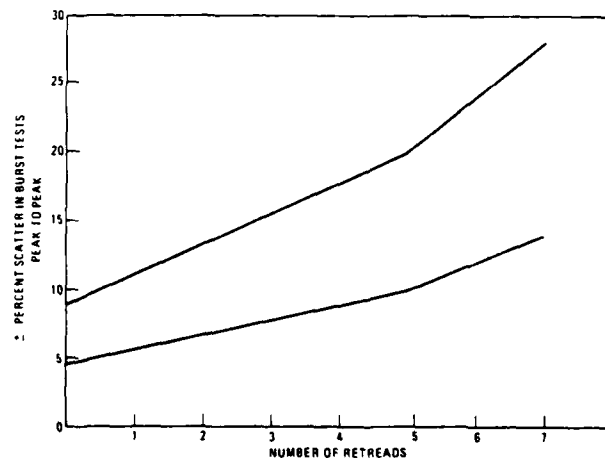


FIGURE 43.  DATA SCATTER IN BURST TESTS AS A FUNCTION OF NUMBER OF RETREADS

## DYNAMOMETER TESTS.

Several different groups of dynamometer tests were made using two different size tires (50 x 20-20, 34 PR and 40 x 14, 24 PR). For one 50 x 20-20 size tire, both new and service tires were used. One group of tests was made to determine the rate of heat build-up and the equivalent radial load needed to represent combined radial and lateral loads. A second group of tests was made to compare the life remaining on service tires exposed to various numbers of flights. A third group of tests provided data from which tire carcass fatigue curves were developed.

## TEST PROCEDURE.

Test Measurements. All tire tests were performed on the 120-inch diameter, 350 miles per hour, dynamometer located in Building 31 at the Wright/Patterson Air Force Base. Table 13 is a list of the measurements made during the dynamometer tests. Figure 44 shows the location of the thermocouples in the apex of the tire. All measurements were made at 5-second intervals.

TABLE 13. MEASUREMENTS MADE DURING DYNAMOMETER TESTS

| Test | Tire Size | Apex Temp* | Contained Air | | Load | | Number of Revolutions | Time |
|---|---|---|---|---|---|---|---|---|
| | | | Temp | Press | Radial | Lateral | | |
| Temp Rate | 50 x 20 - 20 | 2 | X | X | X | X | X | X |
| | 40 x 14 | – | X | X | X | X | X | X |
| Equivalent Rad. Load | 50 x 20 - 20 | 2 | X | X | X | – | X | X |
| Service Tire Remain Life | 50 x 20 - 20 | 1 S/S | X | X | X | – | X | X |
| Carcass Fatigue | 50 x 20 - 2 | 1 S/S | X | X | X | – | X | X |

*1 = Apex temperature on one side of tire, 2 = apex temperature on both sides of tire
S/S = Thermocouple located on serial number side of tire.

Tire Preparation. All new tires were pressure-soaked for 24 hours at rated pressure. The flat plate deflection at rated load was determined. With the tire on the drum at rated load, the pressure was adjusted to provide the same deflection as that obtained on the flat plate at rated load. The tire was then broken in by rolling at 40 miles per hour for 1,000 revolutions and thⁿ ₁ letting the tire cool to below 150 °F.

To impose the damage on each tire caused by a rejected takeoff (RTO), a simulated RTO was performed as follows:

1. The tire was rolled at 50 miles per hour on the drum at rated load until the apex temperature reached 210°F, to simulate pre-takeoff taxi.

2. The drum was then immediately accelerated to 170 miles per hour at rated load to simulate a takeoff run.

53
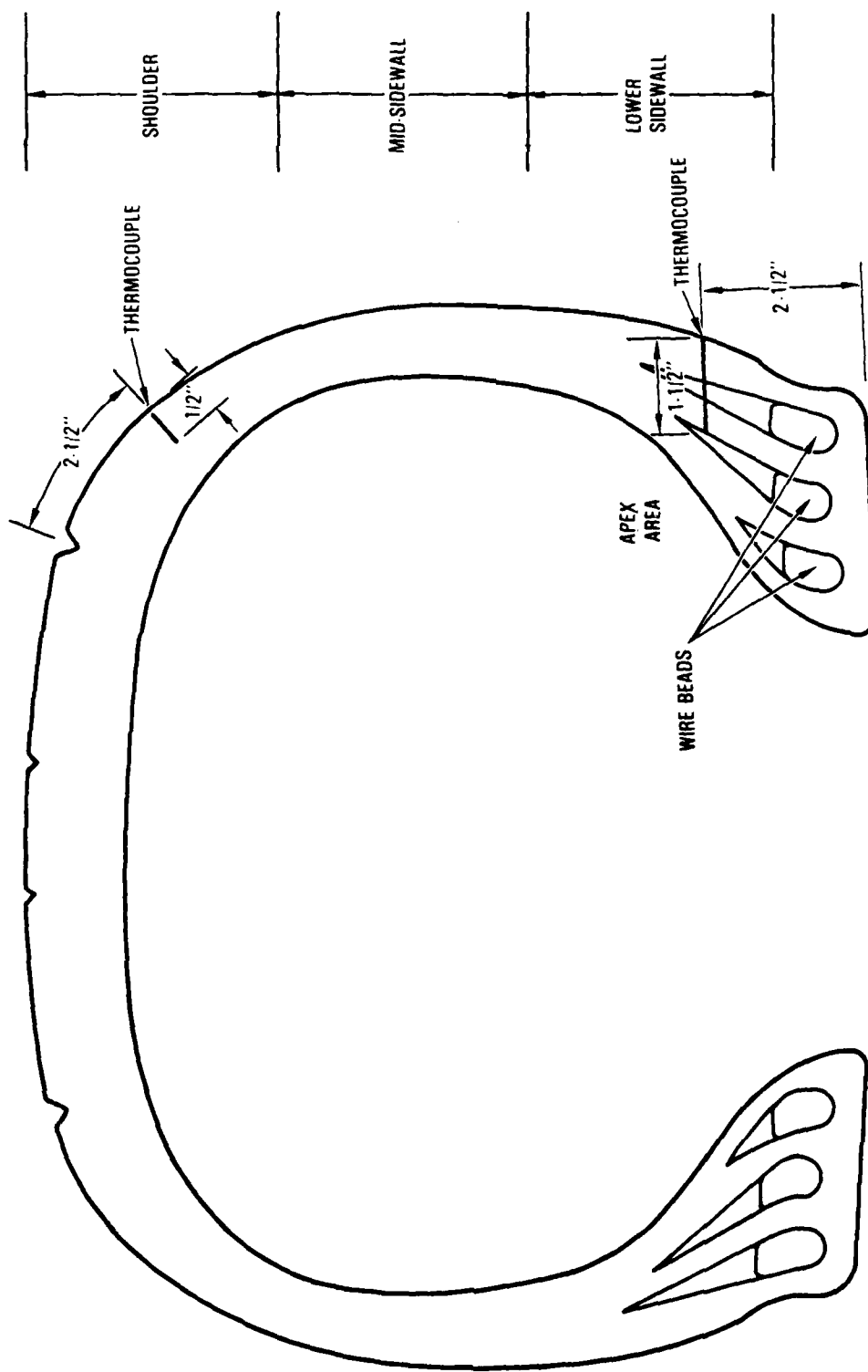
FIGURE 44. LOCATION OF THERMOCOUPLES

3. After the 170 miles per hour was attained, the radial load was increased
   to 1.6 times the rated load to simulate a tire failure cn the same axle.
   (The value of 1.6 times rated load of the tire was selected, rather than 1.9
   to 2.0, because it more normally represents the tire loading encountered in
   service. Items like the 1.07 factor given in TSO 62C and the fact that
   airframe manufacturers generally select a rated pressure higher than the
   minimum in the FAA requirements were also taken into account. The drum was
   slowed from 170 to 0 miles per hour to simulate the braking phase of the RTO.

   Test Methods. Three different test procedures were used to obtain the
types of measurements delineated in table 13.

1. Rate of Temperature Rise and Equivalent Radial Load. - The tires were
   rolled at 50 miles per hour until tire failure occurred. Various
   combinations of radial and lateral loads were used. The matrix of loads used
   in the tests are shown in figure 45.

2. Service Tire Remaining Life. - The tires were rolled at 50 miles per hour
   at a radial load of 1.2 times the rated load until an apex temperature of
   350°F was attained. The tires were then cooled to less than 150°F and the
   process repeated until tire failure.

3. Carcass Fatigue. - Each new tire used in the test was rolled at 50 miles
   per hour, at a given radial load (1.2 to 1.6 times rated) to a given
   temperature (310 to 350°F) and then cooled to less than 150°F. The process
   was repeated until tire failure. See table 14 for details.

TABLE 14. CARCASS FATIGUE TESTS

| Max. Temp. °F | Ratio of Radial Load to Rated Load |
|---|---|
| 310 | 1.2 |
| 330 | 1.2 |
| 350 | 1.2 |
| 310 | 1.4 |
| 330 | 1.4 |
| 350 | 1.4 |
| 310 | 1.6 |
| 330 | 1.6 |
| 350 | 1.6 |

| Lateral Load \ Radial Load | 0.4 | 0.6 | 0.8 | 1.0 | 1.2 | 1.4 | 1.6 | 1.8 | 2.0 |
|---|---|---|---|---|---|---|---|---|---|
| 0.0 | – | – | 22N ① CROWN ② | 1N S/W ③ | 15N S/W | 30N S/W | 13N S/W | 10N S/W | 28N S/W |
| 0.1 | 23N CROWN | 16N CROWN | 8N S/W | 12N S/W | 18N S/W | 19N S/W | 7N S/W | 6N S/W | 5N S/W |
| 0.2 | – | 11N CROWN | 9N S/W | 4N S/W | 25N S/W | 14N S/W | 21N S/W | 26N S/W | – |
| 0.3 | – | – | 2N ABORTED | 20N S/W | 20N S/W | 3N S/W | – | – | – |

a. 50 x 20-20 Tire, 34 Ply Rating, Rated Load 57,000 Pounds

| Lateral Load \ Radial Load | 0.4 | 0.6 | 0.8 | 1.0 | 1.2 | 1.4 | 1.6 | 1.7 | 2.0 |
|---|---|---|---|---|---|---|---|---|---|
| 0.0 | – | – | 7N SHOULDER ④ | 5N S/W | 8N S/W | 1N S/W | 10N S/W | 12N S/W | 4N S/W |
| 0.1 | 15N ⑤ ABORTED | 3N CROWN | 6N SHOULDER | 26N S/W | 2N S/W | 9N S/W | 11N S/W | 17N S/W | 14N S/W |
| 0.2 | – | 22N CROWN | 19N S/W | 29N S/W | 21N S/W | 24N S/W | 27N S/W | 25N S/W | – |
| 0.3 | – | – | 16N S/W | 20N S/W | 23N S/W | 28N S/W | – | – | . |

b. 40 x 40 Tire, 24 Ply Rating, Rated Load 27,700 Pounds

NOTES

① XX N Tire Code Number

② Failure occurred in tire crown

③ Failure occurred in tire sidewall (S/W)

④ Failure occurred in tire shoulder

⑤ Run was stopped excessive smoke from friction

FIGURE 45. TEST MATRIX FOR 50 x 20-20 AND 40 x 14 TIRES

TEST RESULTS.

Rate of Temperature Rise. Appendix B presents a summary of the dynamometer test results for the 50 x 20-20 and 40-14 tires.

Figure 46 shows the incremental temperature rise as a function of number of revolutions for the 50 x 20-20 tire at different radial loads. As would be expected, the temperature rise is quite dramatic at the higher radial loads where the tire deflections are greater. The contained gas pressure rise which occurs from the gas heating in response to the rise in carcass temperature is shown for the corresponding radial loads in figure 47. The data in figures 46 and 47 are from the same dynamometer runs made at 50 miles per hour. However, the relationship between the contained gas pressure and apex temperature will change if a different roll speed is employed.

The incremental apex temperature rise for different dynamometer roll velocity and load combinations are shown in figures 48, 49 and 50. Given that a tire is rolled the same distance but at different velocities, the effect on apex temperature rise of a change in velocity of 100 miles per hour is about 37 percent. A 40 percent increase in radial load will result in about a 50 percent change in apex temperature rise. Figures 51, 52 53 and 54 show the incremental contained gas pressure rise for different combinations of dynamometer roll velocities and loads. On the basis of time there is a substantial difference in temperature when comparing the different roll velocities. However, if the number of revolutions are compared, the difference between roll velocities is substantially reduced for each of the three loading conditions.

Equivalent Radial Load. Testing using combined lateral and vertical loads on dynamometers is difficult. The test equipment has to have a sensor servo system to assure the lateral load remains constant because the tread rubber deposited on the drum changes the interface friction. In addition, it is not practical to simulate taxi operations on a one-for-one basis because of the relatively small amount of time spent on each turn. Accordingly, a number of turn conditions are normally lumped together. However, this technique can cause excessive tread heat which is not encountered in service. Thus, if an equivalent radial load can be used in place of the combined lateral and radial road encountered in turns, the dynamometer testing can be made simpler.

In the development of an equivalent radial load, the assumption is made that a given radial load can be substituted for a combined radial and lateral loading if the number of revolutions to failure for the combined load is the same as that of the radial load. Accordingly, by plotting the radial load as a function of revolutions to failure for various combinations of lateral and radial loads in a convenient form (shown in figure 55), a graph to obtain equivalent loads can be developed (see figure 56).

It is not known whether these relationships will hold for other size tires. Figures 57 and 58 show the ratio of tire radial load to rated load as a function of number of revolutions to failure for a 50 x 20-20 and 40 x 14 tires, respectively. A cursory comparison indicates that, while there are differences between the two figures, there is also a general trend to similarity.
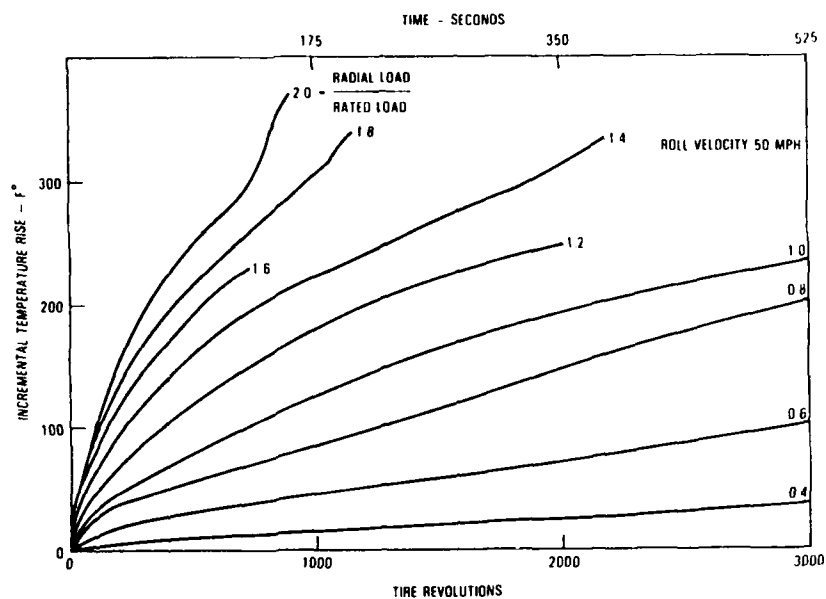
FIGURE 46. 50 x 20-20 TIRE APEX TEMPERATURE RISE
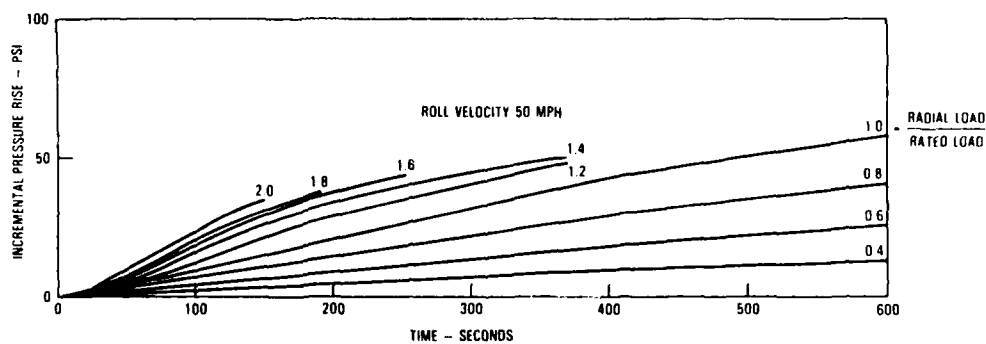


FIGURE 47. 50 x 20-20 TIRE CONTAINED GAS PRESSURE RISE

58
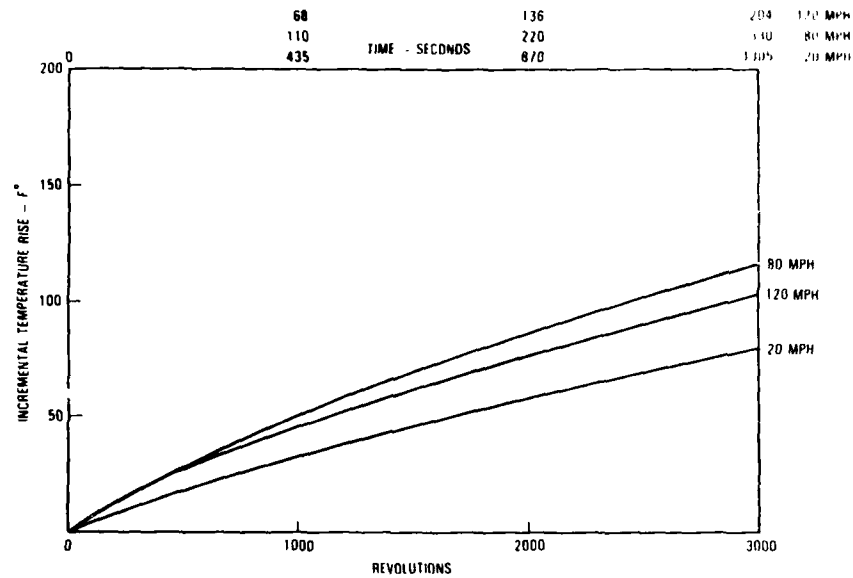
FIGURE 48.   50 x 20-20 TIRE APEX TEMPERATURE RISE
             AT A LOAD OF 0.6 TIMES TIRE RATED LOAD
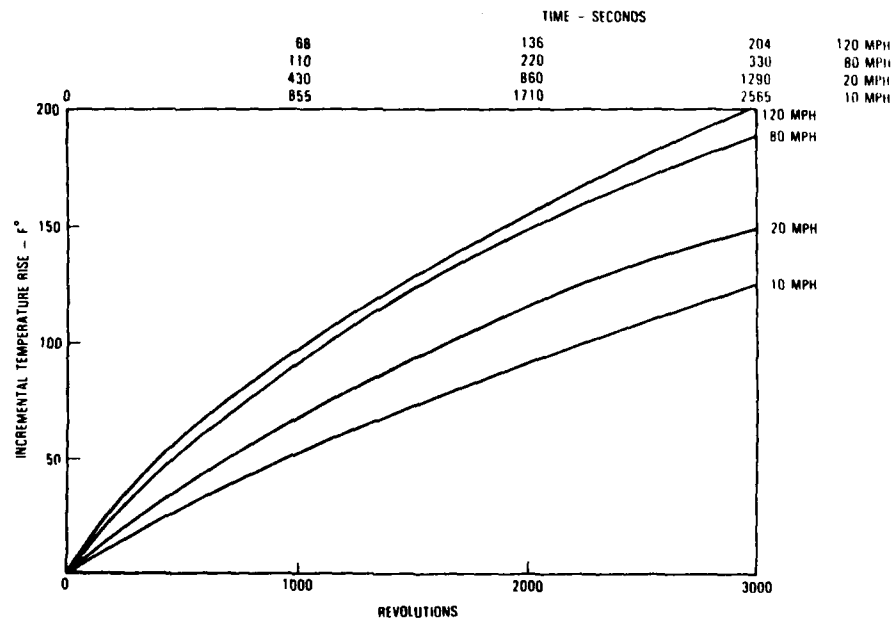


FIGURE 49.   50 x 20-20 TIRE APEX TEMPERATURE RISE
             AT A LOAD OF 0.8 TIMES TIRE RATED LOAD

59
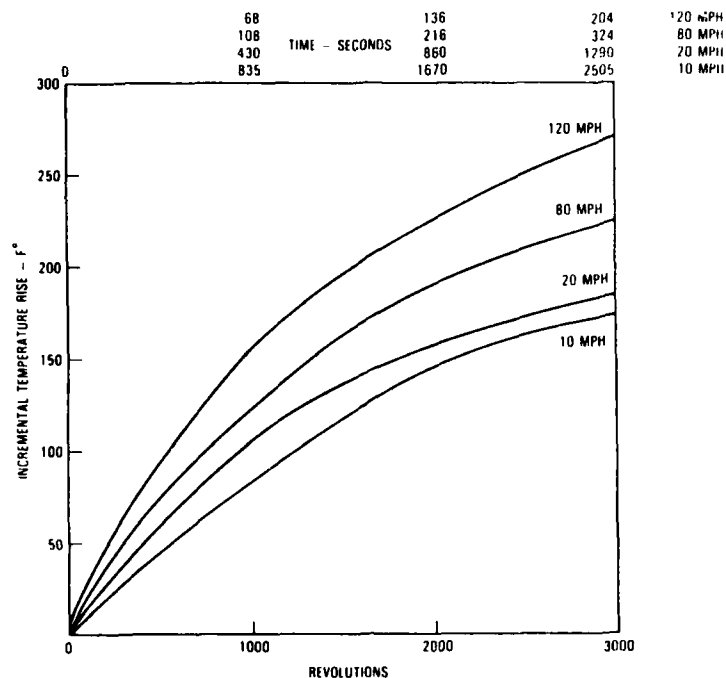
FIGURE 50. 50 x 20-20 TIRE APEX TEMPERATURE RISE
AT A LOAD EQUAL TO THE TIRE RATED LOAD
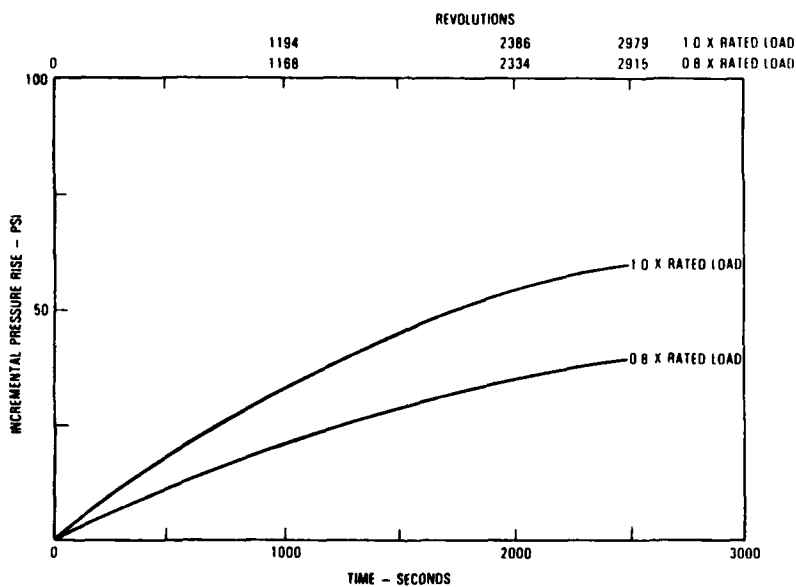


FIGURE 51. 50 x 20-20 TIRE CONTAINED GAS PRESSURE RISE
AT A ROLL VELOCITY OF 10 MPH

60

REVOLUTIONS

| 934 | 1865 | 2794 | 1 0 X RATED LOAD |
| 830 | 1859 | 2787 | 0 8 X RATED LOAD |
| 924 | 1848 | 2772 | 0 6 X RATED LOAD |
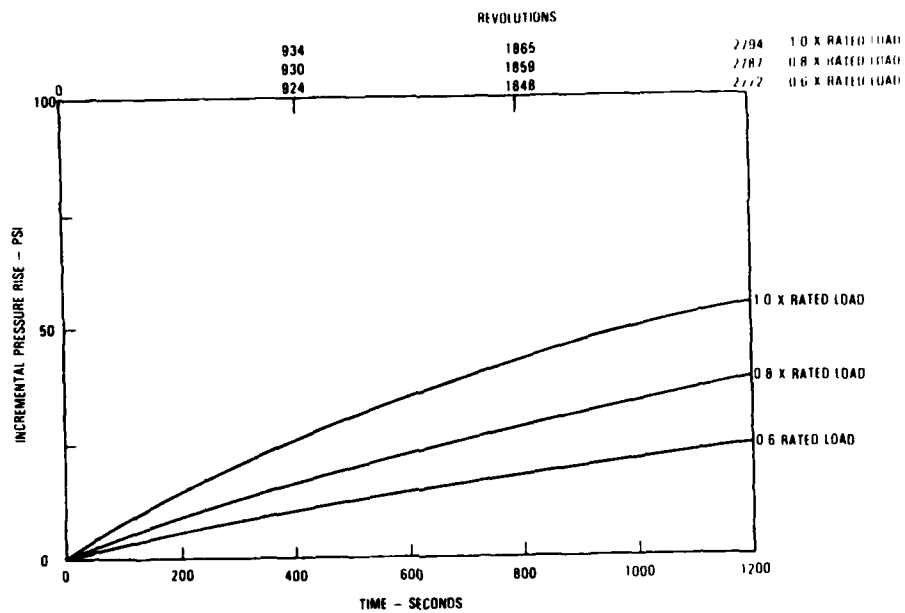


FIGURE 52.  50 x 20-20 TIRE CONTAINED GAS PRESSURE
RISE AT A ROLL VELOCITY OF 20 MPH

REVOLUTIONS

| 925 | 1851 | 2776 | 1 0 X RATED LOAD |
| 924 | 1849 | 2774 | 0 8 X RATED LOAD |
| 916 | 1836 | 2756 | 0 6 X RATED LOAD |
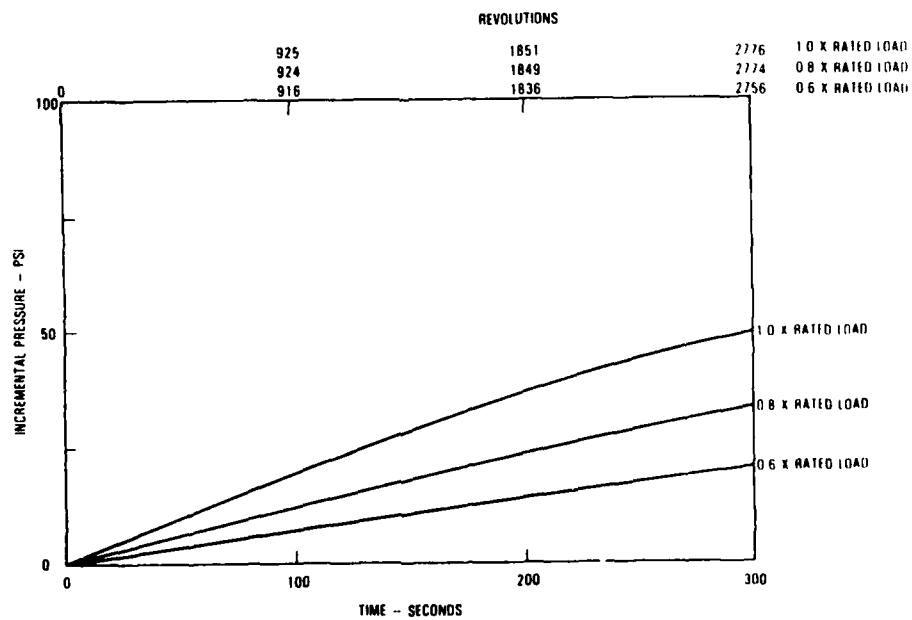


FIGURE 53.  50 x 20-20 TIRE CONTAINED GAS PRESSURE
RISE AT A ROLL VELOCITY OF 80 MPH

61
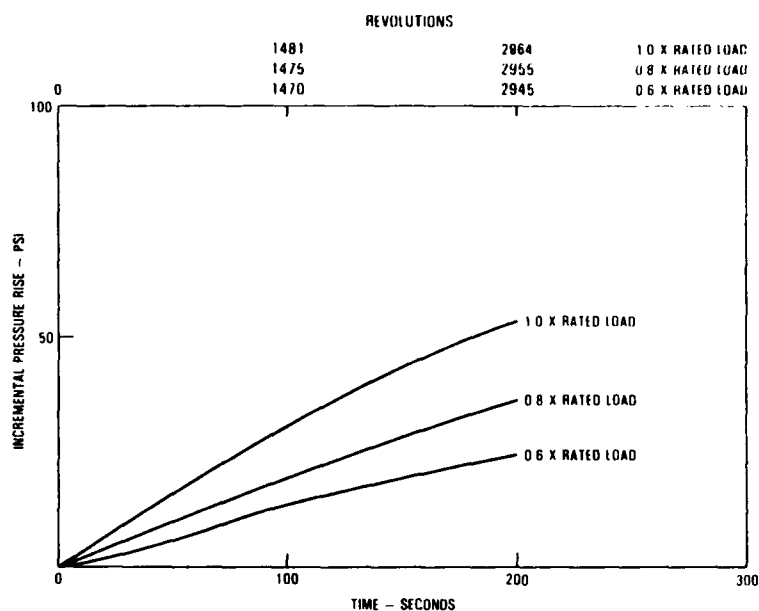
FIGURE 54.   50 x 20-20 TIRE CONTAINED GAS PRESSURE
RISE AT A ROLL VELOCITY OF 120 MPH
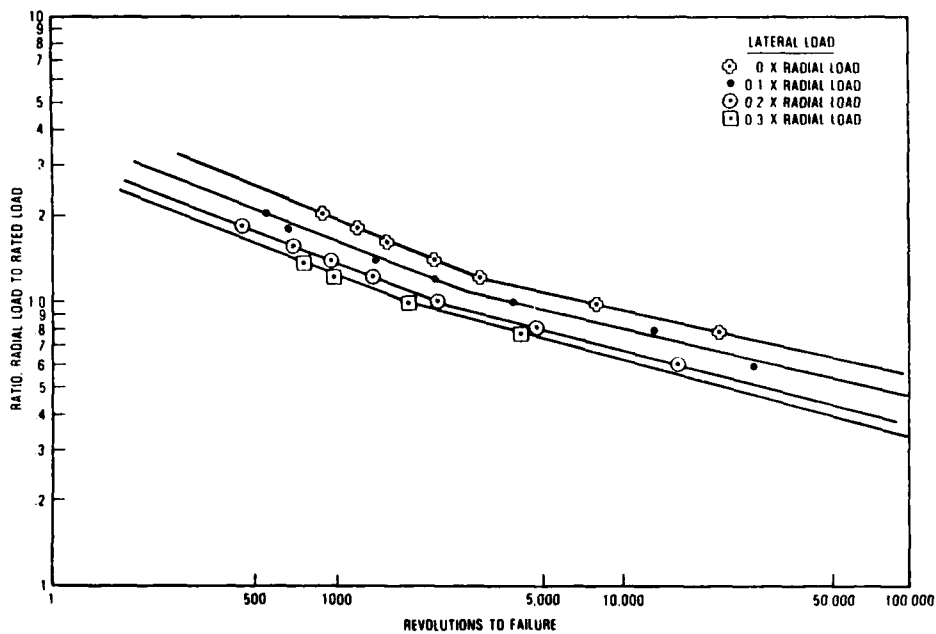


FIGURE 55.   50 x 20-20 TIRE, VARIATION OF RADIAL LOAD WITH
NUMBER OF REVOLUTIONS TO FAILURE
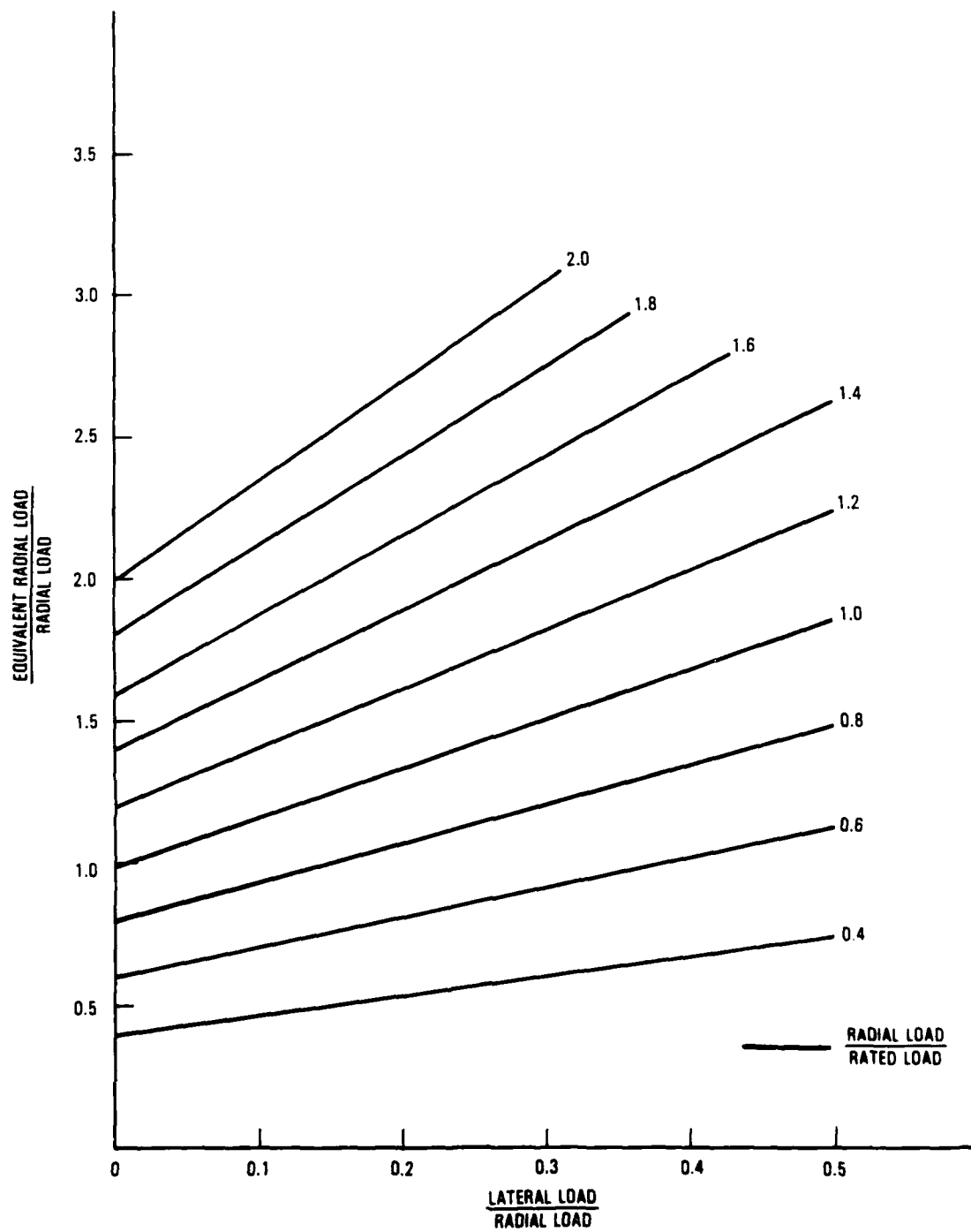
FIGURE 56. EQUIVALENT RADIAL LOAD FOR COMBINED RADIAL AND LATERAL LOAD

63
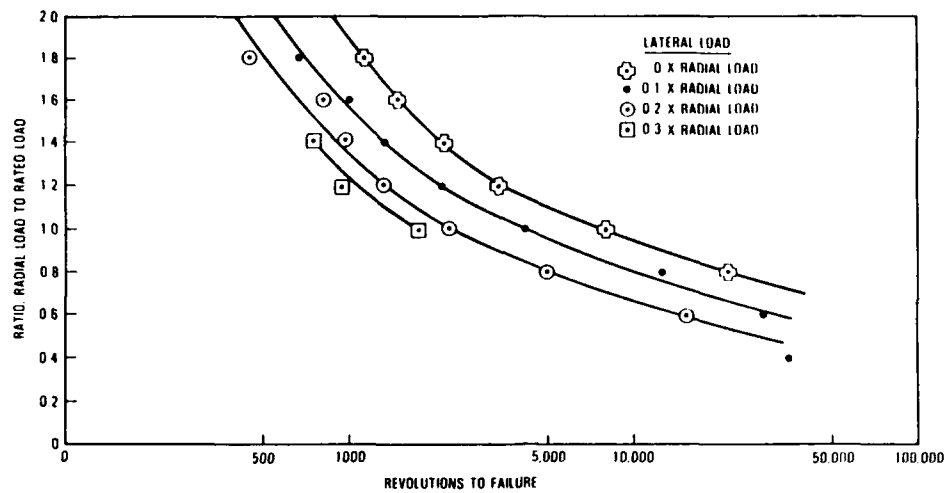
FIGURE 57.  50 x 20-20 TIRE, NUMBER OF REVOLUTIONS TO FAILURE
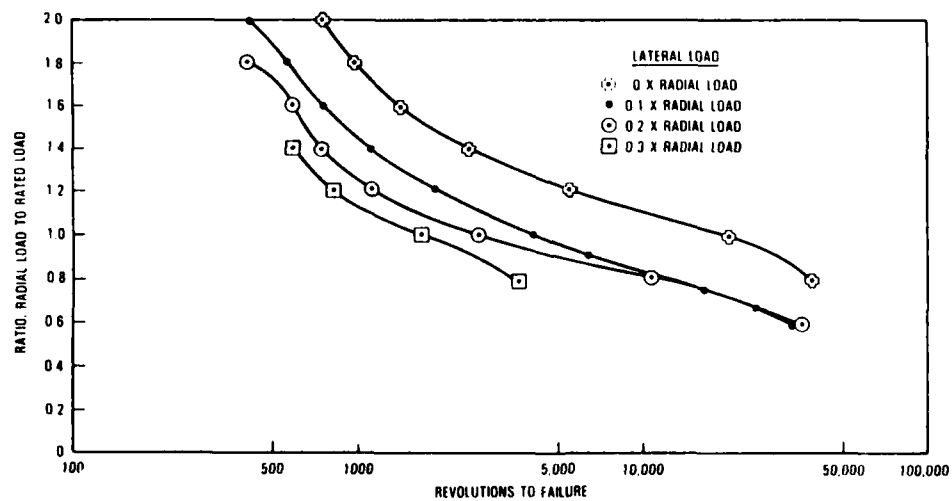


FIGURE 58.  40 x 14 TIRE, NUMBER OF REVOLUTIONS TO FAILURE

64

Service Tire Remaining Life.  A summary of the cycles to failure tests is
presented in table 15.  The  number of flights accumulated on the service tires
as a function of cycles to failure is shown in figure 59.  The figure
illustrates the large data scatter encountered when cycling to 350°F.  However,
the trend to lesser numbers of cycles as the cycling load is increased, is
demonstrated.


TABLE 15.   CYCLES TO FAILURE TEST RESULTS SUMMARY

| Tire Number | Retread Number | Number of Flights | Test Load* | Number of Cycles to Failure | Number of Revolutions to Failure |
|---|---|---|---|---|---|
| 48N | New | 0 | 1.2 | 18 | 36,650 |
| 34N | New | 0 | 1.2 | 20 | 45,175 |
| 30R3 | 2 | 413 | 1.2 | 16 | 28,232 |
| 21R4 | 3 | 670 | 1.2 | 27 | 45,185 |
| 19R4 | 3 | 527 | 1.2 | 11 | 28,388 |
| 7R5 | 4 | 652 | 1.2 | 15 | 29,425 |
| 27R2 | 1 | 383 | 1.2 | 11 | 22,427 |
| 32R5 | 5 | 806 | 1.2 | 19 | 35,643 |
| 31R3 | 2 | 428 | 1.2 | 26 | 44,793 |
| 25R2 | 1 | 257 | 1.2 | 21 | 42,606 |
| 2R5 | 4 | 739 | 1.2 | 6 | 17,557 |
| 9R3 | 4 | 775 | 1.4 | 9 | 14,856 |
| 14R4 | 3 | 548 | 1.4 | 3 | 4,859 |
| 28R2 | 1 | 263 | 1.4 | 2 | 2,806 |
| 1R3 | 2 | 412 | 1.4 | 10 | 13,338 |
| 23R6 | 4 | 734 | 1.6 | 1 | 1,227 |
| 22R2 | 1 | 256 | 1.6 | 6 | 4,598 |
| 33N | New | 0 | 1.6 | 3 | 3,782 |
| 10R5 | 4 | 775 | 1.8 | 1 | 919 |
| 20R4 | 3 | 558 | 1.8 | 4 | 3,581 |
| 13R3 | 1 | 251 | 1.8 | 2 | 1,023 |
| 39N | New | 0 | 1.8 | 7 | 4,490 |

*Ratio of Radial Load to Rated Load

65
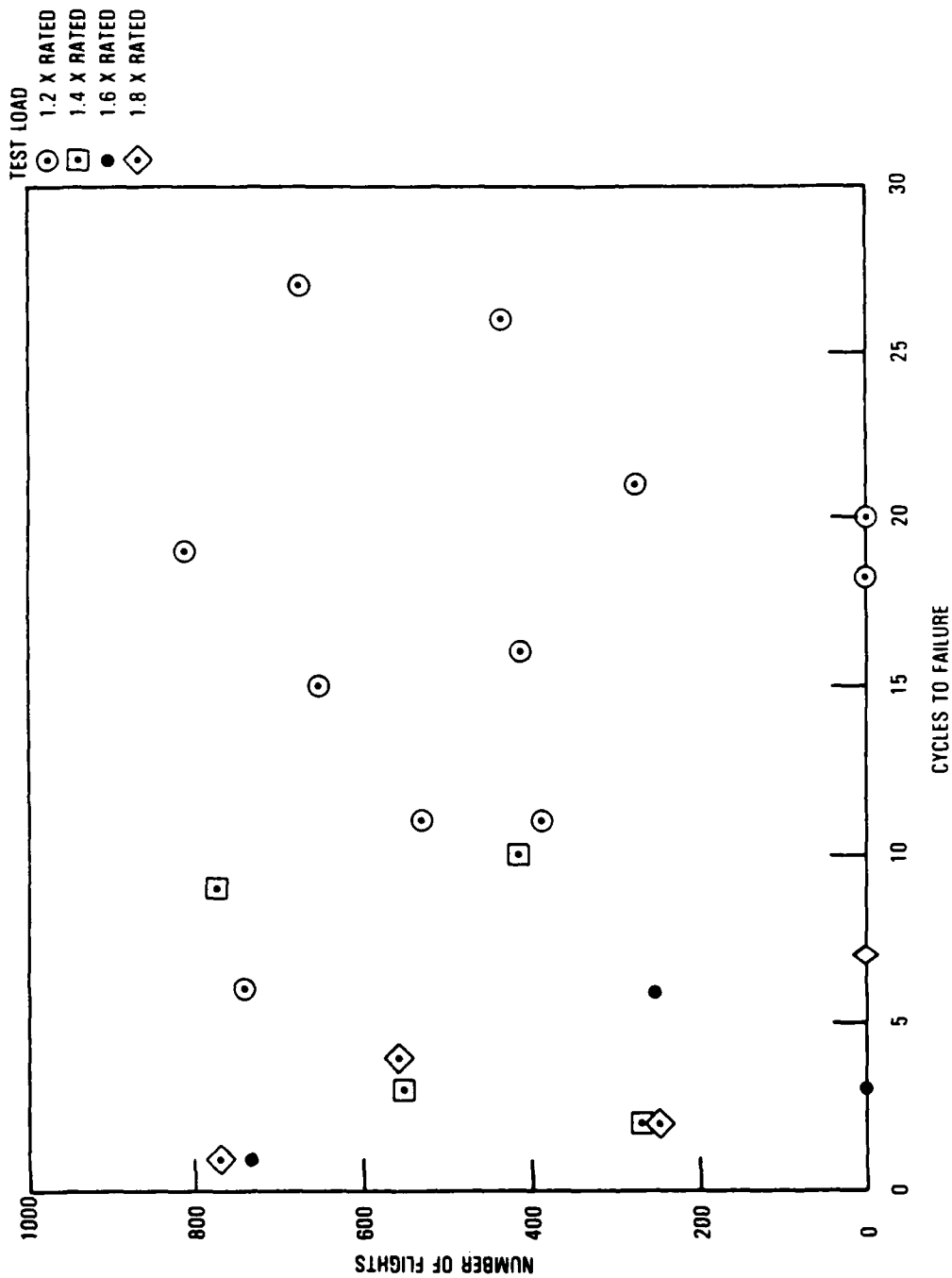
FIGURE 59.   50 x 20-20 TIRE, SERVICE TIRES CYCLES TO FAILURE

There are several potential reasons for the data scatter. Among them are: (1) the actual point at which failure occurred may not in fact be the point at which failure started; (2) a large difference in service experience although the number of landings were comparable; (3) the cycling test temperature of 350°F, while providing a margin of 75 percent of burst pressure, may have been too high; (4) manufacturing difference between tires; and (5) combinations of (1) through (4). The following comments are made regarding these potential causes for the data scatter:

1. Onset of Tire Failure - One evidence of the onset of tire failure is a change in the rate of temperature rise in successive cycles. An indication of the rise can be obtained by dividing the incremental increase in apex temperature by the number of revolutions in a cycle. Figures 60 and 61 show a distinct increase in the temperature rise per cycle. This rise occurs at 12 cycles in each case. Figure 62 shows the number of cycles to failure for a radial load of 1.2 times rated. The catastrophic failures are shown as crosses and the points at which the temperature rise occurred are denoted by circles (the number adjacent to each symbol indicates the test number). Except for test 21, the data show a much improved agreement. Using an exponential curve fitting technique, a curve is drawn as indicated in figure 62 for the points delineated as cycles to failure onset. The curve is based on all data except for test number 21, which was omitted because the number of cycles for both failure onset and catastrophic failure indicated an exceptional tire or a test condition deficiency.

2. Service Experience - There is indication that service experience with tires can vary, as can be seen in table 11. Although the number of landings varied only $\pm1.8$ percent, the variation in burst strength was $\pm9.5$ percent.

3. Cycle Test Temperature - The 350°F temperature used in the cycling tests was based on providing a test that would involve a reasonable number of cycles to failure in order to evaluate the life remaining in the service tires. An examination of figure 42 indicates that at 350°F the margin in average burst pressure is 75 percent; however, if scatter is included, this value is reduced to 48 percent. Taking into account that the tires were tested under a radial load of 1.2 times rated load, the margin at the 350°F level may have been too low for obtaining consistent results.

4. Manufacturing Differences - Burst pressure consistency is about the only measure of strength performance differences between tires of the same size. Examination of tables 11 and 12 indicates that, for 50 x 20-20 and 49 x 17 tires, the scatter in burst strength of new tires is $\pm5$ and $\pm4$ percent, respectively, which accounts for very little of the scatter encountered.

5. Combination of (1) through (4) - The combination of service experience and manufacturing differences is to be expected. Combining the variation of each and removing the variation attributed to the number of landings gives for the 50 x 20-20 tires a variation of about 1? percent. If the hypothesis that the increase in the rate of temperature rise can be considered as the onset of failure, the variation is about 19 percent. This indicates that there is about 8 percent variation that could be attributed to the cycling temperature used in the tests.
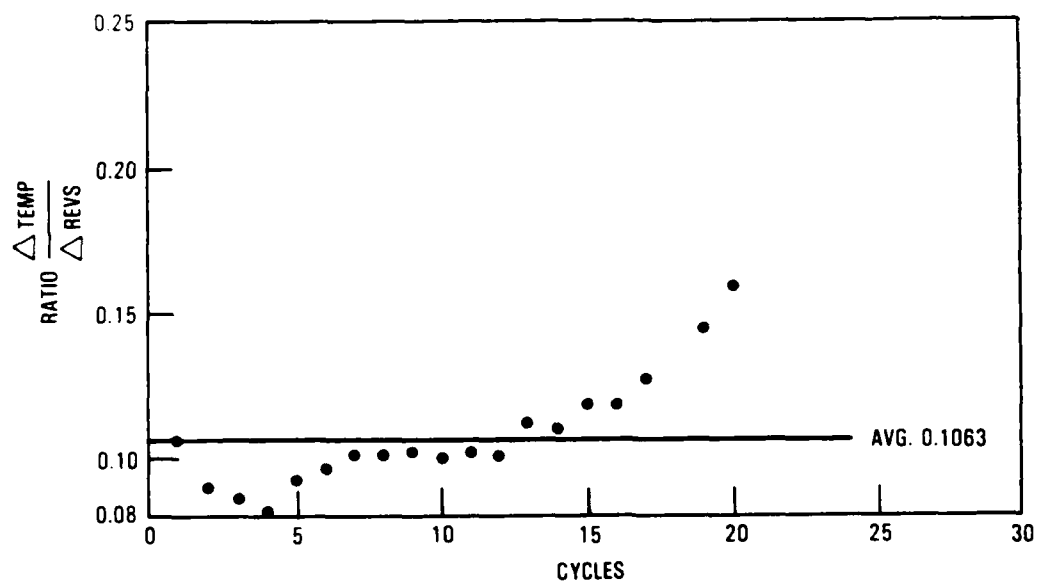
FIGURE 60.   50 x 20-20 TIRE, TEMPERATURE RISE PER REVOLUTION AS
A FUNCTION OF TEST CYCLES, NEW TIRE 34N
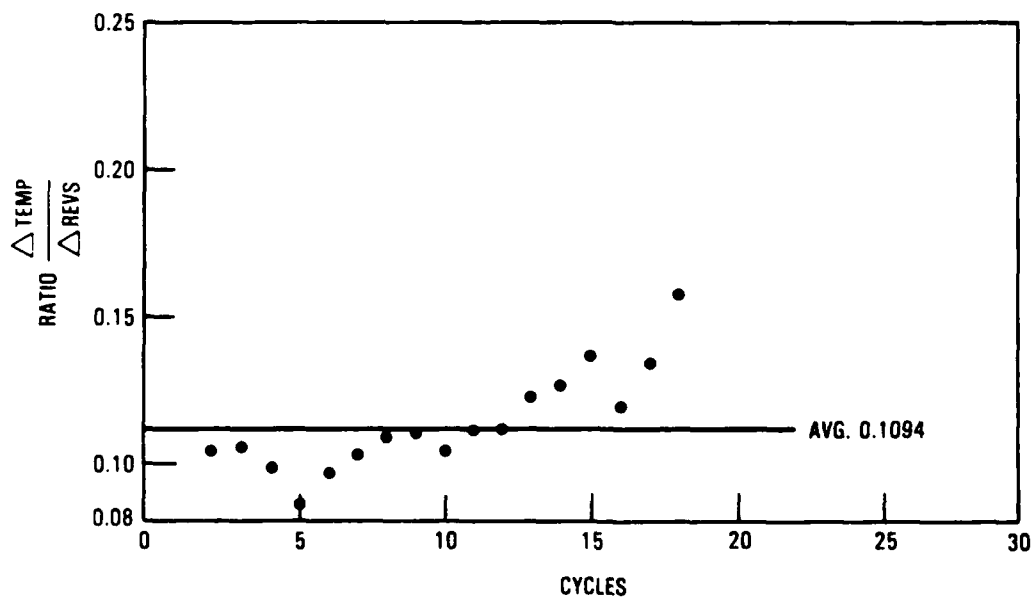


FIGURE 61.   50 x 20-20 TIRE, TEMPERATURE RISE PER REVOLUTION AS A
FUNCTION OF TEST CYCLES, NEW TIRE 48N
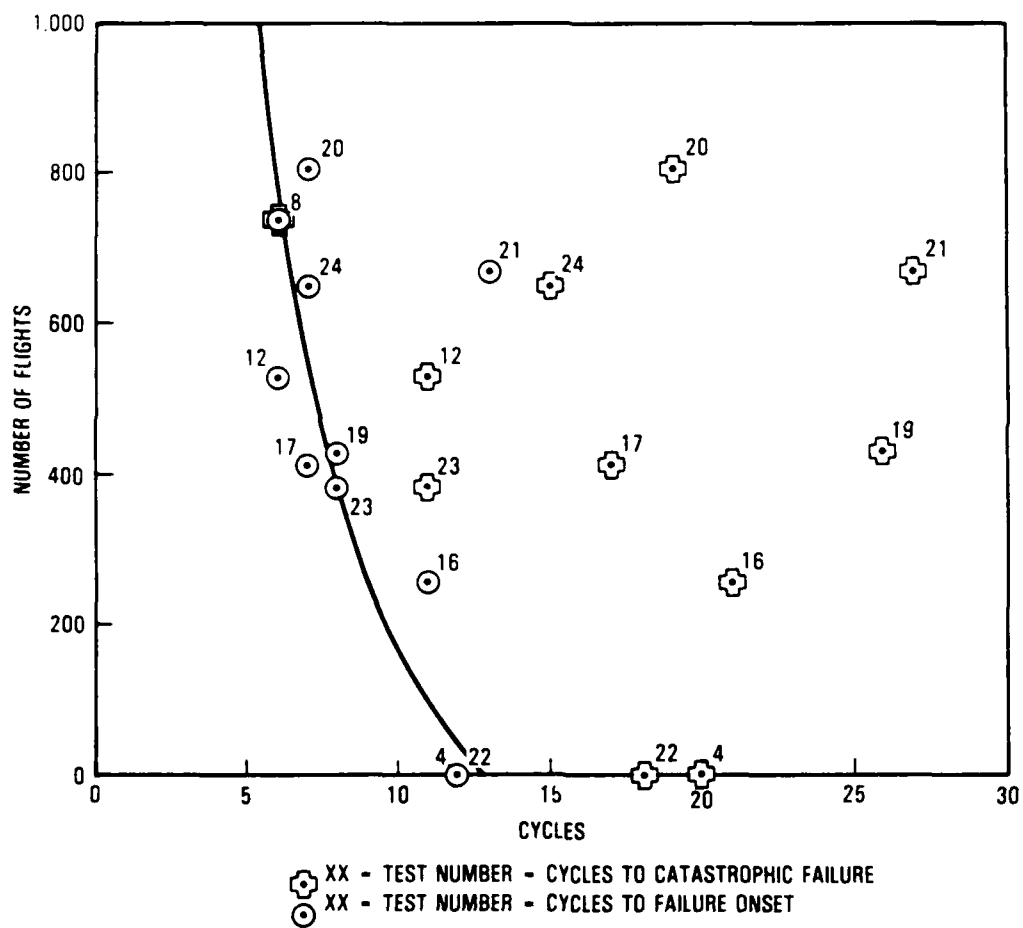
FIGURE 62. 50 x 20-20 TIRE, SERVICE TIRE TEST DATA SCATTER

Because of the scatter encountered during the cycling endurance tests, another method of testing to obtain consistent tire endurance data was tried. The method used requires that the tire apex temperature be kept constant at a certain value by varying the roll velocity. These tests are performed for various combinations of radial and apex temperatures until failure occurs. Prior to the failure of the test mandrel, the three data points given in table 16 were obtained. Using the temperature at which the tire will burst from the increase in tire pressure and the degradation of the carcass burst strength with temperature (see figure 42) as that temperature at which the tire will fail without rolling, the following exponential equation is developed:

$$N_R = 0.000491e^{\frac{4841.5}{T_A}}$$

TABLE 16.        DATA FROM CONSTANT APEX TEMPERATURE ROLL TESTS

| NUMBER | LOAD - KIPS | STABILIZED SPEED - MPH | | APEX TEMPERATURE DEGREES FAHRENHEIT | | | REVOLUTIONS AT TEMPERATURE |
|---|---|---|---|---|---|---|---|
| | | MIN | MAX | MIN | MAX | AVG | |
| 44-R-1 | 79.8 | 4.4 | 37.0 | 303 | 338 | 317 | 1,214 |
| 47-R-1 | 79.8 | 7.9 | 15.9 | 285 | 300 | 295 | 7,628 |
| 40-R-1 | 79.8 | 8.8 | 15.0 | 281 | 294 | 290 | 11,374 |

where
    $N_R$ = Number of revolutions and $T_A$ = Tire apex temperature - $^{\circ}F$

The correlation coefficient for the equation is 0.977, which is a satisfactory curve fit.

Carcass Fatigue. Using the exponential equation obtained from the constant apex temperature roll tests, a fatigue curve for the 1.4 times rated load is estimated, as shown in figure 63. In order to illustrate the method for developing the fatigue life, other curves have been arbitrarily drawn to represent other loading conditions.

To illustrate the procedure for developing the fatigue life, only the takeoff portion of the long range scenarios (see figures 25 through 30) will be used. The average tire apex temperature, the incremental tire revolutions, and the percent of flights are arranged as shown in table 17. The number of revolutions per flight is obtained by multiplying the percent of flights by the number of revolutions for takeoff for each of the missions. If the manufacturer desires the tire carcass to perform for 2,000 flights, the revolutions per flight are multiplied by 2,000. The damage that the tire will incur is obtained by dividing the number of revolutions under a given combination of temperature and load by the allowable revolutions for that condition using figure 63. The first point on table 17 is used as an illustration in figure 63.

70
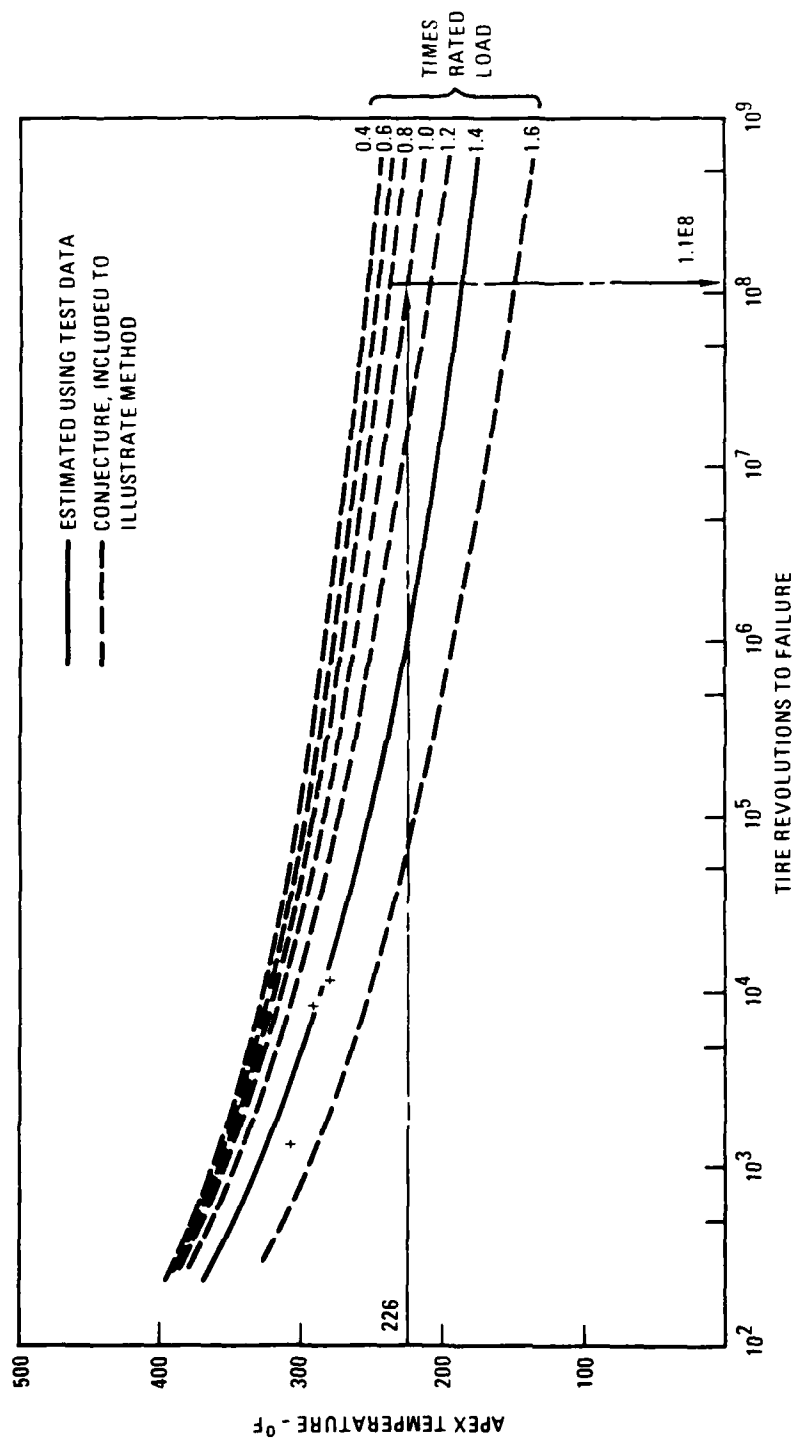
FIGURE 63. ESTIMATED CARCASS LIFE FOR VARIOUS COMBINATIONS OF APEX TEMPERATURES AND LOADS

71

To obtain the total damage the tire will incur during all takeoffs made with the carcass, add the damages in table 17. The value for this illustration is 0.116. The same procedure is followed for all the other events which constitute a flight in the scenarios. When all the damages are added, they should not exceed a value of 1.0. If a value of 1.0 is exceeded, the tire can be expected to fail. Since tire failures can result in costly repairs to the airplane, some margin of safety needs to be established. Some airframe manufacturers try to demonstrate by tests that their product has twice the planned life. If this value is applied to the tire, it would mean that the life of the tire will be exceeded when the damage reaches 0.5.

## FLIGHT TESTS.

Flight tests were performed with instrumented 50 x 20-20 34 ply rating tires simulating a flight which included taxi to takeoff, takeoff, landing, taxi after landing and parking at the ramp.

## TEST PROCEDURE.

Test Measurements. The test measurements included the following:

1.  Tire apex temperature (see figure 44) on the inside and outside of the inboard and outboard rear tires of the left main landing gear.

2.  Tire shoulder temperature (see figure 44) the inside and outside of the inboard and outboard rear tires of the left main landing gear.

3.  Tire pressure for the inboard and outboard rear tires of the left main landing gear.

4.  Left main landing gear vertical, lateral and drag loads.

5.  Brake pressure and temperature of the inboard and outboard rear wheels of the left main landing gear.

6.  Ground speed.

Test Method. Because it was not practical to take measurements continuously, records were made at significant events such as turns, takeoff and landings. In the case of each event, measurements on a time history basis were taken for the entire length of the event.

TEST RESULTS. Table 18 presents a summary of data for various taxi events for Test 1648. The start and ending times are given for each event, along with the corresponding measurements. Plotting the tire apex and shoulder temperatures on a time history basis, such as shown in figure 64, indicates that the greatest increase in temperature was experienced during the takeoff and landing runs. The periods from 8:29:20 to 8:34:36 and 8:46:05 to 8:49:30 show a decline in apex temperature which, since the airplane was being taxied, is opposite to what would be expected. One explanation may be that during this period the airplane, having been taxied, stood still, allowing the temperature to drop sufficiently to overcome the increase from taxiing during these periods. The shoulder temperature is much lower, which is consistent with extensive dynamometer tests performed by a tire manufacturer prior to this program.

72

TABLE 17. SAMPLE SPECTRUM DEVELOPMENT

| AVERAGE TAKEOFF SEGMENT APEX TEMP. °F | TAKEOFF ROLL INCREMENTAL REVOLUTIONS PER TAKEOFF SEGMENT | PERCENT OF FLIGHTS | REVOLUTIONS FOR ONE FLIGHT | REVOLUTIONS FOR 2000 FLIGHTS | LOAD RADIAL/RATED | ALLOWABLE REVOLUTIONS (FROM FIGURE 3 20) | DAMAGE ACT. REVS/ALLOW. REVS |
|---|---|---|---|---|---|---|---|
| 226 | 53 | 5.2 | 2.8 | 5,600 | 1.01 | 1.1E8 | 0 |
| 236 | 133 | | 6.9 | 13,800 | | 2.0E7 | 0.001 |
| 255 | 194 | | 10.1 | 20,200 | | 2.0E6 | 0.010 |
| 274 | 161 | | 8.4 | 16,800 | | 2.0E5 | 0.084 |
| 216 | 53 | 17.4 | 9.2 | 18,400 | 0.91 | ∞ | 0 |
| 227 | 133 | | 23.1 | 46,200 | | 3.0E8 | 0 |
| 246 | 194 | | 33.8 | 67,600 | | 1.5E7 | 0.005 |
| 261 | 78 | | 13.6 | 27,200 | | 2.0E6 | 0.014 |
| 206 | 46 | 12.2 | 5.6 | 11,200 | 0.818 | ∞ | 0 |
| 214 | 116 | | 14.2 | 28,400 | | ∞ | 0 |
| 230 | 168 | | 20.5 | 41,000 | | 1.5E8 | 0 |
| 246 | 140 | | 17.1 | 34,200 | | 1.5E7 | 0.002 |
| 184 | 36 | 12.2 | 4.4 | 8,800 | 0.736 | ∞ | 0 |
| 190 | 91 | | 11.1 | 22,200 | | ∞ | 0 |
| 202 | 132 | | 16.1 | 32,200 | | ∞ | 0 |
| 214 | 110 | | 13.4 | 26,800 | | ∞ | 0 |
| 183 | 36 | 26.5 | 9.5 | 19,000 | 0.729 | ∞ | 0 |
| 189 | 91 | | 24.1 | 48,200 | | ∞ | 0 |
| 200 | 132 | | 35.0 | 70,000 | | ∞ | 0 |
| 212 | 110 | | 29.2 | 58,400 | | ∞ | 0 |
| 170 | 30 | 26.5 | 8.0 | 16,000 | 0.652 | ∞ | 0 |
| 174 | 74 | | 19.6 | 39,200 | | ∞ | 0 |
| 182 | 108 | | 28.6 | 57,200 | | ∞ | 0 |
| 191 | 90 | | 23.9 | 47,800 | | ∞ | 0 |

TABLE 18. SUMMARY OF TAXI TESTS 50 x 20-20 TIRE, FLIGHT 1702, 6/3/81, TEST 1648

| TIME | LEFT MAIN GEAR LOADS – KIPS | | | TIRE TEMPERATURE – °F | | | | | | | | TIRE PRESS – PSI | | BRAKE TEMP – °F | | GROUND SPEED – KNOTS | EVENT |
| | | | | APEX | | | | SHOULDER | | | | | | | | | |
| | VERT. | LAT. | DRAG | ① IIR | ② OIR | ③ I2R | ④ O2R | IIR | OIR | I2R | O2R | IR | 2R | IR | 2R | | |
|---|---|---|---|---|---|---|---|---|---|---|---|---|---|---|---|---|---|
| 8:28:50 | 190 | 0 | 3.0 | 118.4 | 118.4 | – | – | -.- | 105.8 | 96.8 | 116.6 | 190 | 194 | 113.0 | 113.0 | 15.5 | } LEFT TURN |
| 8:29:20 | 200 | 0 | 3.0 | 120.2 | 120.2 | – | – | – | 105.8 | 96.8 | 118.4 | 190 | 194 | 127.4 | 138.2 | 15.5 | |
| 8:34:36 | 200 | 0 | 3.0 | 116.6 | 118.4 | – | – | – | 104.0 | 104.0 | 111.2 | 194 | 201 | 190.4 | 185.0 | 0 | } TAKEOFF RUN |
| 8:35:21 | 0 | 0 | 0 | 176.0 | 185.0 | – | – | – | 132.8 | 123.8 | 176.0 | – | – | 190.4 | 183.2 | 164.9 | |
| 8:39:43 | 0 | 0 | 0 | 141.8 | 136.4 | – | – | – | 98.6 | 100.4 | 105.8 | 197 | 205 | 141.8 | 120.2 | 158.4 | } LANDING RUN |
| 8:40:29 | 200 | 0 | – | 199.4 | 206.6 | – | – | – | 120.2 | 113.0 | 134.6 | – | – | 266.0 | 246.2 | 52.5 | |
| 8:40:30 | 200 | 0 | – | 199.4 | 206.6 | – | – | – | 120.2 | 113.0 | 134.6 | – | – | 266.0 | 246.2 | 52.5 | } RIGHT TURN |
| 8:41:00 | 210 | 0 | 3.0 | 194.0 | 194.0 | – | – | – | 116.6 | 111.2 | 131.0 | 207 | 219 | 379.4 | 352.4 | 11.1 | |
| 8:41:18 | 198 | 0 | – | 190.4 | 190.4 | – | – | – | 114.8 | 111.2 | 131.0 | 207 | 220 | 415.4 | 428.0 | 8.9 | } LEFT TURN |
| 8:41:48 | 205 | 0 | – | 190.4 | 190.4 | – | – | – | 114.8 | 111.2 | 131.0 | 207 | 222 | 453.2 | 437.0 | 17.8 | |
| 8:45:35 | 195 | 0 | – | 210.2 | 208.4 | – | – | – | 122.0 | 120.2 | 131.0 | 213 | 232 | 496.4 | 498.2 | 8.9 | } RIGHT TURN |
| 8:46:05 | 203 | 0 | – | 210.2 | 210.2 | – | – | – | 122.0 | 123.8 | 136.4 | 215 | 233 | 503.6 | 510.8 | 6.3 | |
| 8:49:30 | 195 | 0 | 15.0 | 197.6 | 195.8 | – | – | – | 132.8 | 143.6 | 145.4 | 216 | 233 | 540.5 | 539.6 | 0.4 | } SMALL RADIUS PUSH BACK TURN |
| 8:50:00 | 193 | 26 | 20.0 | 197.6 | 192.2 | – | – | – | 132.8 | 143.6 | 147.2 | 223 | 234 | 536.0 | 536.0 | 0 | |

① INSIDE OF TIRE, OUTBOARD REAR WHEEL
② OUTSIDE OF TIRE, OUTBOARD REAR WHEEL
③ INSIDE OF TIRE, INBOARD REAR WHEEL
④ OUTSIDE OF TIRE, INBOARD REAR WHEEL

74
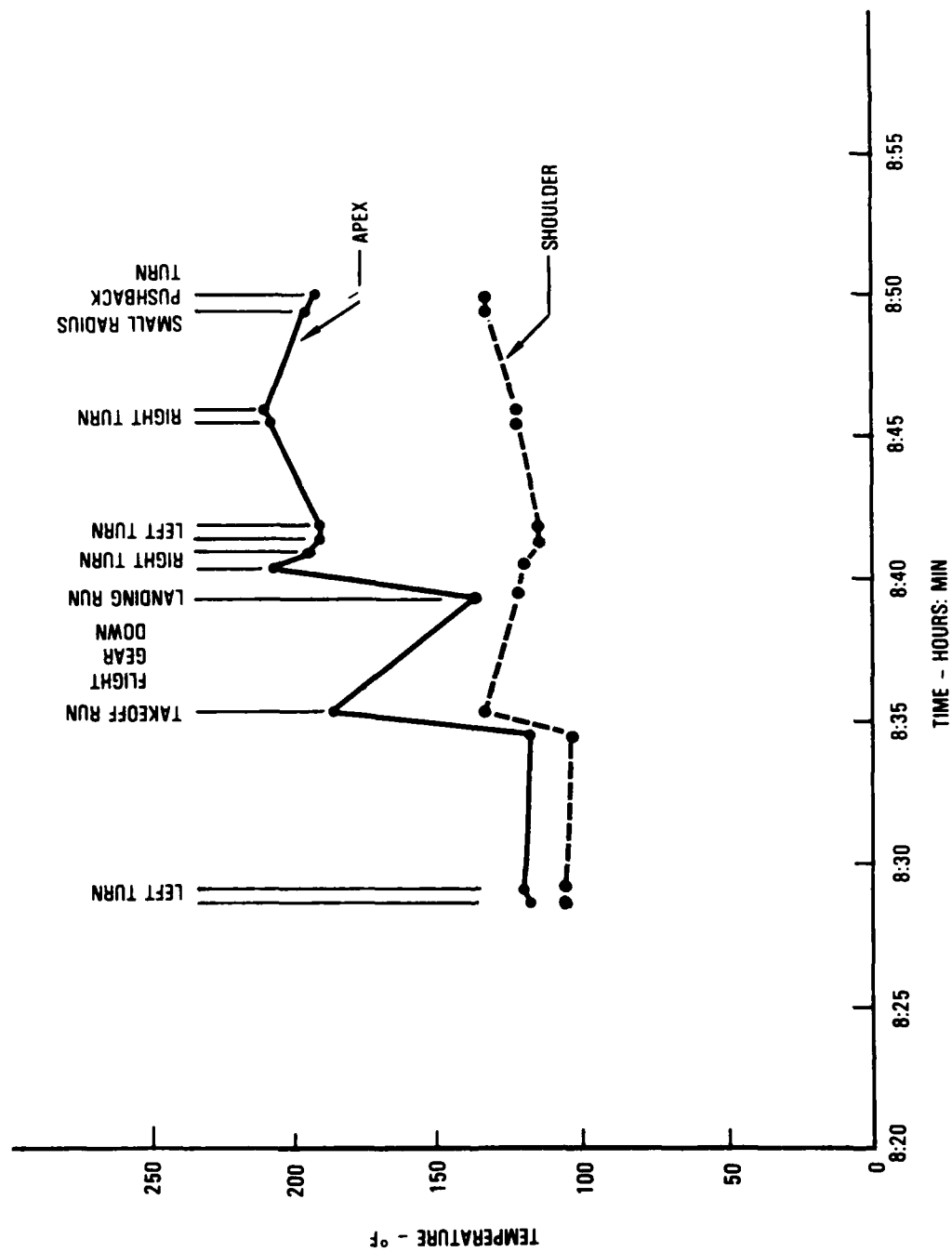
FIGURE 64.   50 x 20-20 TIRE TEMPERATURE, OUTSIDE OF OUTBOARD REAR TIRE, FLIGHT 7026, 6/3/81, TEST 1640

75

ADHESION TESTS.

In an attempt to set appropriate minimum adhesion values for rulemaking, a study
was undertaken.  Adhesion values were obtained from an extensive sample of the
tires in service from the national population of large U.S. aircraft.  The study
(reference 5) concluded that the adhesion values followed a normal distribution;
hence, small samples taken from the production of a single manufacturer could be
used to determine whether the process was in control.

The study determined that the national mean values for the outer ply adhesion of
a tire is 39.8 lb/inch.  The three sigma point, based on a sample having normal
distribution, is about 20 lb/inch.  These values form the basis for the
algorithm used in determining the lower threshold limits used in AC 145-4.

The study did not permit reliable correlation of adhesion values with retread
level.  Figure 65 shows data taken from a sample of about one hundred and fifty
tires, consisting of seven sizes from three different manufacturers (reference
6).  The difficulty in concluding that the adhesion degrades with time comes
from the fact that the sample is small with respect to the number of variables,
and the measurement data spread is very great.

Also, while existing data provides an indication that some degradation occurs in
an aircraft tire with use, no conclusive proof was found to indicate when
unairworthy tires needed to be removed from service.  Therefore, another study
was undertaken, which provided sufficient data to estimate, from an engineering
analysis basis, the point at which tires may fall below an airworthiness limit.

In this study, an experiment was conducted to correlate adhesion values in tires
with time at temperature (reference 7).  The two primary causes of degradation
were found to be cyclic stress from rolling through the contact patch, and heat
from internal friction within the tire body due to flexing.  Of the two factors
- stress and temperature - temperature is the more important, since under proper
conditions, tires can operate over distances and times far in excess of those
required in service.

TEST PROCEDURE.  The test procedure consisted of taking sample coupons 1 inch by
about 4 inches from the shoulder of a tire retreaded once; exposing them to
different periods of aging in an oven at elevated temperature; slitting the end
between the outermost ply and the next outermost; and conducting tensile tests
of the samples.  Two sets of test specimens were aged, one in air, and the other
in nitrogen.  The test is further described in AC 145-4, and in reference 4.

TEST RESULTS.  Figure 65 shows the results of the experiment.  It seems clear
that adhesion is related to time at temperature.  In particular, tires exposed
to temperatures of as low as 220°F encounter reduced adhesion values.

To determine the impact of temperature on the service life of a tire, the
relationship between time-at-temperature and the time-in-service (during which a
tire is above a given temperature threshold) was established as follows:
Retread operations occur at roughly fixed intervals during the service life of a
tire, which varies with aircraft type, load, and the severity of the service
environment.  A reasonable industry average is about 225 landings between
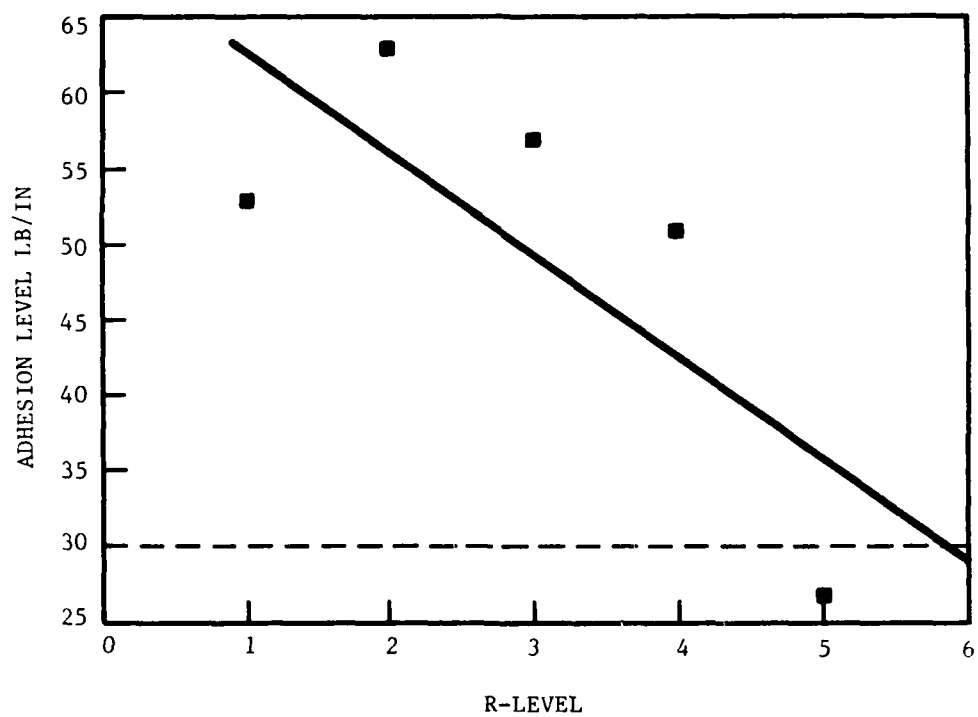
FIGURE 65. PLY ADHESION AS A FUNCTION OF R-LEVEL

77

retreads. From scenario data included herein, it can be determined that tires on long and intermediate haul aircraft above 85 percent gross takeoff weight spend about 40 minutes above 220°F during each takeoff-landing cycle. From figure 66, an approximately 50 percent loss of adhesion in nitrogen for a sample exposed to 200°F for about 1000 hours can be seen. Thus, it will require about 1500 landings, or, at 225 landings per retread, 6.7 retreads for the average tire in severe service, to reach its lower adhesion threshold of 50 percent.

## CONCLUSIONS

### GENERAL.

It is clear that, given the diversity of performance parameters, there are no hard-and-fast rules for establishing the fatigue life of tires. Indeed, tires having been retreaded ten times are not uncommon; particularly on nosewheels or under light load conditions. Similarly, particularly severe service conditions can necessitate limitations of as little as one or two retreads. Using a more rigorous application of the principles described here, it may be possible to predict the life of a tire for a given service environment. The data in this report suggest a finite safe upper service limit for tires used in service having some threshold level of severity.

### SPECIFIC.

1.  A correlation exists between the tire heating model developed in this work and dynamometer experiments.

2.  Although no rigorous correlation was obtained, a close relationship was established between the temperature performance of tires during flight testing and dynamometer testing.

3.  A relationship exists between the time above a given temperature of a tire and its rubber-ply adhesion values. Adhesion varies inversely with exposure to time at temperature.

4.  It is possible to rigorously determine the fatigue state of a tire if sufficient information is known about its service history.

5.  Tire burst pressure is lower at increasing R-levels.
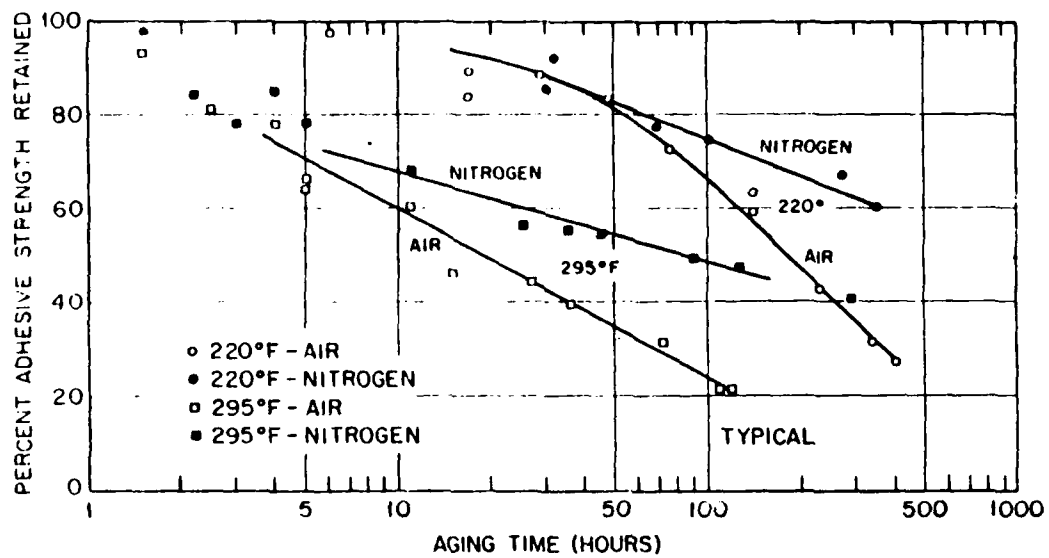
FIGURE 66. ADHESIVE STRENGTH RETAINED VS. AGING TIME

## REFERENCES

1. Trivisonno, N.M., <u>Thermal Analysis of a Rolling Tire</u>, SAE700474, 1970.

2. Prevorsek, D.C. et al., <u>Analysis of Tire Deformation in Operation from the Data of Temperature Rise</u>, SAE800181, 1980.

3. Brookwan, B.J., <u>Transient Thermal Effects in Disc Brakes</u>, AFFDL-TR-79-3112, 1979.

4. Durup, P.C., <u>Improvement of Overload Capability of Air Carrier Aircraft Tires</u>, FAA RD-78-133, 1978.

5. Bobo, S.N., <u>Adhesion Testing of Aircraft Tires</u>, NASA Publication 2264. Proceedings of workshop held at Langley Research Center, Hampton, VA, September 7-9, 1982.

6. Private Communications with S. Bobo, October 1981:

   H.E. Davis, Thompson Aircraft Tire Co.
   J. Ripley, Goodyear Tire and Rubber Co.
   Z.S. Lee, B.F. Goodrich
   C. Shaver, Air Treads Inc.

7. Clark, S.N., <u>Loss of Adhesion in Cord-Rubber Composites</u>, U.S. Department of Transportation, Transportation Systems Center, Cambridge, MA, October 1984.

## APPENDIX A

### SCENARIO APPLICATION FORMAT FOR TIRE APEX
### AND GAS TEMPERATURE RISE

The following procedure presents a step-by-step method for application of the apex and contained air heating equations to operational scenarios.

1. NONRECURRING DATA FOR A GIVEN TIRE (See Table A-1 for data of selected tires)

$\delta_O$ = Tire stiffness no load intercept - in.

$w$ = tire width - in.

$d_O$ = Tire undeflected diameter - in.

$P_R$ = Tire rated pressure - psi

$\delta_{100}$ = Maximum tire deflection-in.

$R$ = Tire stiffness factor

$A$ = 1/3 tire exposed area - sq. in.

$m$ = 1/3 tire weight - pounds

$Vol$ = Total tire contained gas volume - cub. in.

$\nu$ = Ratio of convective heat transfer coefficients

$T_A$ = Ambient temperature - $^O$F

2. TIRE DEFLECTION EQUATION - PERCENT

$$\delta_{TZ} = \frac{7.5 F_Y}{\delta_{100}(P_{a1} + 0.24 P_R)\{w - 0.7(\delta_O + RF_Z)\}}$$

$$+ \frac{100(\delta_O + RF_Z)}{100} + \frac{16.67 F_x}{\delta_{100}(P_{a1} + 4P_R)\{d_O^2(\delta_O + RF_Z)\}^{\frac{1}{3}}}$$

$$P_{a1} = \frac{P_{ao}(459 + T_{a1})}{(459 + T_{ao})}$$

TABLE A-1.   TIRE DATA

| Tire | $\delta_o$ in. | w in. | $d_o$ in. | $P_R$ psi | $\delta_{100}$ in. | R | m lbs. | Vol. cu. in. | $\upsilon$ | A sq. in. |
|---|---|---|---|---|---|---|---|---|---|---|
| 52 x 20.5 - 20 36 PR | 0.8 | 20.05 | 51.27 | 200 | 14.4 | $0.000128e^{(-0.00416P_a)}$ | 110 | 45,210 | 0.43 | 1501 |
| 50 x 20 - 20 34 PR | 0.75 | 19.7 | 49.13 | 205 | 12.69 | $0.000134e^{(-0.00420P_a)}$ | 100 | 39,194 | 0.43 | 1414 |
| 50 x 20 - 20 30 PR | 0.60 | 19.49 | 49.60 | 175 | 12.61 | $0.000141e^{(-0.00398P_a)}$ | 90 | 39,194 | 0.43 | 1414 |
| 40 x 14 28 PR | 0.70 | 13.87 | 39.37 | 200 | 10.06 | $0.000174e^{(-0.00384P_a)}$ | 41 | 11,592 | 0.49 | 729 |
| 40 x 14 24 PR | 0.50 | 13.79 | 39.54 | 170 | 10.5 | $0.000206e^{(-0.00488P_a)}$ | 46 | 11,592 | 0.49 | 729 |

• Recurring Data

$F_Z$ = Tire radial load - pounds

$F_Y$ = Tire lateral load - pounds

$F_X$ + Tire drag load - pounds

$P_a$ = Tire pressure - psi

3.  INCREMENTAL TIRE APEX TEMPERATURE - $^{O}F$

$$\Delta T = \Delta T_f (1 - e^{-\frac{t}{\tau}})$$

where

$$\Delta T_f = \frac{\mu_o F_Z V + H T_A}{H + \alpha F_Z V} - T_o$$

$$= \frac{338.43m}{H + \iota F_Z V}$$

$$t = \frac{\tau N_s}{12V}\left[d_o - \frac{2}{3}(\ell_o + RF_Z)\right]$$

$$\mu_o = 0.01432 C_V C_\iota$$

$$H = 0.0003A(5 + 0.614V_A)$$

$$\iota = (32.58E - 6)C_V C_\ell$$

• Recurring Data

$T_o$ = Starting apex temperature - $^{O}F$

$V$   = Airplace velocity - fps

$V_A$ = Air Velocity over wheel - fps

$N_S$ =  Number of Revolutions

4. INCREMENTAL TIRE CONTAINED GAS TEMPERATURE - °F

$$\Delta T_A = Me^{-\frac{t}{\tau_a}} + Ne^{-\frac{t}{\tau}} + T_{af} - T_{do}$$

$$M = T_{ao} - T_{af} - N$$

$$N = \beta 3 \Delta T_f$$

$$T_{af} = \nu(T_o + \Delta T_f - T_w) + T_w$$

$$\beta = \frac{\tau}{\tau_a - \tau}$$

$$\tau_a = 0.01095 \text{ Vol}$$

- Recurring Data

  $T_{ao}$ = Starting contained gas temperature - °F

  $T_w$ = Wheel temperature - °F

Sequence

1. Solve for $\delta TZ_{RATED}$ by inputting rated load and pressure.

2. Solve for $\delta_{TZ}$ for initial conditions.

3. Determine $C_\delta$ from $\delta_{TZ}/\delta_{TZ_{RATED}}$ versus $C_\delta$ curve (see figure 5).

4. Determine $C_V$ from $C_V$ versus V curve (see figure 4).

5. Enter recurring data: $F_Z$, $F_Y$, $F_X$, $P_A$, $T_O$, V, $V_A$, $N_S$, $T_{AO}$, $T_W$.

6. Solve for $\Delta T$

7. $T_{o1} = \Delta T + T_o$

8. Solve for $\Delta T_a$

9. $T_{ao1} = \Delta T_a + T_{ao}$

10. Solve for $P_{a1}$; $P_{a1} = P_{ao}$ for next iteration.

11. Enter recurring data for next step: $F_{Z1}$, $F_{Y1}$, $F_{X1}$, $P_{a1}$, $T_{o1}$, $V_{A1}$, $N_{s1}$, $T_{ao1}$, $T_{w1}$, $C_{\delta 1}$, $C_{v1}$

(Usually $T_{W1} = T_{ao1}$ and $V_1 = V_{A1}$ if no outside wind velocity. Direction of wind relative to taxi direction determines value of $V_{A1} = V + V_W$.)

Process repeats for each step in taxi. Changing velocity such as takeoff and landing is performed in increments of velocity (around 20 fps increments).
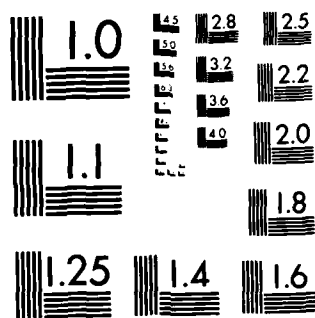
MICROCOPY RESOLUTION TEST CHART

NATIONAL BUREAU OF STANDARDS-1963-A

# APPENDIX B

## SUMMARY OF RADIAL AND LATERAL
## DYNAMOMETER LOADS

Tables B-1 and B-2 present a summary of the dynamometer test results for the 50 x 20-20 and 40 x 14 tires, respectively. Tables B-3 and B-4 give a synopsis of the tire failure modes for the 50 x 20-20 and 40 x 14 tires, respectively. The test conditions can be obtained from table 12 in the text by use of the tire code numbers. Twenty-two out of 27 50 x 20-20 tires and 22 out of 27 40 x 14 tires failed in the lower sidewall. Of the tires that did not fail in the lower sidewall, four of each size failed under the same test conditions and failed in the crown or shoulder areas. Of the lower sidewall failures, all but two occurred on the nonserial number side of the tire. In the case of the 50 x 20-20 tires, 9 failures occurred, with the thermocouples being in the failure areas. Of these cases, 6 were failures that went 360 degrees around the sidewall of the tire, thus casting some doubt as to the thermocouple being the point of origin of some of these failures.

TABLE B-1.  SUMMARY OF 50 x 20-20 TIRE DYNAMOMETER TEST RESULTS

| Number | Load | | | | | | | | Temperature °F | | | | | | Contained Gas Press Loaded – PSI | | Number of Revolutions |
|---|---|---|---|---|---|---|---|---|---|---|---|---|---|---|---|---|---|
| | Radial | | | | Lateral | | | | Apex | | | | Contained Gas | | | | |
| | Kips | | Radial/Rated | | Kips | | Lateral/Radial | | Inside | | Outside | | | | | | |
| | Req. | Act | Req | Act | Req | Act | Req | Act | Start | Failure | Start | Failure | Start | Failure | Start | Fail | |
| 22-N | 45.6 | 45.7 | 0.80 | 0.80 | 0 | 0.19 | 0 | 0 | 63 | 415 | 65 | 415 | 65 | 270 | 244 | 324 | 21,786 |
| 1-N | 57.0 | 55.8 | 1.00 | 0.98 | 0 | 0.28 | 0 | 0 | 89 | – | 89 | 460 | 80 | 158 | 245 | 307 | 8,030 |
| 15-N | 68.4 | 69.6 | 1.20 | 1.22 | 0 | 0.29 | 0 | 0 | 66 | 436 | 73 | 425 | – | – | 249 | 300 | 3,181 |
| 30-N | 79.8 | 79.0 | 1.40 | 1.39 | 0 | 0.19 | 0 | 0 | 85 | 417 | 89 | – | 90 | 196 | 251 | 299 | 2,176 |
| 13-N | 91.2 | 89.7 | 1.60 | 1.57 | 0 | 0.27 | 0 | 0 | 84 | – | 83 | – | 93 | 183 | 254 | 296 | 1,498 |
| 10-N | 102.6 | 99.5 | 1.80 | 1.75 | 0 | 0.16 | 0 | 0 | 80 | 419 | 83 | – | 88 | 166 | 257 | 292 | 1,142 |
| 28-N | 114.0 | 113.2 | 2.00 | 1.99 | 0 | 0.36 | 0 | 0 | 84 | 454 | 84 | – | 85 | 152 | 260 | 293 | 880 |
| 23-N | 22.8 | 21.8 | 0.40 | 0.38 | 2.28 | 2.56 | 0.10 | 0.12 | 79 | 264 | 78 | 198 | 85 | 220 | 240 | 281 | 35,265 |
| 16-N | 34.2 | 33.7 | 0.60 | 0.58 | 3.42 | 3.72 | 0.10 | 0.11 | 70 | 388 | 72 | 266 | 79 | 240 | 241 | 297 | 28,693 |
| 8-N | 45.6 | 45.3 | 0.80 | 0.79 | 4.56 | 4.97 | 0.10 | 0.11 | 65 | – | 55 | 290 | – | 241 | – | 294 | 11,500 |
| 12-N | 57.0 | 57.5 | 1.00 | 1.01 | 5.70 | 5.78 | 0.10 | 0.10 | 95 | – | – | – | 87 | 206 | 248 | 300 | 4,176 |
| 18-N | 68.4 | 67.8 | 1.20 | 1.19 | 6.84 | 7.39 | 0.10 | 0.11 | 72 | 359 | 73 | 242 | 82 | 174 | 248 | 289 | 2,126 |
| 19-N | 79.8 | 79.2 | 1.40 | 1.39 | 7.98 | 8.69 | 0.10 | 0.11 | 63 | 400 | 65 | 254 | 77 | 156 | 250 | 287 | 1,341 |
| 7-N | 91.2 | 90.2 | 1.60 | 1.58 | 9.12 | 10.01 | 0.10 | 0.11 | 74 | 400 | 74 | 255 | 92 | 155 | 254 | 284 | 929 |
| 6-N | 102.6 | 100.8 | 1.80 | 1.77 | 10.26 | 11.17 | 0.10 | 0.11 | 63 | 426 | 65 | 224 | 70 | 122 | 257 | 282 | 664 |
| 5-N | 114.0 | 110.5 | 2.00 | 1.94 | 11.40 | 12.47 | 0.10 | 0.11 | 88 | 444 | 94 | 270 | 99 | 134 | 260 | 283 | 546 |
| 11-N | 34.2 | 33.0 | 0.60 | 0.56 | 6.84 | 7.11 | 0.20 | 0.22 | 86 | 415 | 88 | 214 | 90 | 233 | 241 | 295 | 15,530 |
| 9-N | 45.6 | 44.8 | 0.80 | 0.79 | 9.12 | 9.56 | 0.20 | 0.21 | 84 | 468 | 82 | 179 | 93 | 196 | 244 | 287 | 4,943 |
| 4-N | 57.0 | 57.5 | 1.00 | 1.01 | 11.40 | 11.56 | 0.20 | 0.20 | 82 | – | 83 | – | 81 | 161 | 246 | 284 | 2,253 |
| 25-N | 68.4 | 66.6 | 1.20 | 1.17 | 13.68 | 14.20 | 0.20 | 0.25 | 81 | 399 | 82 | 179 | 101 | 161 | 248 | 276 | 1,328 |
| 14-N | 79.8 | 78.2 | 1.40 | 1.37 | 15.96 | 16.69 | 0.20 | 0.21 | 72 | 402 | 75 | 172 | 89 | 142 | 251 | 277 | 889 |
| 21-N | 91.2 | 89.6 | 1.60 | 1.57 | 18.24 | 19.19 | 0.20 | 0.21 | 71 | 435 | 71 | 166 | 80 | 278 | 254 | 278 | 688 |
| 26-N | 102.6 | 101.5 | 1.80 | 1.78 | 20.52 | 21.64 | 0.20 | 0.21 | 85 | 400 | 84 | 185 | 98 | 129 | 257 | 277 | 449 |
| 2-N | | | 0.8 | | | | 0.30 | | Aborted | | | | | | | | |
| 20-N | 57.0 | 56.7 | 1.00 | 0.99 | 17.10 | 16.50 | 0.30 | 0.29 | 90 | 380 | 90 | 120 | 83 | 147 | – | – | 1,744 |
| 27-N | 68.4 | 68.7 | 1.20 | 1.21 | 20.52 | 21.40 | 0.30 | 0.31 | 89 | 407 | 88 | 135 | 96 | 142 | 249 | 274 | 947 |
| 3-N | 79.8 | 80.3 | 1.40 | 1.41 | 23.94 | 24.90 | 0.30 | 0.31 | 67 | 421 | 67 | 122 | 80 | 127 | 251 | 277 | 744 |

TABLE B-2.  SUMMARY OF 40 x 14 TIRE DYNAMOMETER TEST RESULTS

| | Load | | | | | | | | Contained Gas | | | | |
|---|---|---|---|---|---|---|---|---|---|---|---|---|---|
| | Radial | | | | Lateral | | | | Temperature °F | | Press Loaded – PSI | | |
| | Kips | | Radial Rated | | Kips | | Lateral Radial | | | | | | |
| Number | Req | Act | Req | Act | Req | Act | Req | Act | Start | Failure | Start | Fail | Number of Revolutions |
| 7-N | 22.2 | 21.7 | 0.80 | 0.78 | 0.00 | 0.20 | 0.00 | 0.01 | 70 | 287 | 196 | 270 | 39,574 |
| 5-N | 27.7 | 27.8 | 1.00 | 1.00 | 0.00 | 0.14 | 0.00 | 0.00 | 66 | 266 | 198 | 271 | 12,015 |
| 8-N | 33.2 | 32.7 | 1.20 | 1.18 | 0.00 | 0.43 | 0.00 | 0.01 | 72 | 247 | 199 | 264 | 5,638 |
| 1-N | 38.8 | 38.8 | 1.40 | 1.40 | 0.00 | 0.21 | 0.00 | 0.01 | 81 | 210 | 197 | 254 | 2,517 |
| 10-N | 44.3 | 44.9 | 1.60 | 1.62 | 0.00 | 0.15 | 0.00 | 0.00 | 80 | 179 | 206 | 245 | 1,446 |
| 12-N | 49.9 | 50.0 | 1.80 | 1.81 | 0.00 | 0.14 | 0.00 | 0.00 | 90 | 148 | 209 | 237 | 996 |
| 4-N | 55.4 | 54.9 | 2.00 | 1.98 | 0.00 | 0.17 | 0.00 | 0.08 | 91 | 151 | 212 | 236 | 762 |
| 15-N | | | 0.40 | | | | 0.10 | | Aborted | | | | |
| 3-N | 16.6 | 15.6 | 0.60 | 0.56 | 1.66 | 1.84 | 0.10 | 0.12 | 92 | 254 | 197 | 250 | 33,663 |
| 6-N | 22.2 | 20.6 | 0.80 | 0.74 | 2.22 | 2.41 | 0.10 | 0.12 | 86 | 257 | 196 | 254 | 12,859 |
| 26-N | 27.7 | 27.8 | 1.00 | 1.00 | 2.77 | 3.00 | 0.10 | 0.11 | 77 | 220 | 197 | 248 | 4,186 |
| 2-N | 33.2 | 33.2 | 1.20 | 1.20 | 3.32 | 3.66 | 0.10 | 0.11 | 88 | 179 | 199 | 236 | 1,912 |
| 9-N | 38.8 | 39.2 | 1.40 | 1.41 | 3.88 | 4.16 | 0.10 | 0.11 | 70 | 148 | 203 | 235 | 1,127 |
| 11-N | 44.3 | 44.3 | 1.60 | 1.60 | 4.43 | 4.76 | 0.10 | 0.11 | 82 | 141 | 206 | 229 | 765 |
| 17-N | 49.9 | 49.6 | 1.80 | 1.79 | 4.99 | 5.40 | 0.10 | 0.11 | 85 | 133 | 208 | 228 | 577 |
| 14-N | 55.4 | 55.8 | 2.00 | 2.01 | 5.54 | 6.06 | 0.10 | 0.11 | 85 | 126 | 212 | 231 | 427 |
| 22-N | 16.6 | 17.1 | 0.60 | 0.62 | 3.32 | 3.73 | 0.20 | 0.22 | 75 | 257 | 195 | 254 | 35,515 |
| 19-N | 22.2 | 22.2 | 0.80 | 0.80 | 4.44 | 4.64 | 0.20 | 0.21 | 106 | 208 | 197 | 235 | 10,725 |
| 29-N | 27.7 | 27.7 | 1.00 | 1.00 | 5.54 | 5.78 | 0.20 | 0.21 | 79 | 188 | 198 | 242 | 2,666 |
| 21-N | 33.2 | 33.9 | 1.20 | 1.22 | 6.64 | 6.88 | 0.20 | 0.20 | 76 | 144 | 200 | 225 | 1,131 |
| 24-N | 38.8 | 38.7 | 1.40 | 1.40 | 7.76 | 8.20 | 0.20 | 0.21 | 85 | 138 | 202 | 224 | 757 |
| 27-N | 44.3 | 42.9 | 1.60 | 1.55 | 8.86 | 9.29 | 0.20 | 0.22 | 86 | 134 | 205 | 226 | 608 |
| 25-N | 49.9 | 49.8 | 1.80 | 1.80 | 9.98 | 10.42 | 0.20 | 0.21 | 88 | 128 | 209 | 229 | 422 |
| 16-N | 22.2 | 22.3 | 0.80 | 0.80 | 6.66 | 6.70 | 0.30 | 0.30 | 75 | 191 | 196 | 240 | 3,591 |
| 20-N | 27.7 | 26.9 | 1.00 | 0.97 | 8.31 | 8.53 | 0.30 | 0.32 | 78 | 159 | 197 | 230 | 1,696 |
| 23-N | 33.2 | 33.3 | 1.20 | 1.20 | 9.96 | 10.40 | 0.30 | 0.31 | 86 | 139 | 200 | 223 | 823 |
| 28-N | 38.8 | 39.2 | 1.40 | 1.42 | 1.64 | 12.13 | 0.30 | 0.31 | 68 | 118 | 203 | 227 | 603 |

TABLE B-3.  50 x 20-20 TIRE FAILURE ANALYSIS

| Tire Code Number | Serial Number | Failure Origin |
|---|---|---|
| 1N | 93190035 | S/S ① Lower Sidewall, NSS ② Sidewall Separation 180° from T/C ③ |
| 2N | 03260054 | Test Aborted Before Failure Excessive Tread Wear |
| 3N | 03260055 | NSS Lower Sidewall     for 360° |
| 4N | 93030065 | NSS Lower Sidewall 180° from T/C |
| 5N | 93030067 | NSS Lower Sidewall for 180° at 45° from T/C |
| 6N | 03230083 | NSS Lower Sidewall for 180° with T/C at one end |
| 7N | 03150086 | NSS Lower Sidewall 180° from T/C, Heat in S/S shoulder |
| 8N | 93310087 | NSS Lower Sidewall for 360°; Heat in Both Shoulders, Excessive on NSS Shoulder |
| 9N | 03250121 | NSS Lower Sidewall for 360°, Tread Worn |
| 10N | 03250122 | NSS Lower Sidewall 180° from T/C |
| 11N | 03250123 | Crown Blowout toward NSS |
| 12N | 03250124 | NSS Lower Sidewall 360°, Separation on NSS |
| 13N | 03170181 | NSS Lower Sidewall 90°, NSS Sidewall Separation with T/C at One End |
| 14N | 03220182 | NSS Lower Sidewall 180° from T/C |
| 15N | 03240189 | NSS Lower Sidewall for 180° with T/C in the Middle, S/S Lower Sidewall Separation |
| 16N | 03240187 | Crown Blowout 180° from T/C |
| 18N | 00100194 | NSS Lower Sidewall 180° from T/C |
| 19N | 03220211 | NSS Lower Sidewall for 90° at 60° from T/C |
| 20N | 03250251 | NSS Lower Sidewall 180° from T/C, Heat in Tread |
| 21N | 03250252 | NSS Lower Sidewall for 360° |
| 22N | 03250253 | Crown Break in Tread Area Toward S/S |
| 23N | 03250254 | Crown Centerline Blowout, Both Sidewalls OK |
| 25N | 03240283 | NSS Lower Sidewall 90° from T/C |
| 26N | 03160284 | NSS Lower Sidewall for 360° |
| 27N | 03150306 | NSS Lower Sidewall 180° from T/C |
| 28N | 03260323 | S/S Lower Sidewall for 150° at 150° from T/C |
| 30N | 93000488 | NSS Lower Sidewall 180° from T/C |

NOTES:

① Serial Number Side of Tire

② Non-serial Number Side of Tire

③ Thermocouple

TABLE B-4.  40 x 14 TIRE FAILURE ANALYSIS

| Tire Code Number | Serial Number | Failure Origin |
|:---:|:---:|:---|
| 1N | 03040142 | NSS ① Lower Sidewall ② |
| 2N | 03040144 | NSS Lower Sidewall, S/S Sidewall Separation |
| 3N | 03040146 | Crown — Excessive Heat |
| 4N | 03040147 | NSS Lower Sidewall, S/S Lower Sidewall Separation |
| 5N | 03040166 | NSS Lower Sidewall, Heat in Both Shoulders |
| 6N | 03040168 | NSS Shoulder |
| 7N | 03040169 | S/S ③ Shoulder — Heat |
| 8N | 03040171 | NSS Lower Sidewall, Heat in Both Beads, Heat in Both Shoulders |
| 9N | 03040172 | NSS Lower Sidewall |
| 10N | 03020202 | NSS Lower Sidewall |
| 11N | 03020203 | NSS Lower Sidewall, Heat in Both Shoulders |
| 12N | 03050221 | NSS Lower Sidewall |
| 14N | 03050229 | NSS Lower Sidewall, Slight Tread Abrasion |
| 15N | 03050230 | Test Aborted Before Failure |
| 16N | 03050231 | NSS Lower Sidewall, Severe Tread Abrasion |
| 17N | 03050241 | NSS Lower Sidewall, Heat in S/S Shoulder |
| 19N | 03050243 | NSS Lower Sidewall, Heat in Crown |
| 20N | 03050244 | NSS Lower Sidewall, NSS Sidewall Separation |
| 21N | 03050245 | NSS Lower Sidewall, Heat in Crown |
| 22N | 03050247 | NSS Lower Sidewall, Heat in Crown, S/S Lower Sidewall Separation |
| 23N | 03050248 | NSS Lower Sidewall |
| 24N | 03030249 | NSS Lower Sidewall, Heat in NSS Shoulder, Slight Tread Abrasion |
| 25N | 03050249 | NSS Lower Sidewall |
| 26N | 03050251 | NSS Lower Sidewall, NSS Shoulder Separation, S/S Sidewall Separation |
| 27N | 03030262 | NSS Lower Sidewall, Slight Tread Abrasion |
| 28N | 03030264 | NSS Lower Sidewall, Slight Tread Abrasion |
| 29N | 03030230 | NSS Sidewall, Slight Tread Abrasion |

NOTES:

① Non-serial Number Side of Tire

② See Figure 44 for Location on Tire

③ Serial Number Side of Tire

# APPENDIX C

## MISCELLANEOUS TIRE INFORMATION

During the progress of the program, the following data were obtained that were not directly pertinent to the program, but may be of interest.

### EFFECT OF CENTRIFUGAL FORCE

The carcass of a rolling tire experiences centrifugal forces. When the tread area contacts the ground, or-in the case of the dynamometer contacts the drum, the effective portion of the tread and crown rubber will partially support the radial load imposed on the tire. Figure C-1 illustrates this point by showing a reduction in tire deflection as the tire roll velocity increases.
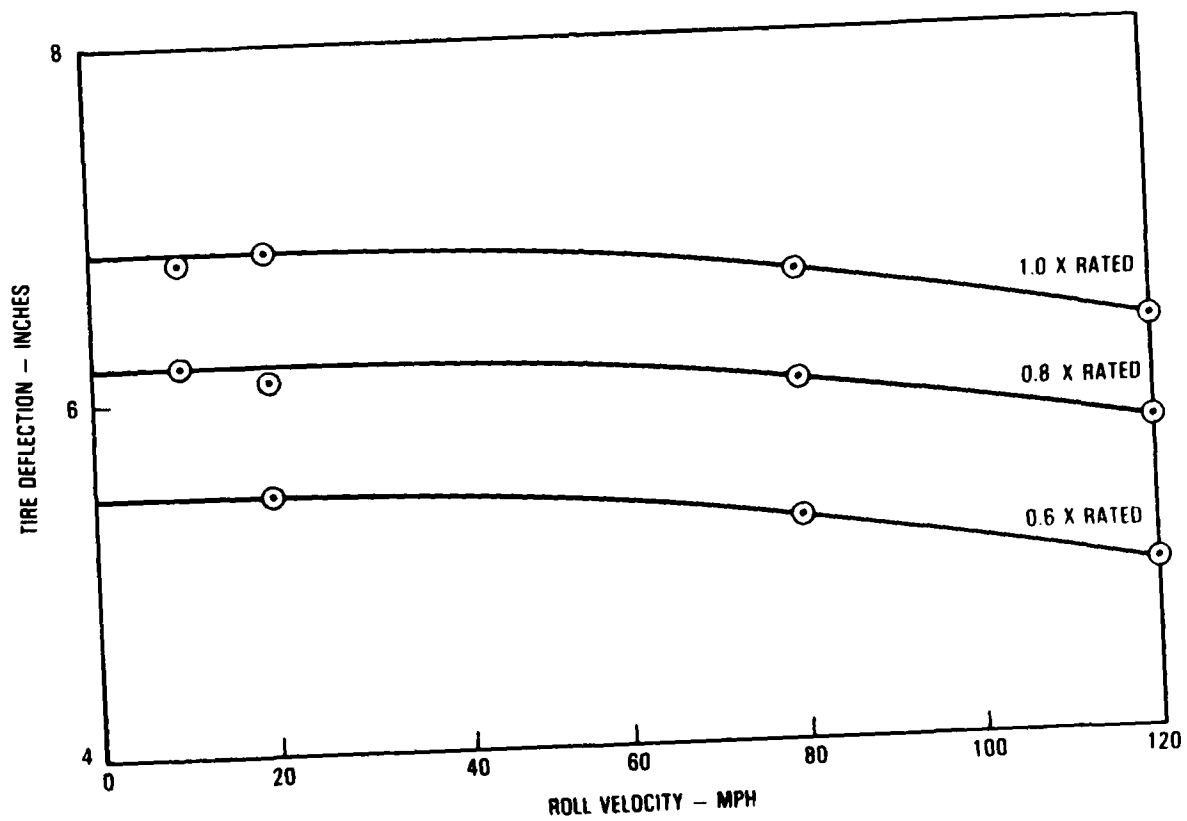
FIGURE C-1.   50 x 20-20 TIRE, EFFECT OF ROLL VELOCITY ON TIRE
DEFLECTION UNDER CONSTANT RADIAL LOADS

# APPENDIX D

## STANDARD DISTRIBUTION LIST

### Region Libraries

| | |
|---|---|
| Alaska | AAL-64 |
| Central | ACE-66 |
| Eastern | AEA-62 |
| Great Lakes | AGL-60 |
| New England | ANE-40 |
| Northwest-Mountain | ANM-60 |
| Western-Pacific | AWP-60 |
| Southern | ASO-63d |
| Southwest | ASW-40 |

### Headquarters (Wash. DC)

ADL-1
ADL-32 (North)
APM-1
APM-13 (Nigro)
ALG-300
APA-300
API-19
AAT-1
AWS-1
AES-3

### Center Libraries

| | |
|---|---|
| Technical Center | ACT-64 |
| Aeronautical Center | AAC-44.4 |

### OST Headquarters Library

M-493.2 (Bldg. 10A)

Civil Aviation Authority
Aviation House
129 Kingsway
London WC2B 6NN England

University of California
Sers Dpt Inst of Trsp Std Lib
412 McLaughlin Hall
Berkely, CA 94720

Embassy of Australia
Civil Air Attache
1601 Mass Ave. NW
Washington, D. C. 20036

British Embassy
Civil Air Attache ATS
3100 Mass Ave. NW
Washington, DC 20008

Scientific & Tech. Info FAC
Attn: NASA Rep.
P.O. Box 8757 BWI Aprt
Baltimore, Md. 21240

Dir. DuCentre Exp DE LA
Navigation Aerineene
941 Orly, France

DOT-FAA AEU-500
American Embassy
APO New York, N. Y. 09667

Northwestern University
Trisnet Repository
Transportation Center Lib.
Evanston, Ill. 60201

DISTRIBUTION LIST

| GOVERNMENT | No. of Copies |
|---|---|

FAA NATIONAL HEADQUARTERS                                      66
800 Independence Ave., SW
Washington, DC  20591

ATTN:   Thomas McSweeney, AWS-100 (2)
        Phil Akers, AWS-120 (2)
        Raymond Ramaskis, AWS-300 (2)
        Leo Weston, AWS-340 (10)
        Angelo Masstrulo, AWS-340 (50)


FAA CENTRAL REGION HEADQUARTERS                                4
601 East 12th Street
Federal Building
Kansas City, MO  64106

ATTN:   John Reebling, ACE-250 (2)
        Walter Horn, ACE-115C (2)


FAA ALASKAN REGION HEADQUARTERS                               2
701 C Street, Box 14
Anchorage, AL  99513

ATTN:   Paul Donohoe, AAL-250 (2)


FAA MIKE MONRONEY AERONAUTICAL CENTER                         2
P.O. Box 25082
Oklahoma City, OK  73125

ATTN:   Lyle Combs, AAC-950 (2)


FAA WESTERN-PACIFIC REGION HEADQUARTERS                       2
P.O. Box 92007
Worldway Postal Center
Los Angeles, CA  90009

ATTN:   William Sullins, AWP-250 (2)

FAA SOUTHWEST REGION HEADQUARTERS
P.O. Box 1689
Fort Worth, TX   76101

ATTN:  George House, ASW-250 (2)


FAA SOUTHERN REGION HEADQUARTERS                          2
3400 Norman Berry Drive
P.O. Box 20636
Atlanta, GA   30320

ATTN:  George Mattern, ASW-250 (2)


FAA NORTHWEST MOUNTAIN REGION HEADQUARTERS                2
17900 Pacific Highway South
C-68966
Seattle, WA   98168

ATTN:  Stanley Magnuson, ANM-250 (2)


FAA NEW ENGLAND REGION HEADQUARTERS                       2
12 New England Executive Park
Burlington, MA   01803

ATTN:  Gerald Nash, ANE-250 (2)


FAA GREAT LAKES REGION HEADQUARTERS                       2
O'Hare Lake Office Center
2300 East Devon Avenue
Des Plaines, IL   60018

ATTN:  Roger Gordon, AGL-250 (2)


FAA EASTERN REGION HEADQUARTERS                           2
JFK International Airport
Fitzgerald Federal Building
Jamaica, NY   11430

ATTN:  Arvid Hanson, AES-250 (2)

FAA EUROPEAN OFFICE HEADQUARTERS                                2
15 Rue de la Loi (3rd Floor)
B-1040 Brussels, Belgium
c/o American Embassy APO, NY   09667

ATTN:  Joseph Pontecorvo, AEU-250 (2)


DOT TRANSPORTATION SYSTEMS CENTER                              20
Kendall Square
Cambridge, MA   02142

ATTN:  Steve Bobo, DTS-48 (20)


FAA LOS ANGELES AIRCRAFT CERTIFICATION OFFICE                  2
4344 Donald Douglas Drive
Long Beach, CA   90808

ATTN:  Anthony Bonano, ANM-130L (2)


USAF FLIGHT DYNAMICS LAB.                                       8
Wright Patterson AFB, OH   45433

ATTN:  Paul Wagner, AFWAL/FIEM (2)
       Igors Skribliss, AFWAL/FIEM (2)
       Avar Peterson, AFWAL/FIEM (2)
       Bruce Tremblay, ASD/ENFE (2)


NATIONAL AERONAUTICS AND SPACE ADMINISTRATION                  2
Mail Stop 497
Langley Rearch Center
Hampton, VA   23665

ATTN:  John Tanner (2)


CIVIL AVIATION AUTHORITY                                        2
CAA Brabazon House
Redhill, Surrey U.K.   RH1SQ

ATTN:  Roger Christmas (2)

## NONGOVERNMENT

ATTN:  Thomas Dwenger                                    2
Goodyear Tire Company
1144 East Market STreet
Akron, OH  44316


ATTN:  Richard R. Batten                                 2
TWA
KC International Airport
Kansis City, MO  64195


ATTN:  Harry Davis                                       2
TATCO
7775 N.W. 12th Street
Miami, FL  33120


ATTN:  Yukio Tadokoro                                    2
C/O Harry Davis, TATCO
7775 N.W. 12th Street
Miami, FL  33120


ATTN:  Dave Lundquist                                    2
American Airlines
P.O. Box 582809
Tulsa, OK  74158-2809


ATTN:  Gregory L. Felder                                 2
B.F. Goodrich
500 S. Main Street
Akron, OH  44318


ATTN:  Ronald L. Olds                                    2
Michelin Tire Corp.
Patewood Exec. Park
P.O. Box 19001
Greenville, SC  29602

```
ATTN:  Neal Billeran                                          2
McDonnell Douglas Corp.
3855 Lakewood Blvd.
Mail Code 36-94
Long Beach, CA  90846


ATTN:  Prof. S. K. Clark                                      2
Mech. Eng./Appl. Mech.
315 Auto Lab.
University of Michigan
Ann Arbor, MI   48109


ATTN:  W. E. Dunning                                          2
C1-250, Mail Code 36-94
Douglas Aircraft Co.
3855 Lakewood Blvd.
Long Beach, CA  90846


ATTN:  Stanley Glen Mays                                      2
Sir Treads Inc.
P.O. Box X
5075 Pine Tree Street
Forest Park, GA   30051


ATTN:  Dave Zitzman                                           2
Goodyear Tire & Rubber Co.
1144 E. Market Street
Akron, OH   44316


ATTN:  W. C. Shaver                                           2
Air Treads, Inc.
1864 Sullivan Road
College Park, GA 30337


ATTN:  Carl Topinka                                           2
Eng. Dept. 178
Cessna
P.O. Box 7704
Wichita, KS   67277
```

ATTN: W. W. Witt                                          2
United Air Lines/SFOEG
San Francisco National Airport
San Francisco, CA  94128


ATTN: Charles Westlund                                    2
1250 Knoxville Avenue
Long Beach, CA  90815


ATTN: Yosekui Okado                                       2
Bridgestone Research Inc.
P.O. Box 66120
Washington, DC  22035

DATE
FILMED
-8